DTIC FILE COPY

AD-A215 534

AN EXPLORATORY ANALYSIS OF MOTION SICKNESS DATA: A TIME SERIES APPROACH

THESIS

David C. Thompson
Captain, USAF

AFIT/GSO/ENS/89D-15

DTIC
ELECTE
DEC 19 1989
S D
B

DEPARTMENT OF THE AIR FORCE
AIR UNIVERSITY
AIR FORCE INSTITUTE OF TECHNOLOGY
Wright-Patterson Air Force Base, Ohio

DISTRIBUTION STATEMENT A
Approved for public release;
Distribution Unlimited

89 12 18 083

(1)

AFIT/GSO/ENS/89D-15

AN EXPLORATORY ANALYSIS OF MOTION SICKNESS DATA: A TIME SERIES APPROACH

THESIS

David C. Thompson
Captain, USAF

AFIT/GSO/ENS/89D-15

DTIC
ELECTE
DEC 19 1989
S B D

Approved for public release; distribution unlimited

AFIT/GSO/ENS/89D-15

AN EXPLORATORY ANALYSIS OF MOTION SICKNESS: A TIME SERIES APPROACH

THESIS

Presented to the Faculty of the School of Engineering
of the Air Force Institute of Technology
Air University
In Partial Fulfillment of the
Requirements for the Degree of
Master of Science in Space Operations

David C. Thompson, B.S.

Captain, USAF

December, 1989

Approved for public release; distribution unlimited

Preface

This study applied time series methods in the analysis of motion sickness data obtained in experiments at AFIT. The research showed the usefulness of these methods by analysis of the data in both the time and frequency domains.

The analysis indicated a definite boundary may exist in some subjects between healthy and sickness-induced brain data. A significant model change occurred approximately halfway through the primary subjects trial run. The addition of Dilantin (phenytoin) appears to slow the effects of motion sickness and its effects were noted in the model.

I would like to thank my faculty advisor, Lt Col James Robinson for his encouragement and undying support. He was instrumental in the initial design and conduct of the research effort. I am grateful to Dr. Matthew Kabrisky for his patience and the use of his data and laboratory equipment. And most importantly, I wish to thank my wife Michelle for enduring this effort along with me and putting up with the long nights and weekends of work.

David C. Thompson

Accession For
NTIS GRA&I ☑
DTIC TAB ☐
Unannounced ☐
Justification
By
Distribution/
Availability Codes
Dist | Avail and/or Special
A-1

Table of Contents

List of Figures

List of Tables

Abstract

A methodology was developed in order to characterize the prodigious amount of electroencephalographic (EEG) data collected during motion sickness experiments at the Air Force Institute of Technology. The analog data are sampled and digitized into a time series. Stationarity transformations and a windowing operation are performed on the data to produce local areas of stationarity.

Windowed versions of the autocorrelation function, partial autocorrelation function and periodogram are discussed and employed. The windows are analyzed over time in order to view the underlying structure of the model that is hidden in the data. These functions are converted into image files to aid interpretation. The images are directly interpreted for model determination, model changes, artifact assessment and stationarity determination.

A primary subject and two confirming subjects are analyzed. Both a placebo trial and Dilantin trial were analyzed for each subject to determine the nature of motion sickness and the efficacy of the drug treatment. The results are inconclusive as all three subjects brain data proved to be unique with respect to the placebo trials. A definite model change or pattern can not be determined based on the

subjects used. The effects of Dilantin on the brain signals, however, were marked in two of the three subjects.

The methodology is shown to be an effective means of representing the underlying structure of large amount of data. Both significant and weak periodicities within the data can be highlighted for analysis and interpretation.

AN EXPLORATORY ANALYSIS OF MOTION SICKNESS DATA: A TIME SERIES APPROACH

I. Introduction

Background

Man is not a stationary creature. Unfortunately, the human body is not always well equipped for all types of travel. This lack of fitness often manifests itself as motion sickness. Anyone who has experienced car sickness or sea sickness can attest to the debilitating nature of the illness. The problem becomes more severe in space where a closed environment and tight schedules leave little or no room for sickness.

Approximately fifty percent of all astronauts experience some degree of space adaptation syndrome (SAS) (6:542). SAS is a form of motion sickness that occurs the first few days on orbit while the astronaut becomes accustomed to the weightless environment. Although not a significant problem for long duration flights, three workdays lost for sickness out of a four to seven day flight could jeopardize the mission's success.

Two lines of research are underway to tackle the problem of motion sickness. The first is trying to understand the process of motion sickness by observing the physiological changes that take place in the body as the subject transitions through the stages of motion sickness. A good understanding of the physiological process is essential to determine the nature of motion sickness. The second type of research seeks to eliminate the effects of motion sickness by employing drugs or other means such as biofeedback or sensitization therapy (14:2).

Researchers at the Air Force Institute of Technology (AFIT) are actively pursuing both interests with motion sickness experiments (4;12;14). A drug treatment is being tested and based on preliminary results, is a likely candidate as a cure for motion sickness (3).

NASA considers SAS a high priority problem to be solved. It is estimated that SAS may cost $10 million per shuttle flight. In addition, SAS poses several real dangers to the crew, particularly when spacesuits must be worn (12:3-4).

Summary of Current Knowledge

Motion Sickness and Treatment. The generally accepted theory behind the occurrence of motion sickness is the sensory conflict theory. This theory asserts that motion

sickness results when certain visual or vestibular cues do not match the other signals received by the brain or match those already known from previous experiences (14:2). The conflicting signals result in a sensory mismatch resulting in motion sickness as the brain attempts to resolve the situation based on previous experience to similar stimulus.

As an example of this theory, consider a person sitting on the edge of a spinning merry-go-round. If he were to close his eyes and tilt his head downward, the ear would send signals suggestive of a change in rotation. The body on the other hand, would continue to send signals to the brain that the spinning motion was unchanged. These conflicting signals then cause motion sickness to occur.

The classical symptoms of motion sickness are nausea, pallor, cold sweats, and vomiting (14:1). Additional symptoms associated with space motion sickness (SMS) reported during the first nine space shuttle missions were abdominal fullness and discomfort, anorexia, lethargy, malaise, and headache. These symptoms agree closely with ground reported motion sickness symptoms (12:6-7). Thus it has been proposed that a treatment that is effective in the laboratory also may work in space (12:11).

Scott cited three promising treatments to motion sickness (14:2-4). These treatments are drugs, biofeedback, and desensitization. Certain specific drugs are currently

the preferred form of treatment on shuttle flights today (12:7-10). Unfortunately these drugs are depressants and carry with them unpleasant side effects that impair alertness and degrade performance (12:27-28). The drug of choice is a combination of the depressant scopolamine and a stimulant, (dexedrine) used to offset the negative effects of the depressant. Side effects of this treatment are tremors, restlessness, increased motor activity, insomnia and agitation (12:28).

A new use for the drug Dilantin (phenytoin) is undergoing testing at the Air Force Institute of Technology (AFIT). The drug has been shown to be effective in eliminating motion sickness symptoms in studies performed at AFIT. Three subjects out of the 18 tested have been cured of all symptoms and the average improvement in symptom onset time has improved over 500 percent per subject (14:70-81). Dilantin would be an excellent course of treatment because of its low incidence of side effects (3).

Biofeedback and desensitization have been effective in curing airsickness (14:3). Cowings et al. suggest motion sickness may result after a build-up of sympathetic activity within the autonomic nervous system. Autogenic feedback training would then be useful to slow or eliminate the generation of these signals (6:548-550). Unfortunately,

these courses of treatment are not likely candidates for implementation due to the nature of space operations.

Past Research at AFIT. Motion sickness research has been active at AFIT since 1983. The first team assembled the motion chair and designed the first physiological sensors (14:3). The current motion chair is a flight disorientation simulator adapted with bio-sensors and has been modified so that it can only rotate about the subjects' z-axis (11:4-15).

In 1985, Jarvis and Uyeda continued the spin chair research and reported the first experimental results (14:4). Many of the unique physiological sensors that are in use today were designed and built by Chelen after his arrival on the team as principal investigator.

The 1986 research team applied the first statistical methods to the data (11:10). They were able to identify trends among the physiological indicators associated with the onset of motion sickness. A multiple linear regression was used to develop an initial predictive model (11:57-60). The major finding of the research was the initial discovery of a low frequency, high amplitude brain wave that occurs during motion sickness (11:63).

Chelen et al. identified this brain pattern as a seizure equivalent originating from the temporal lobe (4:7-8). Their study suggested the use of the anticonvulsant drug

Dilantin (phenytoin). Dilantin was considered a good choice because of its efficacy in controlling epilepsy, and long history of use with few known side effects (3).

In 1987, Drylie, Fix, and Gaudreault automated the collection procedure by adding computers for data analysis. They added new sensors and standardized the experiment to improve the reliability of the results (14:4-5).

Fix first suggested the use of a neural net in predicting the subject's instantaneous sickness level (7:6). The neural net model involves developing a unique motion sickness equation for each subject. Weighted linear combinations of these equations are then taken to form the overall motion sickness equation (7:19-25).

Scott and Morales continued this line of research in 1988 (14;11). The neural net model was applied to the 1986 data and resulted in a nonlinear equation containing 34 terms with only five independent variables. These five variables were used to predict the subject reported symptom level on a scale from one (well) to ten (sick). The model was correct to within one level in only 60% of the cases and within two in 77% of the cases (14:28-31). The results were only slightly better using the 1987 data (14:31-32).

Morales (12:86-91) used a similar technique using only three of Scott's five variables. His model contained 96 nonlinear terms. Morales suggested that the

electroencephalographic (EEG) activity is a defense mechanism of the brain, and Dilantin may enhance that defense capability (12:107). He recommended further research in this area because the EEG may be the key physiological parameter of interest (12:106).

Measurements. Motion sickness research continues to produce conflicting results concerning physiological measurements and their interpretations. Cowings et al. reported the findings of Graybiel and Lackner that show no relationship between the physiological measurements and subject-reported symptoms (6:543). A different protocol by Cowings et al. showed that heart rate, basal skin resistance, pulse volume of blood, and respiration are all correlated with the levels of symptoms reported by the subject (6:547-549).

Changes in physiological measurements as an indicator of motion sickness are still a topic of debate in the literature. It seems there are almost as many sets of indicators as there are experiments (6;7;11;12;14). For example, Cowings et al. cites the findings of Money that the autonomic nervous system can play no part in motion sickness research, therefore eliminating the need to take measurements of heart rate, blood pressure, and respiration (6:542-543). Graybiel and Lackner also reported no change in heart rate and no relationship between blood pressure and

onset of motion sickness symptoms as cited by Cowings et al. (6:543).

Other findings contradict these results. Cowings et al. report a significant relationship exists between heart rate, basal skin resistance, blood pulse volume, respiration rate and the level of motion sickness reported by the subject (6:547-548). They also cite the work done by Crampton (6:543) that suggested a relationship between several physiological variables, to include heart rate and pallor, and onset of motion sickness. Cowings et al. conclude that time series analysis of physiological data may be the key to understanding the subtle relationships among the variables of motion sickness (6:550).

AFIT studies substantiate the findings of Cowings et al. that physiological measurements are correlated with onset of motion sickness (7;11;12;14). McPherson showed that thoracic respiration, finger pallor, and galvanic skin response are highly correlated with reported symptoms while heart rate, skin temperature, and respiration rate were correlated to a lesser degree (11:63). Fix reported stomach activity, eye motion, respiration rate, galvanic skin resistance, and skin temperature as having been highly correlated with motion sickness (7:14).

Scott determined that eye movement, stomach activity, and respiration rate are good indicators of motion sickness

(14:49,56). Morales, using the same data determined heart rate, respiration rate, and stomach activity to be effective indicators (12:72-93).

Problem Statement

This study was designed to be an exploratory analysis of the physiological data obtained during a typical AFIT motion sickness experiment. Selected channels were analyzed to determine the nature and extent of a hypothetical "motion sickness generator". The analysis was accomplished for both a placebo run and Dilantin treatment run to determine the drug's effect, if any, on the generator.

Scope

This bulk of the analysis was limited to one subject for several reasons. First, an extensive amount of analysis was required in order to establish the results to be shown later. It was also determined that a thorough, complete analysis of one subject would give more insight into the nature of the phenomena under study than would a less thorough study using many subjects. By limiting the analysis to a few subjects, these new methods could be properly validated for use in continued research across a wider range of subjects. Once the primary analysis was complete, two additional subjects were analyzed for comparison.

The research was further limited to the analysis of five key channels of motion sickness data. The channels chosen for the analysis were the five brain channels. These selections were made based on previous recommendations (12:108) that the brain channels required further investigation. The other channels were considered to be either uncorrelated with motion sickness or subject to artifacts and error.

Assumptions

The primary assumption of this research was that the data could be treated as a time series process. With this assumption made, traditional time series methods and more specifically, Box-Jenkins methods for model fitting could be applied to the data (2:18-19).

A second assumption assumes an autoregressive integrated moving average (ARIMA) model can be fit to the data. A further assumption is that any changes in the body as a result of motion sickness will manifest itself as a change in this model. Model change being defined as an obvious shift in the underlying process. These changes may manifest themselves as shifts in the autocorrelation function, partial autocorrelation function, periodogram or combinations of all three. By observing changes in the model over time, inferences about the motion sickness generator

and its effects can be drawn.

A final assumption involved the concept of stationarity. It was assumed that the data to be analyzed was initially stationary or could be made stationary by means of some transformation. Stationarity transformations were limited to simple differencing.

II. Experimental Procedure

Subject Screening

The experiment began with a volunteer subject filling out a questionnaire and medical history on himself. Because of the protocol in effect, the subject pool was limited to healthy male active-duty DOD personnel only. The history was then reviewed by the resident physician who performed a physical to determine whether the subject was fit for the experiment.

Specific items of interest were any previous instances of possible neurologic damage or occurrences of motion sickness. These indicators are then used to help determine experimental parameters and aid in data analysis after the experiment. For instance, if the subject showed a predisposition toward motion sickness, a slower spin rate would be used to induce motion sickness. Similarly, a subject who showed no history of motion sickness would be spun at a higher rate. The spin rate was adjusted from subject to subject to normalize the experiment duration and keep most trials under 15 minutes.

A susceptibility trial is then run on the subject. The purpose of this trial is to familiarize the subject with the protocol and to determine how susceptible the subject really is to the stimulus.

The AFIT protocol employs a flight motion simulator that has been modified to spin only about the subjects' z-axis. The spin chair can spin either clockwise or counter-clockwise and the rotation can be switched from trial to trial. This is usually done in order to minimize any possible adaptation effects the subject may experience when the experiment is performed a second time.

The subject is blindfolded and placed in the chair. The trial begins after the chair has been brought up to speed and stabilized. A series of taped commands directing random head motions (up, down, left, right) is then played and the subject performs these movements. The motions are randomized in an attempt to minimize any adaptation effects that might be experienced due to repeated head movement in the same plane. It is this movement of the head, into and out of the plane of rotation, that causes the stimulus that induces the motion sickness.

The head motions continue until the subject experiences frank sickness and is near emesis. During the course of these motions, experimenters ask the subject to comment on his current state using the scale of 1 (well) to 10 (emesis). The experimenters also query the subject as to the symptoms he is experiencing and what caused any change in subject reported symptom level (SSL).

If the subject appeared to have a normal susceptibility trial, and decided to continue with the experiment, a cognitive test battery is then given. The battery consists of a grammatical reasoning test, unstable tracking test, and visual perception test. The results are then used for comparison against later tests, specifically under the influence of the drug Dilantin, to determine any possible side effects that might influence cognitive skills or visual acuity (14:15).

Instrumented Trials

Following a successful susceptibility trial, the subject performed two instrumented trials to test the efficacy of the drug under investigation. One run is performed under the effect of the drug Dilantin, while on the other run the subject is given a placebo. A double blind environment is adhered to throughout the experiment by which neither the subject nor the experimenters know, which pills were taken. Serum blood levels are taken before each trial with the results not made available by the laboratory until after the second trial is complete.

The protocol of these two trials remained the same. The subject is tested using the cognitive test battery described earlier. These results are compared to the previous performance to determine if there are any possible drug

side-effects. He is then fitted with the various physiological monitoring devices and the chair is spun at the predetermined speed. It is essential that both trials be accomplished using the same speed. Because the stimulus is proportional to the cube of the spin rate, a change in rate may significantly influence the onset and extent of symptoms. To eliminate the possibility of adaptation, one trial is spun clockwise, and one counter-clockwise. The same random head motions are performed to induce motion sickness, and the experiment continues until emesis is achieved.

Monitoring Devices

One thing that makes the AFIT motion sickness research unique is the extent of physiological monitoring that takes place. A Soltec model 8k26 16 channel strip chart recorder and Kyowa Dengyo Beta machine are employed to record the various channels in both analog and hardcopy outputs for later analysis. All channels are band limited to 30 Hertz (Hz) and below by special filters designed by Chelen. This effectively eliminates unwanted artifacts such as AC noise in the 60 Hz range.

Brain activity is measured by means of five pairs of electrodes. Because the frequency of the signals is small, .2-.3 Hz (4:5-6) subdermal electrodes are placed under the scalp to improve reception. The channels measured are EEG1A

corresponding to the midline frontal cortex region, EEG1B (parietal midline cortex), EEG1C (right side temporal lobe), EEG2A (left side temporal lobe), and EEG2B (bilateral frontal cortex region). See Figure 1 for approximate placement of electrodes on the scalp.

Respiration is measured using two pneumographs. A pneumograph is a device that measures the degree of

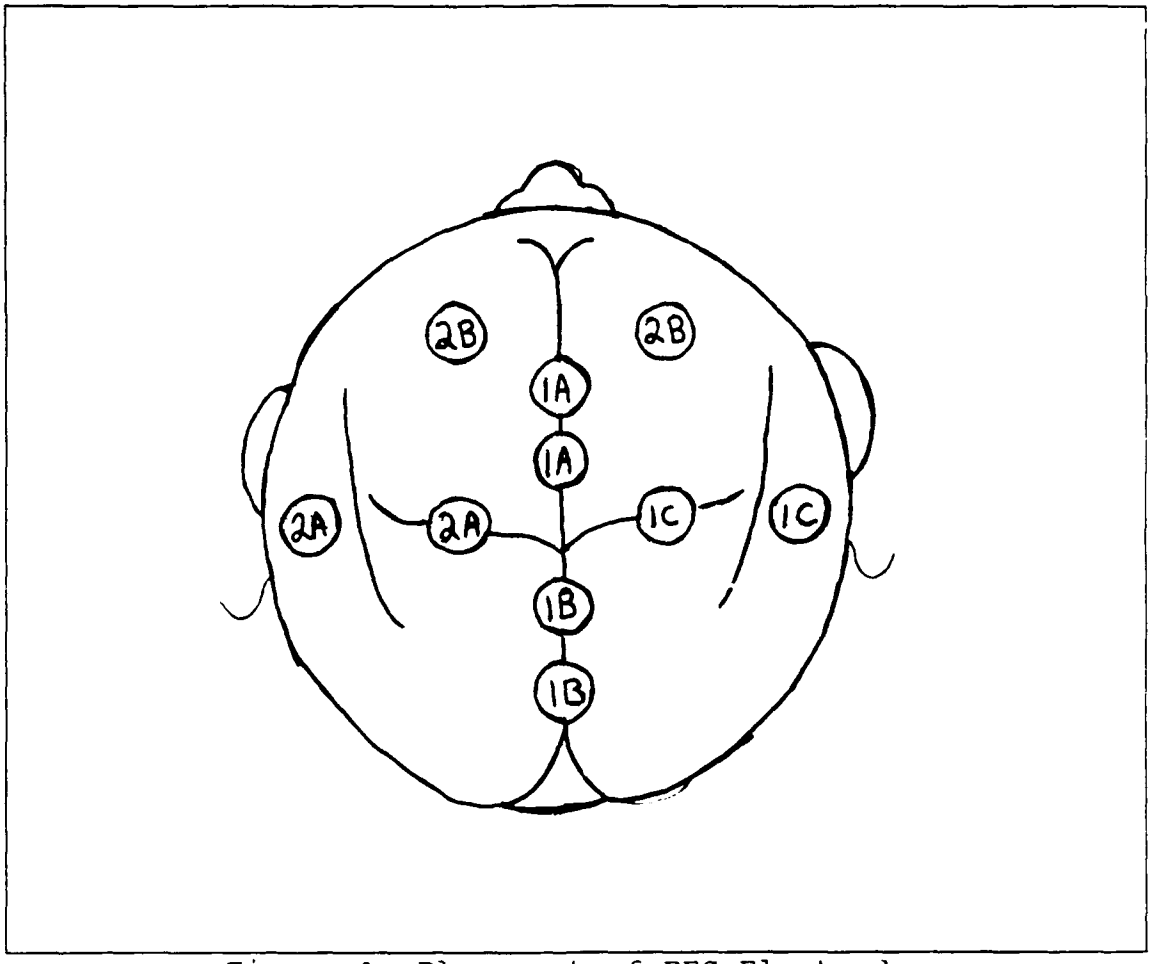

Figure 1. Placement of EEG Electrodes

expansion of the chest due to respiration. Both abdominal and thoracic respiration are monitored. Prior to the start of the experiment these devices are calibrated using a spirometer to compare actual breathing volume with measured values given by the pneumographs.

Heart rate is measured using the standard electrocardiograph (EKG). The EKG measures the electrical activity of the heart. A blood pressure cuff is also used to measure blood pressure at random points throughout the experiment.

Skin pallor measures the blood flow changes that accompany the onset of motion sickness. Two sites have been chosen for measurement. Photoplethysmographs (PPS) are the optical instruments used to measure the skin color of the face and the tip of the little finger. These are referred to as the facial and peripheral PPS values. Previous studies, however, have left some doubt about the accuracy of these measurements (14:8).

Eye motion is measured using two sets of sensors called electronystagmographs (ENG). The ENGs measure the electrical potential produced by the muscles of the eye. Two pairs are used to measure both the vertical and horizontal movements. Unfortunately these sensors may be prone to artifact caused by unnecessary movement and sweating (14:6).

Stomach activity is measured using devices called splanchnograms. Two forms of this device are employed. The electrosplanchnogram measures the electrical activity of the stomach. A phonosplanchnogram is used in obtaining an audio recording of the actual sounds produced by the stomach.

III. Methodology

This thesis deals with the complex issue of how to deal with large amounts of data. Although usually this may be an enviable situation, having too much data can cause many unique problems involving data storage, data manipulation, data presentation and interpretation. Implicit in any thorough analysis of the motion sickness data is the development of a new methodology to analyze and interpret the vast amount of data already generated.

Data Sampling

The data recorded during the experiment consist of multiple channels of analog (continuous waveform) data stored on videotape. The analog data must first be sampled and digitized before any analysis can be performed. The process of sampling converts the analog signal into a discrete representation of the waveform by means of a two step sampling process.

The first step of this process is to sample the waveform at discrete constant time intervals. This interval is equal to the reciprocal of the sampling rate that will be discussed later. This first step results in an intermediate waveform that is now discrete in time but continuous in amplitude. The second step is to digitize the data into discrete amplitudes. The number of levels is dependent on

the sampler and software used, with 256 levels being a representative example. At this point the data are now discrete in both time and amplitude allowing digital processing methods to be employed. Figure 2. illustrates this process and the resulting waveforms that are obtained.

The process of sampling represents a tradeoff between storage capacity and signal reproducability. To reproduce the signal exactly requires a theoretically infinite sampling rate (thousands of Hz) with the accompanying unrealistic data handling and storage requirements. Sampling at a significantly lower rate minimizes the resources needed but also reduces the reproducibility of the waveform. The distortions that occur when restoring the signal are known as aliasing.

The effects of this tradeoff are minimized when the sampling occurs at the Nyquist Limit (5:30). The Nyquist limit is the sampling frequency defined to be twice the maximum frequency of the band-limited signal. Mathematically:

$$w_s = 2w_{max} \tag{1}$$

where w_s is the sampling rate in samples/sec and w_{max} is the largest frequency in Hz of the band-limited signal. Theoretically this sampling rate should be sufficient to reproduce the original signal accurately and without the effects of aliasing. Unfortunately, the process of band-

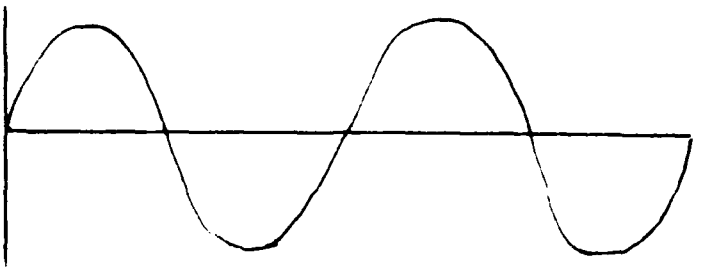

Analog -- Continuous in Time and Amplitude

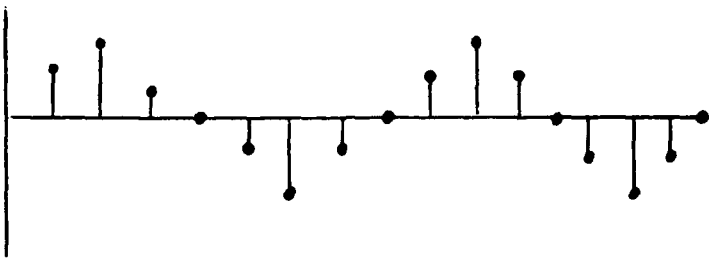

Sampled -- Discrete in Time Continuous in Amplitude

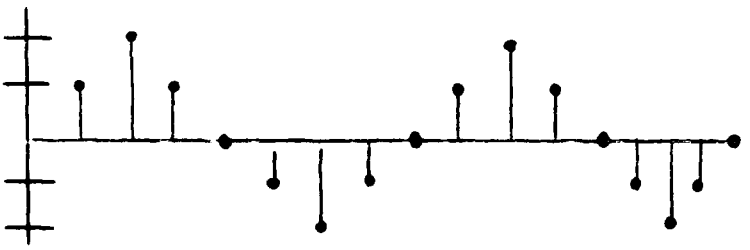

Final Signal -- Discrete in Time and Amplitude

Figure 2. Illustrations of Digital Sampling Effects

limiting the original signal requires that the signal be processed through some form of filter that eliminates the unwanted higher frequencies. Because the filter is not ideal, there will be some degree of high frequency bleed

through. This may cause additional aliasing that the Nyquist limit sampling rate may not account for.

It is for this reason that researchers often sample at higher than the Nyquist rate (5:31). To determine the proper sampling rate, representative channels were sampled at various rates from the Nyquist rate of 60 Hz, up to 300 samples per second. The sample autocorrelation function, to be discussed later, was used to compare the effects of the increased sampling rates. The results were disturbing because the different sampling rates resulted in different functions. As the sample rate is increased above the Nyquist frequency, it is expected that the function will remain relatively constant. Because the sample autocorrelation function changed with the increasing sampling rate, there appears to be random correlations introduced due to the increased number of samples taken.

The hypothesized cause is an inconsistency in the sampling software not sampling properly, thus giving spurious results as the sample rate is increased. The decision was made to continue the research using the more reliable results gained by sampling at the Nyquist rate (10). Thus for all subsequent analyses, the sample rate was to remain at 60 Hz (samples per second).

Data Collection and Manipulation

Data collection and manipulation was a three step process. First the data were sampled and digitized using a Zenith Z-248 computer running CODAS by DATAQ Instruments. Codas is the software that performs the analog to digital conversion of the data. The data files were transferred to a mainframe computer for statistical processing. Data manipulation was accomplished using IMSL and SAS statistical packages. Applicable subroutines included both time series and spectral analysis routines. The output of these routines was then transferred to a microcomputer for final analysis and interpretation.

Graphical data analysis was accomplished on a Sun 386i running Interactive Data Language (IDL) software by Research Systems Inc. This program allowed a real-time display of, and interaction with, the vast amount of data that was generated using the mainframe batch processing.

Analytical Methods

The data collection phase generated approximately 600,000 observations that were sampled over 14 channels of physiological data. This represented only fifty percent of the total data available for one subject. A technique was developed analyze this large data base efficiently and accurately.

Time Series and Stationarity. Each channel was treated as a separate time series. A time series can be thought of as a sequence of data that has been sampled from a time-continuous process. The samples were taken at uniform time intervals equal to the reciprocal of the sampling rate as discussed earlier.

To employ the methods of time series analysis, the series must be assumed stationary. A time series is considered stationary of order 2 if the mean and variance do not change with respect to time (13:106). A plot of the series over time is usually one indication of stationarity. The series is considered stationary if the values appear to fluctuate consistently about a constant mean and appear to have constant variance. Otherwise, the series is considered nonstationary and must be made stationary by means of a stationarity transformation.

Often, the mean is either increasing or decreasing over time. This linear trend can be treated using a technique known as first differencing (1:26). First differencing takes a series Y_t of n observations and transforms it into a new stationary series Z_t of n-1 observations defined by:

$$z_t = y_t - y_{t-1} \qquad (2)$$

To illustrate this concept, consider a basic nonstationary time series Y(t) and its first differenced stationary time series Z(t). Since Z(t) is stationary:

$$z_t = \mu + a_t \qquad (3)$$

where a_t is a random shock associated with observation t. Substituting $z_t = y_t - y_{t-1}$ into Equation 3 yields:

$$y_t - y_{t-1} = \mu + a_t \qquad (4)$$

or

$$y_t = \mu + y_{t-1} + a_t \qquad (5)$$

Thus it can be seen that the original series contains a linear trend in y and is therefore nonstationary, whereas the transformed series is stationary about the new series' mean μ which is constant.

Should the series sample mean appear to be changing at a nonlinear rate, second differencing can be employed to eliminate this trend. Second differencing amounts to taking the first differences of an already differenced series because the differenced series is nonstationary also.

Although transformation to induce stationarity is usually effective, it may only result in local periods of stationarity. Therefore a second method for insuring stationarity is often employed. This method seeks to limit the sample size to the extent that the sample under consideration is stationary.

For example, the assumption that the change in mean is linear may only be valid for a limited time interval at which point a new mean must be computed. Thus the time series as a whole can be nonstationary but individual

segments of the series, with the appropriate transformation, can be considered stationary.

To implement this method of stationarity control requires the discussion of a moving window. A moving window is a segmentation device used to split a large nonstationary time series into a finite set of stationary subseries. According to Cohen, the simplest device is to divide the series into segments of a constant length although more complicated adaptive segmentation techniques can be employed (3:101-102).

The choice of window length is a tradeoff between stationarity considerations and accuracy of spectral estimation. For instance, as the window length is increased, lower frequencies can be estimated but at the expense of decreasing stationarity. Window sizes of 1000, 750, 500, 400, 300 and 250 observations were considered. A representative sample was taken and an attempt at model fitting was made. The best model fitting occurred using a window of 250 observations and was therefore chosen for this analysis. This equates to a window length of 250/60 Hz or 4.167 seconds. This size window allowed spectral estimation down to .24 Hz, within the frequency range as measured by Chelen (4:5), and also satisfied the stationarity assumptions quite well.

Once the appropriate transformation and window size were found, three fundamental time series and spectral analysis methods were applied to the data. They were the sample autocorrelation function, sample partial autocorrelation function and the periodogram.

Sample Autocorrelation Function. The sample autocorrelation function (ACF) is the correlation coefficient between pairs of values of a stationary time series X(t) that are separated by a time lag k (13:107). Mathematically, the ACF is defined for each lag k as:

$$r_k = \frac{\Sigma(x_t - \overline{x})(x_{t+k} - \overline{x})}{\Sigma(x_t - \overline{x})^2} \qquad (6)$$

where $\overline{x}$ is the sample mean of the stationary series. Because r_k is a correlation coefficient, it is restricted to the interval: $-1 < r_k < 1$.

The ACF can be thought of as a measurement of the linear relationship between points of a time series separated by constant time lags. Typically lags of order 25 or less are computed and plotted as is true in this thesis.

Large positive values of r_k imply that observations separated by k time units are positively correlated and tend to move together in a linear relationship. Large negative values of r_k imply observations separated by k time lags are negatively correlated and move together in an opposite direction. Because the values of the ACF decrease as k

increases, the ACF also reflects the amount of "memory" there is in the process under study. In other words, for an autoregressive process, the dependence of future observations on past observations will decrease as the distance between the observations increases. The greater the number of significant lags, the more memory there is in the process. Further properties of the ACF can be found in Priestley (13:108-110).

Examination of the behavior of the ACF can be used to determine the subtle relationships contained in the data and suggest possible model structure. To illustrate this idea, consider the previous nonstationary time series whose values are increasing linearly with time. It is obvious that each successive observation is linearly dependent on the previous one as was the one before it and so on. Thus the autocorrelation function would have a value close to one at lag 1 and would die down slowly at increasing lags but would remain significant even at very large lags.

This behavior can be seen in the plot of the ACF for this nonstationary time series as in Figure 3. As discussed earlier, a time series that exhibits a linear trend is not a stationary process because the mean is increasing. Thus the ACF can also be used to determine if a series is stationary or not. Use of the ACF for model fitting will be discussed later.

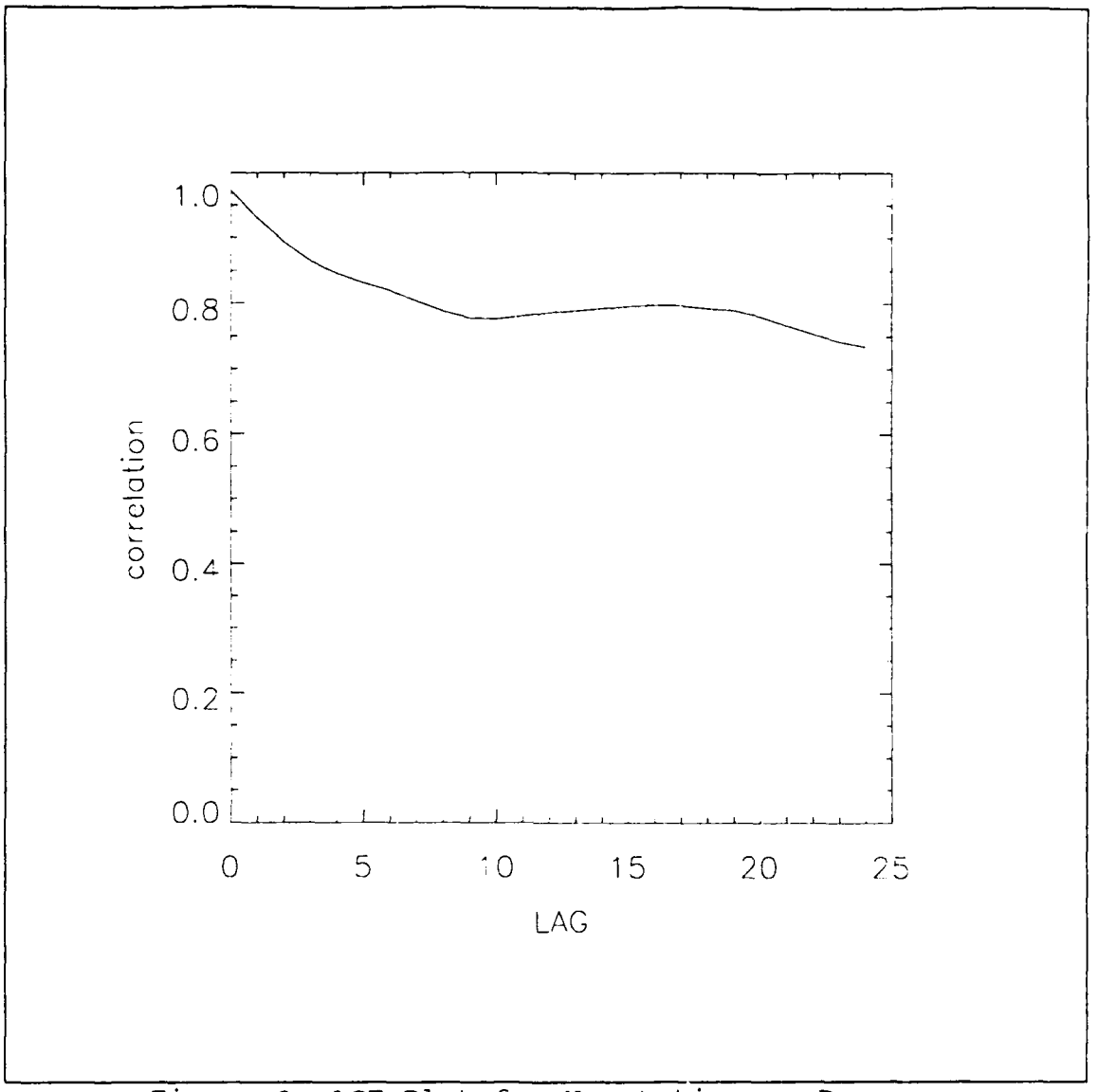

Figure 3. ACF Plot for Nonstationary Process

Sample Partial Autocorrelation Function. The sample partial autocorrelation function (PACF) is also used as an aid in model determination. It is defined as the autocorrelation of the stationary time series values at lag k with the effects of the intervening observations

eliminated (1:43). The PACF can be found by solving the set of Yule-Walker linear equations of lagged autocorrelations (2:64). As was the case with the ACF, the PACF is computed for successive lags and are plotted for interpretation. The PACF is useful in determining the order of the autoregressive process in an ARIMA model as will be discussed next.

Time Domain Modeling. The ACF and PACF are typically the principal tools used to determine the nature of the model that describes the process that has been sampled. The ARIMA model, for Autoregressive Integrated Moving Average is a forecasting technique that fits significant behavior in the ACF and PACF in order to model the underlying structure contained within the data (2:174-178).

An ARIMA model contains autoregressive (AR) and moving average (MA) operators. Assuming a stationary series Z(t), the model takes the following mathematical form:

$$\phi_p(B) z_t = \delta + \theta_q(B) a_t \qquad (7)$$

where $\phi(B)$ and $\Theta(B)$ are polynomials of the backshift operator and δ is a constant term. The backshift operator (B), operates on the succeeding variable by reducing its subscript by the order of the polynomial term.

The process of model fitting begins with an interpretation of the ACF and PACF to determine the type and order of the model. After a tentative identification has

been made, the appropriate parameters are estimated. The model is uniquely determined by the set of estimated parameters (ϕ,θ).

An AR model of order p takes the form:

$$(1 - \phi_1 B - \phi_2 B^2 - \ldots - \phi_p B^p) z_t = \delta + a_t \qquad (8)$$

or

$$z_t = \delta + \phi_1 z_{t-1} + \phi_2 z_{t-2} + \ldots + \phi_p z_{t-p} + a_t \qquad (9)$$

This model expresses the current value of the series as a linear function of previous values at lags up to the order of the model plus a random element, a_t. An AR model is usually indicated if the ACF shows signs of a mixture of exponential decay and damped sine waves while the PACF shows non-zero spikes at lags up to lag p and goes to zero after lag p.

The MA model of order q takes the form:

$$z_t = \delta + (1 - \theta_1 B - \theta_2 B^2 - \ldots - \theta_q B^q) a_t \qquad (10)$$

or

$$z_t = \delta + a_t - \theta_1 a_{t-1} - \theta_2 a_{t-2} - \ldots - \theta_q a_{t-q} \qquad (11)$$

This model expresses the current value of the series as a function of previous random elements up to order q. The MA model is indicated if the PACF shows signs of exponential decay and damped sinusoids while the ACF exhibits non-zero spikes at lags up to lag q and goes to zero after lag q.

A mixed ARMA model of order (p,q) contains both AR and MA terms. The basic form of the model was shown earlier in Equation 6. This model is usually indicated if both the ACF and PACF show signs of exponential decay.

A tentative model identification is made based on the rules already discussed. This model then acts as a filter and is passed through the data which results in a new time series containing the residuals of the model fit. The resulting ACF and PACF of the residuals are computed and analyzed for further significant behavior. The goal is for the residuals to be white noise for a model to be adopted. The reason for this is that the underlying assumption is that the sampled series was originally a white noise process that had been transformed by the linear filter of the model in question. If the series can be filtered back to a white noise process, then the correct model has been found (2:18).

Although the goal of much ARIMA modeling is the actual forecasts, direct interpretation of the ACF and PACF can be used to gain important insight to the process that gave rise to the sampled series. For instance, unknown seasonalities and periodicities within the data may turn up only by direct examination of the series using these tools. Thus to a limited extent the sample ACF and PACF can reflect changes in an underlying model without actually fitting a model to the data. This macroscopic viewpoint enables quick identification of model trends and changes if a succession of results from moving windows are observed.

This was accomplished by plotting the ACF and PACF of each window as a function of time. Because the behavior of

the ACF and PACF determine the nature of the model, any change in the underlying model will manifest itself as changes in one or both functions. Both regularities and irregularities across the windows can be highlighted. This method was tested on several random windows. Preliminary models were identified based on visual inspection of the ACF and PACF. A model was then fit and compared with the original model. The two models agreed closely enough that the visual inspection method was deemed adequate for use in model detection of large samples of data.

Frequency Domain Modeling. Another method for detecting model change is to analyze the data in the frequency domain. The underlying assumption is that a stationary series can be decomposed into the sum of sinusoids of the form (13:390) such that:

$$X_t = \Sigma\ A_i \cos(w_i t + \phi_i) \qquad (12)$$

where the ϕ_i are phase shifts randomly distributed on the interval $(-\pi,\pi)$, A_i are the amplitudes, and the w_i are the frequencies of the model that need to be estimated. Since these frequencies are usually unknown, they must be estimated by means of a periodogram.

The periodogram is a search technique that estimates the squared amplitudes of the sinusoids at a specified, discrete set of frequencies. These frequencies correspond to harmonics of the fundamental frequency $w_f = 2\pi/n$ where n is

the number of observations. The periodogram then is the plot of the squared amplitudes of the frequencies defined by:

$$w_i = 2\pi i/n \quad i=0,1,2,\ldots,n/2 \tag{13}$$

Hypothesis testing is used to determine the significance of each frequency. This is done by testing the value of the largest peak (13:406). Under the null hypothesis of no periodicities, that is all $A_i = 0$, the test statistic:

$$g = \frac{\max(I_i)}{\Sigma I_i} \tag{14}$$

where I_i are the computed ordinates of the periodogram, will be close to zero. A significant value of g invalidates H_o in favor of H_a that a periodicity does exist at the frequency given by the largest peak. The test can be repeated for subsequent smaller peaks by substituting in the next smaller value of I and summing over the remaining frequencies. Thus the underlying frequencies of the periodicities can be found. Just as the parameters of an ARIMA model determine the nature of the model in the time domain, so do the harmonics contained in the periodogram define the series in the frequency domain.

The periodogram can also be viewed as an estimate of the series' spectral density function (SDF). The SDF is a measure of the distribution of power over a range of discrete frequencies. Because the normalized SDF is the Fourier transform of the ACF (13:216), changes in this

function should reflect similar changes in the time domain model. The periodogram can therefore be used as an aid in confirming the significance of model changes that were found using time domain modeling techniques and representing them from another perspective.

Image Processing

The display of a typical windowed ACF, PACF or periodogram resulted in a surface plot of between 2000 and 56000 points. The reason for this large amount of data lies in the windowed nature of the function. For example, the windowed sample autocorrelation function (WACF) is a two dimensional matrix that is formed by stacking the ACFs over time for each window as a row in the matrix. Each row contains the computed correlations for that window. Each column represents the set of lags computed across all the windows. Thus an n x k matrix is formed that is n windows by k (25) lags in dimension. The entries in the matrix represent the kth lagged correlation within the nth computed window in the sample.

This matrix can then be plotted to observe the subtle changes that occur over time. The resultant plot of the data represents the surface that is formed by the intersection of the correlations with each other and across the windows over time. Figure 4 shows an example of an ACF surface plot. This

method of display allows interpretation of the relationships among the windows as they change over time. The disadvantage of this method comes about because of the amount of information that can be obscured from the viewer because of the 3-dimensional nature of the plot. A 2-dimensional analog to this display is needed in order to view all the windows at once without obscuring any of the data. This was accomplished by converting the surface plot into an image.

The method was to turn a two dimensional data array into a displayable image file. Each two dimensional array contained values that were normalized and revalued according to a 256 level scale. These values correspond to the 256 shades of gray supported by the display and printing algorithms. The result is a two dimensional gray scale image that contains the same information as the three dimensional surface plot. Because the resulting image is two dimensional as opposed to the plot, data are not obscured and all the windows of the series can be interpreted simultaneously.

A sample ACF image is shown in Figure 5. The image is the result of stacking successive windows of independent sample autocorrelation functions. The horizontal axis gives the lag number with increasing lags from left to right. The left vertical axis corresponds to the window number of the sampled series with increasing numbers (time) going up. The right vertical axis gives the subject reported symptom level

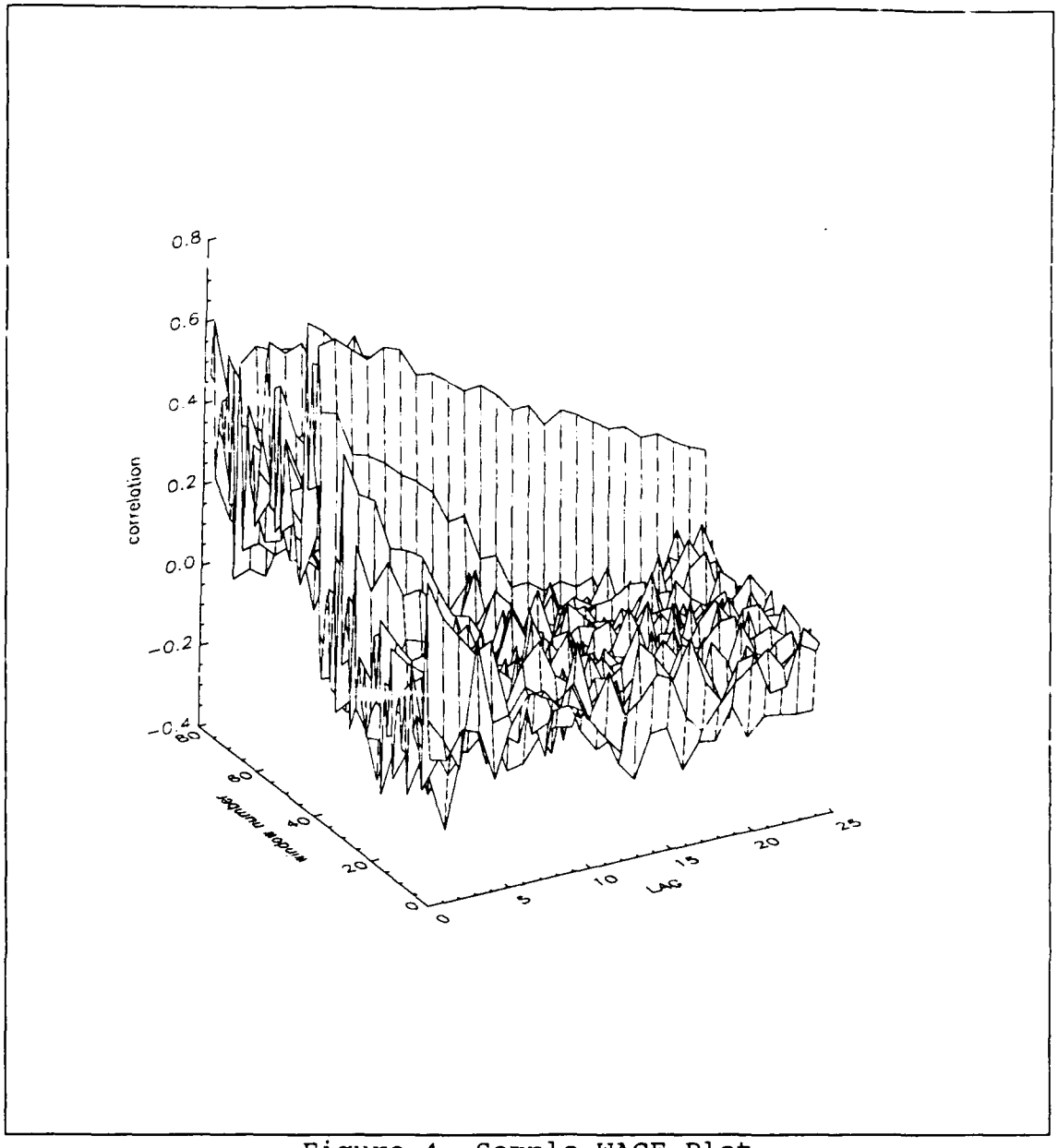

Figure 4. Sample WACF Plot

(SSL) for comparison of model effects with symptom onset. Thus the lower left corner pixel gives the lag 1 correlation for the first window corresponding to the subjects' asymptomatic level. Likewise the upper right pixel gives the

value of the lag 25 correlation for the final window corresponding to frank sickness (emesis).

This image contains the same data as displayed in Figure 4. By comparison of the two, it can be seen that the darker regions of the image correspond to negative correlation levels and the whiter areas correspond to positive levels of correlation. The shade of the white or dark pixel is an indication of the absolute value of the correlation level. For instance, darker pixel values indicate a more negatively correlated series whereas the whiter pixel values indicate a more positively correlated time series.

Interpretation of these images is straightforward. The problem is simply a matter of pattern recognition. Significant behavior manifests itself in the form of striations. The goal then is to highlight the striations that are regularities in the underlying model and those that might appear as artifacts if viewed singly. The more intense the shade of the striation, the more significant the effect. These striations can be either vertical or horizontal. Vertical striations indicate continuing correlation among one lag throughout several windows in time. This is indicative of a long duration periodicity within the data. Horizontal striations give an indication as to the degree of memory in the process or stationarity of the data. In other

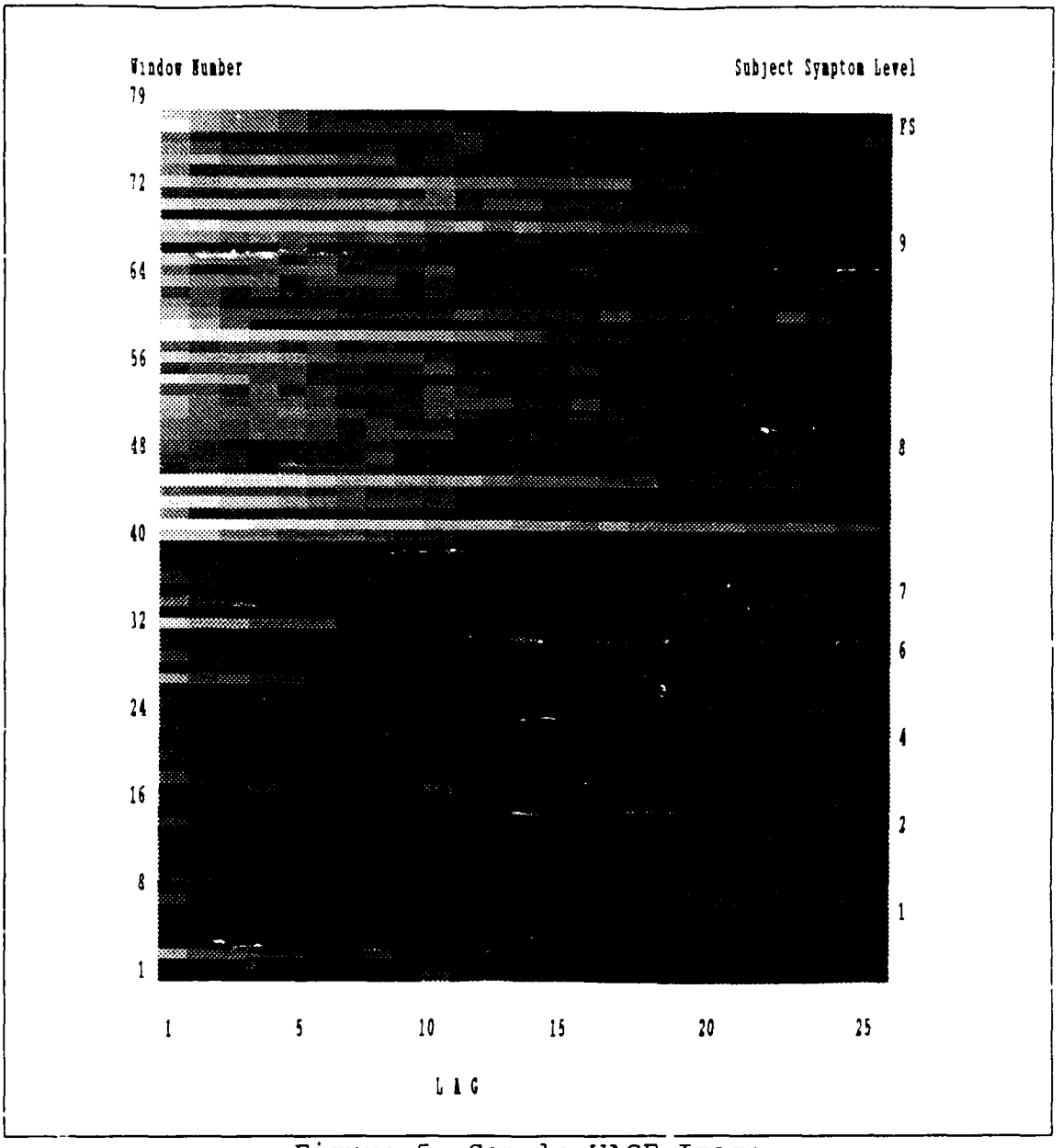

Figure 5. Sample WACF Image

words, as the length of the horizontal striation increases, higher and higher order lags remain significantly correlated. This behavior is valid for that window only,

however, should it persist, it may be an indication of a model change or shift from periodic to nonperiodic behavior.

To illustrate these ideas, again consider Figure 5. There appear to be two regions of correlation behavior. The windows 39 and below show no significant behavior and would suggest a possible white noise process. Windows 40 and above show signs of an abrupt model change in which the process has a significant amount of memory as lags up to 10 appear significant. This would indicate either an autoregressive model or possible nonstationarity of the data. The behavior can also be seen somewhat in Figure 4. but is less dramatic than the image presentation. Furthermore, the true degree of variability in the overall pattern is lost.

The relationship between correlation and image can be seen further in Figure 6. Figure 6a is a plot of lag 1 for each of the 79 windows of the series. Comparing this to previously discussed behavior of Figure 5 illustrates how the correlation values increase with increasing whiteness of the image pixel. Figure 6b graphically illustrates the change in correlation and possible model change that occurs between time windows 39 and 40.

Because the image is superior for use in structure interpretation, only the image will be provided for the time domain functions. The previous images will now be defined as the windowed sample autocorrelation function (WACF) and the

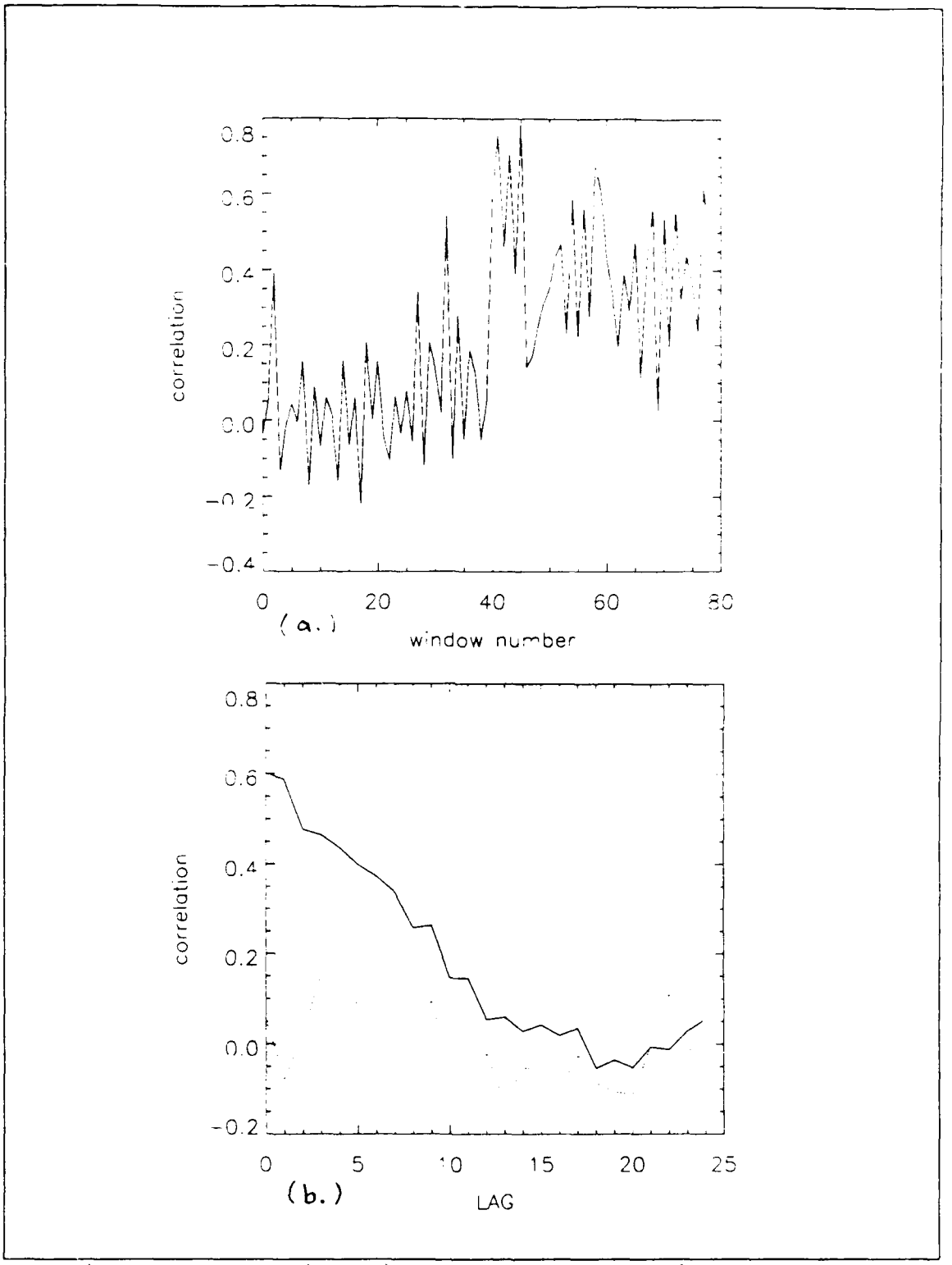

Figure 6. Relationship Between Correlation and Image

windowed sample partial autocorrelation function (WPACF). The reason for this distinction is to further stress the idea that the image is the direct result of the stacking of their respective functions from successive windows in time.

The windowed periodogram will still be discussed but is not presented as an image. The image technique was not as useful in this case due to the much larger range of amplitudes allowed. Imaging is at its best when the levels to be imaged are relatively consistent in relative level. (Remember the ACF and PACF are limited to between plus and minus one.) Techniques such as "stretching" can be used to highlight specific aspects of the periodogram. Stretching limits the number of grey scales to an interval where unique aspects can be seen. All behavior that occurs outside this interval is then effectively blacked-out thereby limiting its usefulness to strictly highlighting and not interpretation. This technique was not employed here, rather the images are all presented in their pristine form with all 256 levels allowed.

Multivariate Time Series

Multivariate time series deals with the interactions that may exist between two or more related time series. To model the effects one time series has on another requires the use of a transfer model. A transfer model predicts

future values of a dependent time series based on past values of both the dependent and independent time series (1;343).

The device used to establish the linear relationships that exist between two stationary time series is the sample cross-correlation function (CCF) (1:351). Consider a dependent time series Y_t and an independent time series X_t that is hypothesized to have a causal relationship with series Y_t. The CCF measures the linear relationship between Y_t and X_{t+k} for each lag k. This is represented mathematically as:

$$r_k = \frac{\Sigma(y_t - \overline{y})(x_{t+k} - \overline{x})}{[\Sigma(y_t - \overline{y})^2]^{1/2}[\Sigma(x_t - \overline{x})^2]^{1/2}} \qquad (7)$$

where $\overline{x}$ and $\overline{y}$ are the respective series' means.

The CCF is then a plot or listing of the computed lags as was the case with the ACF. But unlike the ACF, the CCF plots the 2k+1 values -k, -k+1, -k+2,...,-1,0,1,..., k-2, k-1, k. The reason for the negative lags is that both feed-forward and feedback relationships can exist between the two series. Significant positive lags imply that series Y is related to past values of series X at the significant lag. Significant negative lag values imply that series X is related to past values of series Y at the corresponding lag.

Should the original hypothesis be true, only positive lags will be significant indicating a feed-forward

relationship from series X to series Y. Negative lags negate the null hypothesis in favor of the alternate hypothesis that a feedback relationship exists from series Y to series X. The presence of both positive and negative lags would imply that both a feed-forward and feedback relationship exists. Thus direct interpretation of the CCF can be used to gain insight into the relationships that exist between the two time series and how these relationships change over time.

When fitting transfers functions, the output series is typically prewhitened by the input series and the input series similarly whitened. This is ordinarily done to minimize correlations that result due to the "unwhitened" effects of the input series. These effects are of interest in this research as they give an indication as to the significance of any feed-forward feedback relationships that are indicated by striations in the resulting image. Thus the CCF is computed given the original stationary series.

As was the case with the univariate functions, the CCF is also displayed as an image. The same windowing technique is used and the CCFs are similarly stacked over time. Therefore the WCCF is the image representation of the windowed cross-correlation function used to interpret the multivariate relationships.

IV. Results

The results chapter will be presented in four sections. The first section covers the interpretations of the univariate time series associated with the placebo trial of the primary subject. Section two covers the interpretations of the univariate time series associated with the Dilantin trial of the primary subject. Section three contains the interpretations of the multivariate time series associated with the brain data for the placebo trial. The final section contains the analysis for the additional two subjects.

Univariate Analysis of Placebo Treatment

Four physiological channels were analyzed for the placebo trial. They were four of the five brain channels (EEG1A, EEG1B, EEG2A, EEG2B). Channel EEG1C data were not collected due to equipment trouble. The analysis and figures follow for the first case, channel EEG1A. For each subsequent channel, the analysis follows but its related plots and images can be found in the Appendix. All plots and figures are referenced by figure number.

The placebo trial lasted approximately 6 minutes from the beginning of head motions to frank sickness (emesis). The run is summarized below in Table I. The SSL is the subject symptom level that relates the subjective condition of the subject. Major symptoms are noted as well as the time

of occurrence. All data are referenced to the applicable sample window to which it is associated with.

Table I Summary of Placebo Trial

Time(SEC)	SSL	Window #	Symptoms
0	ASYM	1	NONE
20	1	4.8	NONE
50	2	12	Queasy stomach
90	4	21.6	Increased queasiness
120	6	28.8	SAME
150	7	36	Starting to sweat
200	8	48	SAME
270	9	64.8	Stomach churning
330	FS	76.8	Emesis

EEG1A (Midline Frontal). The raw data are given as the top plot in Figure 7. Note the dramatic change in the amplitude and variance of the data approximately 171 seconds into the experiment. This is indicative of a possible model change. Although difficult to tell from the plot, the raw data do not have a constant mean. First differencing is applied to the data and the resulting stationary series is displayed at the bottom in Figure 7. It can be seen that this series is stationary about zero. It is this differenced series that the analysis is conducted.

Analysis of the WACF image shown in Figure 8 confirms the presence of two distinct model regions. The WACF for windows 1-40 individually show little significant behavior and are indicative of a white noise process. Windows 41-79 show significant positive correlations among lags 1-10 that

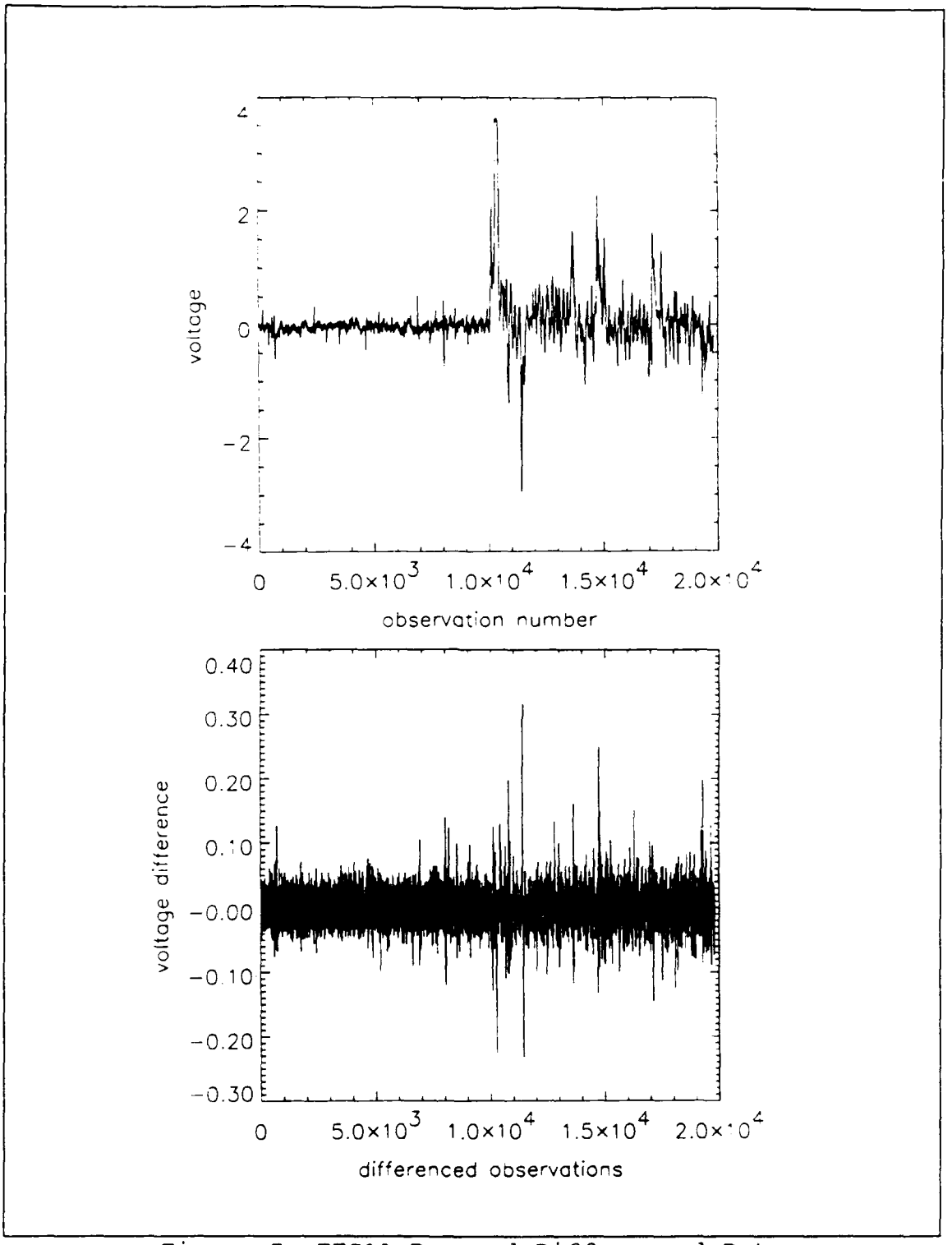

Figure 7. EEG1A Raw and Differenced Data

persist for the duration of the experiment, indicating a transition towards nonstationarity or the development of an autoregressive process.

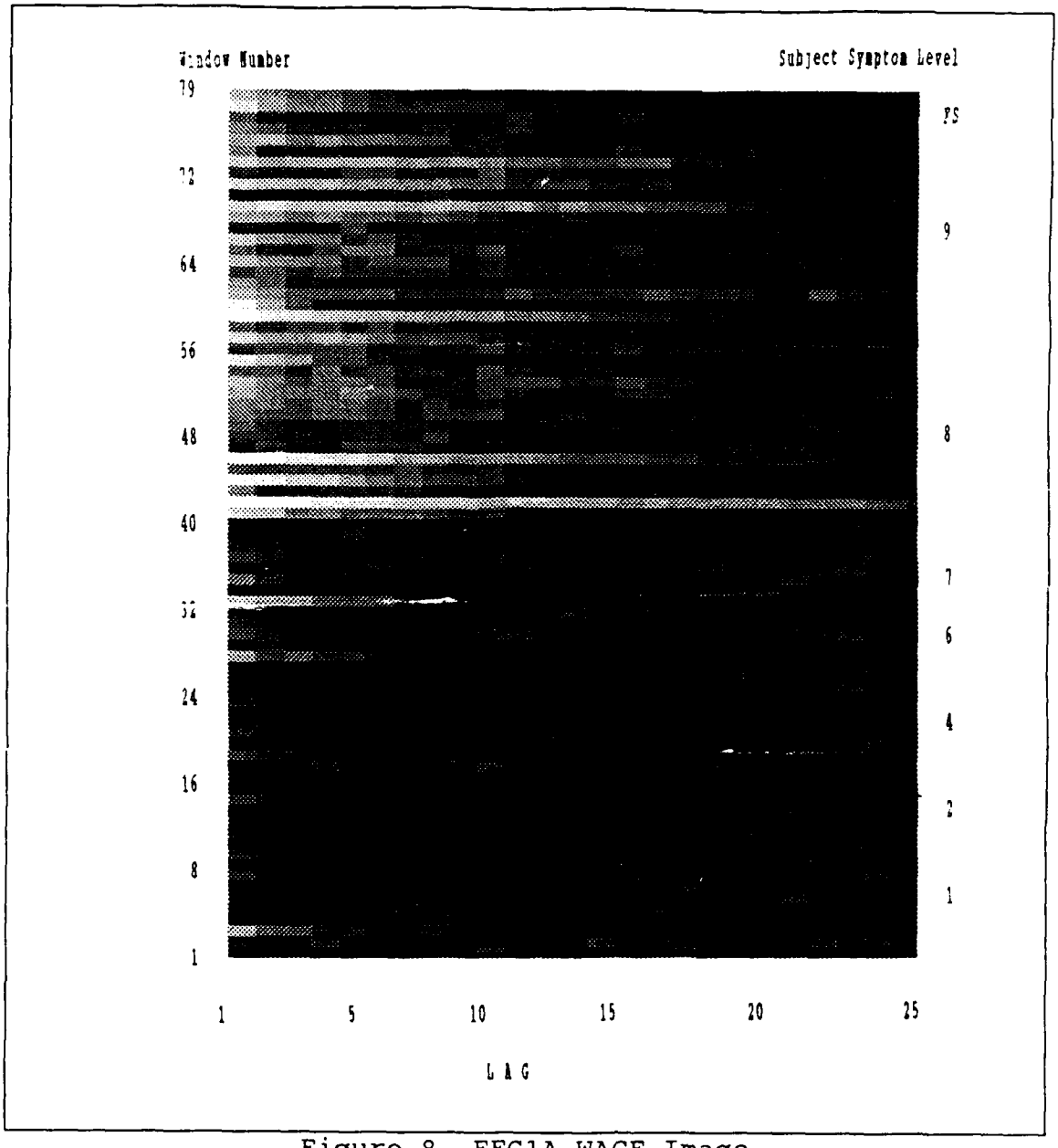

Figure 8. EEG1A WACF Image

This behavior is consistent with that found in the WPACF image as pictured in Figure 9. Although the general shape of the WPACF remains the same throughout the experiment, the lag 1 correlation values follow the pattern set by the WACF. Windows 40 and below exhibit behavior consistent with a white noise process while windows 41 and above are dramatically more positively correlated and indicate an autoregressive order 1 process AR(1). Lags 2 through 5 also appear to be more positively correlated following window 41 and may indicate a higher order AR model.

Thus it can be seen that the underlying process has undergone an abrupt model change during window 41. This occurs approximately 171 seconds into the trial and corresponds to the point midway between SSL 7 and 8.

A vertical inspection of the WACF and WPACF images highlights a mild periodicity at lag 10. Because one lag represents 60^{-1} sec, a lag 10 relationship corresponds to a a period of 1/6 sec or a frequency of 6 Hz. (Because the sampling rate is constant throughout the analysis, this relationship will always hold.)

The frequency of 6 Hz represents the midrange of the theta wave activity of the brain, usually 3-8 Hz (4). Theta waves are normally produced by the brain with increased production of these waves usually associated with a slowdown

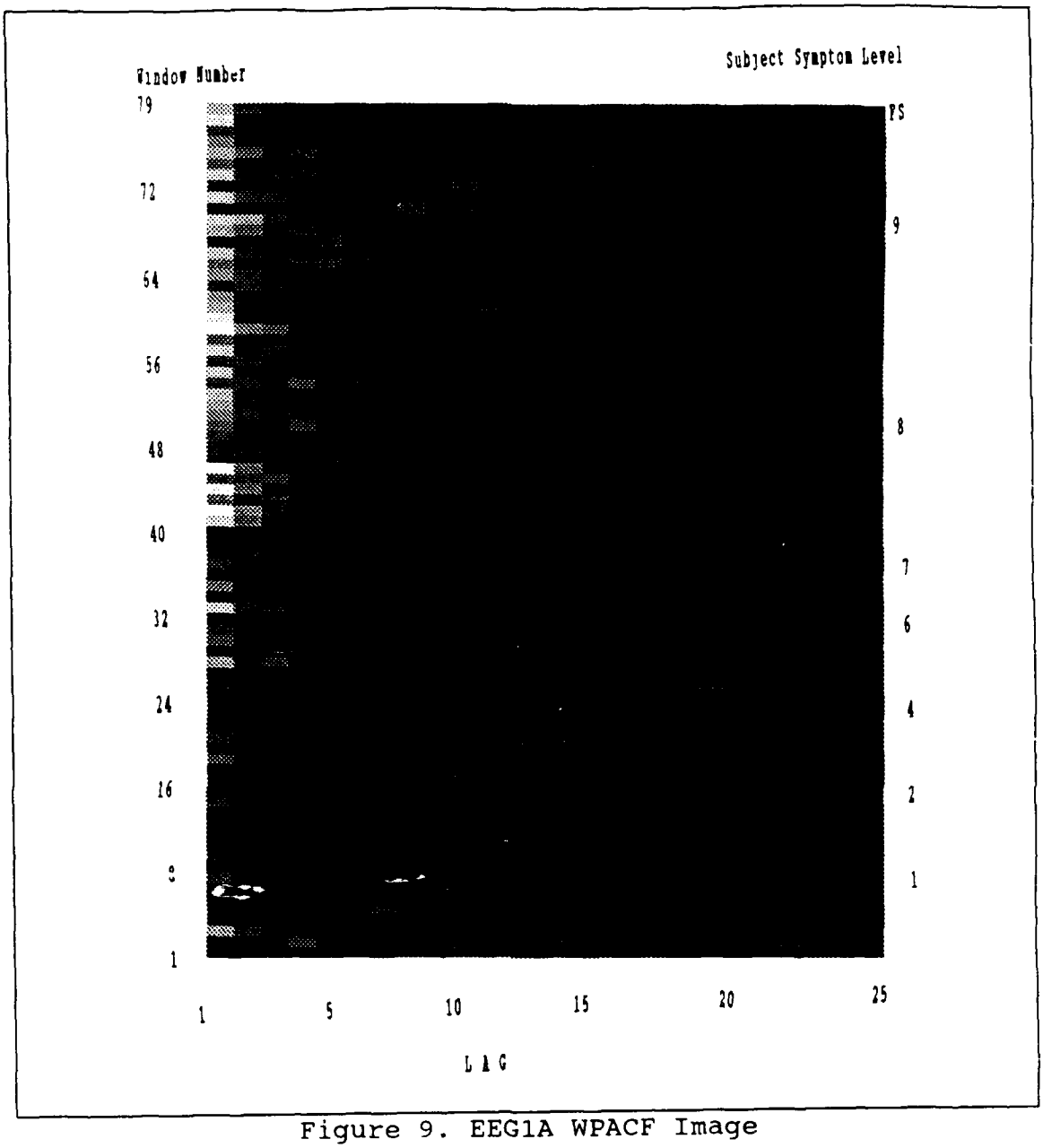

Figure 9. EEG1A WPACF Image

of the brain (4). For example, theta waves increase as the brain enters the sleep state. Note the striation appears in both the WACF and WPACF but is more predominant in the WACF. Also note that the striation becomes more positively

correlated as time goes on. This could indicate a strengthening of the signal accompanied by a subsequent increase in theta wave production and a resulting slowdown in brain activity.

The presence of a model change at window 41 is confirmed by analysis in both the frequency domain and the raw data. The periodogram plot for EEG1A is given in Figure 10. The plot shows the varying nature of the frequency distribution as it changes over time. The x-axis plots the relative frequency with increasing ordinates representing increasing harmonics of the fundamental frequency. The y-axis plots the window number with increasing ordinates representing the experiment elapsed time (each window is 4.167 sec). The z-axis plots the squared amplitude of the normalized frequency.

The periodogram shows a dramatic shift in low frequency power corresponding in time with the model change in the time domain. Windows 1-40 show a flat spectrum indicating no periodic elements are present. Tests on the significance of the highest peaks in these windows fail to reject H_o that no periodicities exist. Windows 41 and up, however, display a significant shift in power to frequencies between .24-1.2 Hz with correspondingly large amplitudes. Tests on these peaks yield significant values and it is concluded that low frequency high amplitude periodicities do exist.

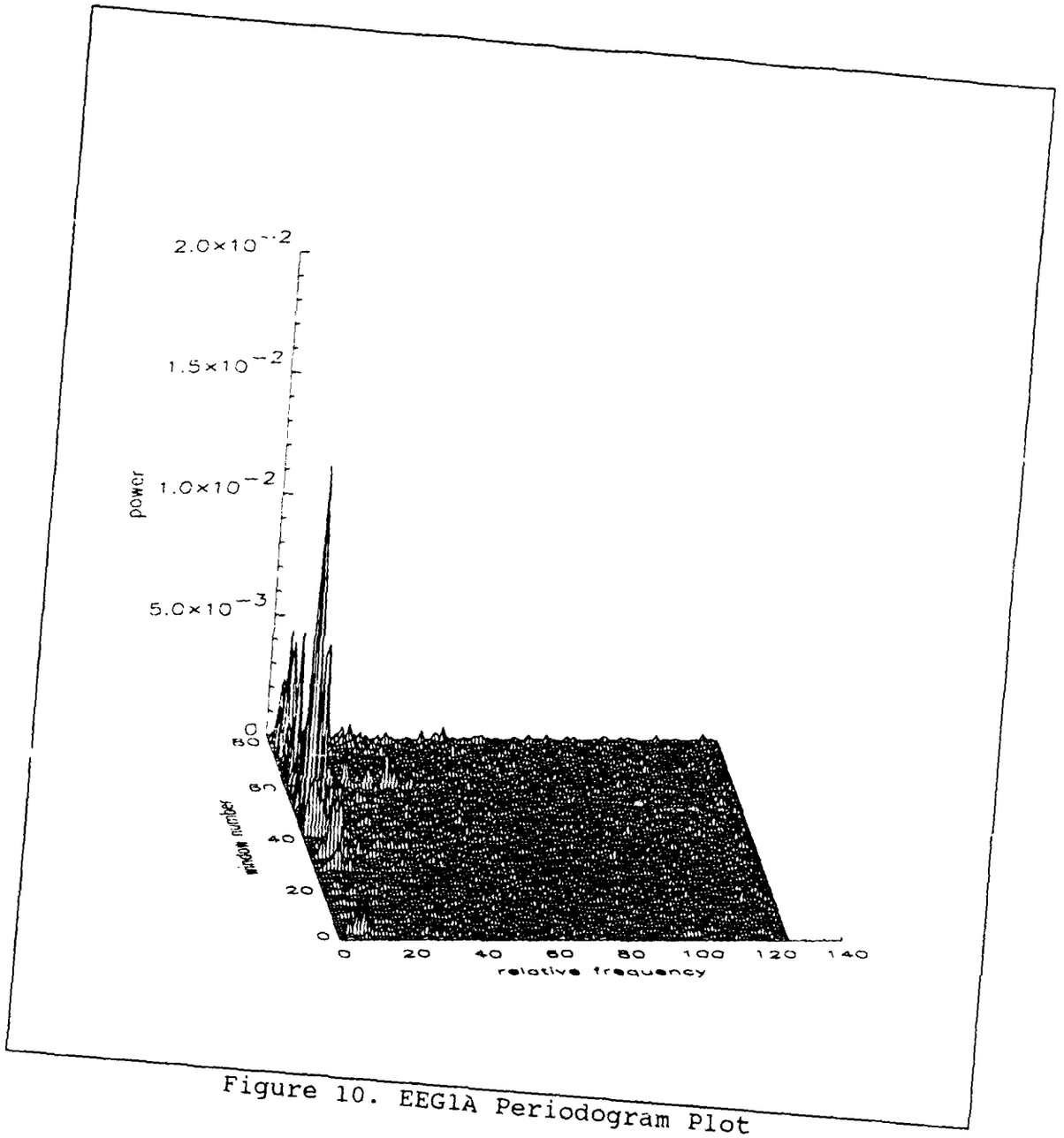

Figure 10. EEG1A Periodogram Plot

The absence of a periodicity at frequency 25 (6 Hz) can be seen in Figure 10. This would correspond to the weak periodicity noted in the WACF and WPACF images. Because the periodicity was weak to begin with and without confirming

evidence in the periodogram, it is concluded that the lag 10 periodicity may not be a true one. This serves to illustrate the power of the time domain imaging technique since very weak harmonics can still be identified and highlighted.

EEG1B (Midline Parietal). The data for EEG1B were also nonstationary and first differences were used to produce local stationarity. The plot of the observations and differenced data can be found in Figure 11 in the Appendix. Looking at the raw data, there does not appear to be an abrupt model change as was present in channel EEG1A. The dominant characteristic of this data are the several areas of motion artifact that can be seen between observations 15000 and 20000. This is especially noticeable in the plot of the differenced data. The artifact is caused by extreme motions of the head and results in abnormally large voltages. These false voltages appear in the WACF plot as a light horizontal striation that has a width equal to the time duration of the artifact and usually does not repeat itself.

The EEG1B WACF in Figure 12 also shows signs of four strong motion artifacts. The location of the striations correspond to the four noticeable artifacts as seen in Figure 11. Note that the duration of the artifact corresponds to the width of the striation and appear to increase in duration as the experiment progresses. The first

artifact at window 44 has a duration of one window, the second is at windows 54-55 and the third covers windows 60-62. The final artifact occurs at windows 69-73 has a duration of about 1100 observations and the corresponding striation appears five windows wide.

Strong evidence of periodic behavior is noted in the four wide vertical striations. They are centered around lags 5, 10, 15 and 20 and indicate a possible seasonal model of order 5. This corresponds to a periodicity of 12 Hz that may be correlated to normal brain activity. The 12 Hz signal is indicative of an alpha wave. The striations appear to be strengthening over time. As the eye averages these striations across all the windows, a pattern is suggested. The pattern suggests increasing strength of the periodicity and its harmonics over time.

The WPACF displays similar behavior and is given in Figure 13. The same periodicities are present but not as well-defined early on as in the WACF. The striations do strengthen and increase in definition as the window number increases. As was the case with the WACF, no indications of an abrupt model change are present. In conjunction with the WACF it appears the underlying model is either white noise or a weak AR(1) process with a definite seasonal operator at lag 5. The seasonal model increases in strength over time and may approach nonstationarity at the seasonal level. Thus

it appears the model is changing at the seasonal level. This change appears as gradual increase in correlation of the harmonics of lag 5. Because the change is gradual, no break point can be determined between the sick and well models as was the case in channel EEG1A. Thus motion sickness appears to affect thic brain channel by altering the seasonal behavior of the data.

The periodogram as given in Figure 14 does not appear to display a power distribution shift similar to that seen in channel EEG1A. Four regions of low frequency power shifts can be seen but are not representative of the seizure discussed earlier. The shifts are not limited to the same low bandwidth (.24-1.20 Hz) and appear only in those windows containing high motion artifact. A vertical ridge can be seen across frequencies 46-47. Tests confirm the significance of this periodicity that correspond to a frequency of approximately 11 Hz. This confirms the periodicity noted in the WACF and WPACF. The amplitude of this periodicity appears to increase over time as the ridge increases in height as the window number increases. This confirms the strengthening of the periodicity associated with the model change.

Thus it is concluded that this channel does not exhibit an abrupt model change but instead exhibits a gradual increase in the strength of its seasonal component. The

significant periodicity associated with the seasonal behavior may be attributable to increased midrange alpha wave activity.

EEG2A (Left Temporal). This is an incomplete channel because the data were lost following the 56th window due to equipment failure. The raw and differenced data are given in Figure 15. A model change may have occurred around observation 11000 (window 44). The signal appears to have a lower frequency than the previous observations as seen in the EEG1A data. This is difficult to determine because of the presence of motion artifact. The situation is made even more difficult by the presence of a clipped signal over the last 600 observations as the sensor output peaked prior to its failure. Thus the final two or three windows may be invalidated due to sensor malfunction.

The WACF is given in Figure 16. With the exception of the final three windows, the WACF remains unchanged. Windows 48, 45, 41 and 39 show signs of motion artifact. The periodicity seen in EEG1B is also present here and is centered on multiples of 5.5 lags. This corresponds to the same 11 Hz frequency as seen earlier. The strength of this activity appears remain constant.

Figure 17 contains the WPACF and supports the analysis of the WACF. A strong positive correlation at lag 1 appears and increases over time as does a negative correlation at

lag 2. This pattern remains unchanged and is indicative of either an AR(1) or AR(2) process. The same periodicities can be found as in the WACF but are less well-defined.

The periodogram given in Figure 18 confirms the analysis of the time domain. No model change is indicated prior to window 52 where the sensor output becomes suspect. The only significant peak prior to this occurs along the ridge centered on frequency 46. This is a frequency of 11 Hz and confirms the presence of a significant periodicity within the alpha wave region of normal brain activity.

EEG2B (Bilateral Frontal). The raw and differenced data are given in Figure 19. Two model regions are obvious in the raw data plot. A motion artifact can be seen between observations 11000 and 12000.

The WACF and WPACF given in Figures 20 and 21 exhibit behavior nearly identical to that previously seen in the EEG1A data. A dramatic model change occurs at window 46 in the WACF and is characterized by significant positive correlations among lags 1 through 10. A faint periodicity can be seen at lags 10 and 11 that increase in strength after window 46. A lag 10 periodicity is a frequency of 6 Hz which is in the midrange of theta wave production of normal brain activity.

The WPACF is characterized by both a strong positively correlated lag 1 and negatively correlated lag 2 prior to

the model change. Window 46 and subsequent windows indicate much higher correlated lag 1 values and associated shift in lag 2 to positive correlations. This can be interpreted as shift from an AR(1) model to a nonstationarity that must be second differenced to re-introduce stationarity. The lag 10 periodicity is present but faint.

Figure 22 shows the shift towards the high amplitude, low frequency pericdicities seen in the later windows of the periodogram. This point corresponds to the change seen in the time domain model at window 46. The 6 Hz periodicity is not supported by the periodogram. No noticeable ridge occurs at frequency 25 (corresponding to 6 Hz). Furthermore, no periodicities are significant (all A_i are zero) prior to the model change at window 46.

In summary, four of the five brain channels were analyzed for the placebo trial. One of these channels remained unchanged while the other three channels can be described as being driven by more than one independent process. Two types of model change were found.

The first type has a well model that is characterized by few significant correlations usually at lags 2 or less and a periodogram with no significant periodicities. This will be called the pre-sickness model. The post-sickness model is characterized by significant correlations at much

higher lags and a shift in the periodogram towards high amplitude, low frequency components.

This behavior has been previously described as a seizure equivalent and is usually indicative of the terminal phase of motion sickness (4:8). The seizure can be seen to be a nonlocalized event because its movement can be traced throughout the brain by observing its occurrence among the five brain channels.

The seizure appears to begin in the frontal cortex and propagates through the brain in a counter-clockwise direction. A definite time lag for the propagation can be measured between the appearance in one brain channel to the appearance in the next. These movements and lags are summarized in Table II. The seizure was confirmed for channels EEG1A and EEG2B. Channel EEG2A was included for comparison only since confirmation of the seizure could not be made, however, the presence of a model change was indicated in the data prior to sensor outage.

Table II Propagation of Seizure Signal-Placebo Trial

Channel	Location	Time(SEC)	Lag(SEC)
EEG1A	Midline Frontal Cortex	171	0
EEG2B	Bilateral Frontal Lobe	192	21
EEG2A	Left Temporal Lobe	217 (?)	25 (?)

The second type of model change was not as abrupt. Motion sickness can also manifest itself as a gradual change in the seasonal components of the model. Both pre-sickness and post-sickness models are fit with a seasonal model. It is the strength or the seasonal periodicities that changes as a result of the stimulus in the experiment. Because this change occurs over time, a clear division between the two cannot be determined as seen in the other channels.

It appears the motion sickness generator may be resident within the frontal cortex in this subject and has, as its primary output, a low frequency seizure equivalent that does not remain localized. The results of this seizure are the symptoms normally attributable to motion sickness (4:8).

Univariate Analysis of Dilantin Treatment

The Dilantin treatment was analyzed to determine what effect the anticonvulsant has on suppressing the seizure noted during the placebo trial. This trial lasted approximately 14 minutes, a 233% improvement in performance attributable to the drug treatment. Table III gives a summary of the experiment including symptoms and subject sickness level and is followed by the analysis of the four brain channels. Channel EEG1C was not collected because of an equipment malfunction.

Table III Summary of Dilantin Trial

Time(SEC)	SSL	Window #	Symptoms
0	ASYM	1	NONE
120	2	28.8	Queasy stomach
160	3	38.4	More queasiness
250	4	60	Cold feeling in legs
420	5	100.8	Sweating
840	FS	201.6	Emesis

EEG1A (Midline Frontal). The increase in trial duration results in a greater number of windows to analyze. This makes the analysis a little more difficult because to fit more windows within the same space, the windows are reduced in size. Thus the resultant pixel associated with each correlation value remains the same length but is proportionately smaller in height. The added benefit is that the additional data will tend to smooth the images and therefore highlight the more significant characteristics.

The raw and differenced data plots are given in Figure 23. There is an obvious model change approximately one-third of the way into the experiment. The change is characterized by high voltages with greater variance. The differenced data show three obvious areas of motion artifact around windows 24000 (window 96), 26000 (104) and 39000 (156).

The WACF and WPACF for are given in Figures 24 and 25 respectively. As indicated in the data plot, the WACF

exhibits signs of two distinct model regions. The first region, windows 1-69, shows no significant correlations. The second region consisting of windows 70 and up, appear to be driven by a new process characterized by high positive correlations up to lag 12. This occurs 292 seconds into the trial and corresponds to the point where the subject first reported a cold feeling in his legs. The WPACF similarly exhibits more highly correlated lag 1 values in windows 70 and up. A weak vertical striation appears centered on lag 6 (10 Hz) indicating a possible alpha wave class periodicity.

It appears the data were originally driven by a white noise process until the point of sickness where the model becomes either an AR(1) process or a nonstationary process that requires second differencing to correct. This behavior continues for the duration of the experiment.

The periodogram given in Figure 26 confirms the presence of two model regions. As seen previously, the three motion artifacts dominate the plot because of its high power and long spectrum. The unaffected windows exhibit the characteristic seizure spectrum of high amplitude periodicities among the frequencies .24-1.2 Hz. Note the time before model change increase from 171 to 292 seconds between the placebo and Dilantin trials, an increase of approximately 2 minutes. The presence of a 10 Hz periodicity

is not confirmed by the periodogram. The first significant peak does not occur until the model change at window 70.

EEG1B (Midline Parietal). The appearance of two model regions is obvious in the plot of the raw data in Figure 27. The change occurs approximately 266 seconds, or 16000 observations into the trial. The change is characterized by higher voltage signals with greater variance about a less constant mean. The differenced data highlight some possible motion artifact between observations 15000 and 30000.

The WACF given in Figure 28, however, is unique in that the second model region does not appear to continue throughout the trial. A model change is indicated at window 65, approximately 271 seconds into the trial, because of increasing correlations among lags 1-6. This behavior disappears at window 162, after a duration of 404 seconds, at which point the previous model regions' behavior resumes. A periodicity exists, centered on lags 5 and 6, that corresponds to the previously discussed alpha wave region. These signals appear to increase in strength with time.

The WPACF in Figure 29 is unremarkable and changes little over time. It is characterized by a strong positive correlated lag 1 and strong negatively correlated lag 2. No periodicities are indicated. In conjunction with the WACF, it appears the first region can be modeled by a low order AR model or white noise process. The second region is

characteristic of an AR model with more significant terms giving way to possible nonstationary behavior. The original model region then reappears following window 162.

The periodogram is given in Figure 30. The characteristic low frequency shift is present at window 65 coinciding with the model change in the time domain. The shift continues for the duration of the experiment. Although the peak of this signal occurs at lag 120, the subject was capable of continuing the experiment for another 80 windows reporting only mild symptoms before the rapid onset of emesis. The time before seizure onset also increased from 225 to 271 seconds. These effects can be attributed to the effects of the drug Dilantin.

EEG2A (Left Temporal). This channel was cut short approximately 6 minutes into the trial due to equipment failure. The raw data up to that point can be found in Figure 31. As can be seen there it is difficult to determine from the raw data alone, whether or not a model change has occurred prior to sensor failure.

Examination of the WACF given in Figure 32 indicates the presence of two possible model regions. A white noise or low order AR model is indicated in the windows 1-52. Windows 53 and above are characterized by strong positive correlations at lags up to 6 and beyond. An AR model or possible shift toward nonstationarity is indicated in these

windows. A vertical striation centered on lags 5 and 6 represents a periodicity of 11 Hz that appears to strengthen over time. The WPACF in Figure 33 is remarkable only for its consistency. It remains consistent with the idea that the underlying process is autoregressive in nature. The lag 2 correlation becomes less significant after the model change indicating a shift from an AR(2) to an AR(1) process. The 11 Hz periodicity is present and also appears to strengthen as the window number increases.

The periodogram given in Figure 34 shows the presence of the high amplitude, low frequency components indicative of the seizure equivalent discussed earlier. The presence of this signal from the outset of the trial is probably due to the anticonvulsant Dilantin. This was not a wholly unexpected result, since one of the effects of the drug is to stimulate the very signals that it attempts to keep under control (1). As long as this behavior remains localized and does not spread, the effects of motion sickness can be tolerated.

The peak power of the low frequency signals increases at the window in which the model change was noted in the time domain. This may be due to the added frequency shift normally seen coincident with the model change added to the alpha activity attributable to the effects of Dilantin. The

11 Hz periodicity is confirmed by the presence of a significant ridge at frequency 46 (11 Hz).

EEG2B (Bilateral Frontal). This channel also suffered a loss of data at approximately 6 minutes into the trial. The loss of these two critical channels plus the lack of data for channel EEG1C underscores the importance of reliable sensors on the successful interpretation of the results of the experiment. The raw and differenced data plots are given in Figure 35. Evidence of a model change can be found in the observations about halfway through the series. The data appear to decrease in frequency accompanied by an increase in variance about its mean.

In this case the WACF and WPACF given in Figures 36 and 37 respectively, are nearly identical in nature to those for channel EEG2A. The same analysis applies with the model change occurring in window 64. The now common 11 Hz periodicity is present in both the WACF and WPACF.

The periodogram as shown in Figure 38 exhibits the same high amplitude, low frequency components that are present from the outset of the experiment as was the case for EEG2A. The power associated with these signals does not remain constant, however, as Figure 39 illustrates. This is a plot of the first five harmonics of the periodogram plotted across all the windows. A slight linear trend indicates the power is increasing with time among the first five harmonics

of the periodogram. The 11 Hz periodicity is confirmed by the presence of a ridge at window 46 in the periodogram.

In summary, all four of the brain channels analyzed exhibited a significant model change indicative of a motion sickness-induced seizure equivalent. It is interesting to note that they are the same three channels that exhibited this behavior in the placebo trial.

The effects of Dilantin were readily apparent as the time before emesis was increased substantially and time before model change increased an average of 67 seconds. Furthermore, two channels contained from the outset, those frequency components usually associated with the onset of motion sickness. The power levels of these components were much smaller than those previously seen in the placebo trial. These components are due to the effects of Dilantin that slow other brain patterns down into the delta and sub-delta region (3). Once again, the seizure can be t acked by following its appearance in the affected channels. Table IV summarizes the path by affected area, time of occurrence and lag between occurrences. The seizure appears to move clockwise beginning in the left temporal lobe and ending in the midline frontal cortex region. This migration takes approximately 71 seconds.

It is interesting to note that the direction of propagation of this signal is the opposite direction to

Table IV Propagation of Seizure Signal-Dilantin Trial

Channel	Location	Time (sec)	Lag (sec)
EEG2A	Left Temporal Lobe	221	0
EEG2B	Bilateral Frontal Lobe	267	46
EEG1B	Midline Parietal Lobe	271	4
EEG1A	Midline Frontal Cortex	292	25

that seen in the placebo trial. No explanation for this behavior can be found because both trials were spun at the same rate and both were spun counter-clockwise.

Multivariate Analysis

The multivariate analysis was employed using the placebo data to confirm the hypothesis that the seizure originates in the frontal cortex and spreads from there. Should this be true, the WCCF would indicate a high correlation between the two affected channels at the point of signal transfer. The WCCF was computed for the six combinations of the four brain channels taken two at a time. The results were surprising.

During the analysis of the WCCF, a new source of artifact was discovered. All WCCF images exhibited the same periodic pattern as seen in the WCCF in Figure 40. The image gives the lag -25, -24, ... -1, 0, 1, 2, ..., 24, 25 cross-correlations between channels EEG1A and EEG1B for the

79 windows of the trial. The same pattern repeats itself like clockwork every five lags. This pattern is too periodic and repetitive to be physiological in origin (10).

The hypothesis is that a low frequency (.05 Hz) signal component is introduced into the data from the Beta recorder or video tapes. The correlation pattern develops as a result of the sampling software that acts as a multiplexer and introduces the artificial correlations. The correlations are artificial because they are the results of noise correlated to noise and are not indicative of any true periodicities in the data.

This hypothesis was confirmed by sampling three channels of the same data. If the hypothesis was true, the same pattern would appear but with a cycle of three lags. This was accomplished and as expected, the pattern appeared with a cycle of three lags.

Some conclusions can be drawn from these images, even though the main characteristics are noise-related. The plot in Figure 41 is the plot of the WCCF image. The x-axis 0 corresponds to lag -25 and 51 corresponds to lag +25. Note the values of the cross-correlations given on the z-axis. The maximum absolute value plotted is .015. The minimum statistically significant correlation for a sample size of 250 observations is .063. Thus all the cross-correlations

across all windows are not considered statistically different from zero.

The conclusion to be drawn is that neither channel has a significant effect on the other. Under the null hypothesis that no relationships exist, the expected WCCF is identically zero. Because the WCCF shows no significant correlations, H_0 can not be rejected. This was the case for all six WCCF images. A second WCCF image, that computed for EEG1A/EEG2B is shown in Figure 42. Note the same replicating five lag pattern.

The lack of a relationship among the channels can also be seen by visually inspecting the data. Items of interest are when two or more series line up over time or exhibit the same shape separated by a time lag. The data can be inspected by creating an image similar to that done for the WACF and WPACF. An array is built that contains one column of data for each brain channel. The array is then converted into an image file that displays the data as a continuous color bar that reflects the original data. Such an image is given in Figure 43.

The image given in Figure 43 shows the data taken for the four brain channels of the placebo trial. The x-axis is the image representation of the observations with increasing observations going from left to right. The y-axis is divided into four sections, one for each channel. It is difficult to

see any obvious lining up of patterns in the observations across two or more channels. The striations appear to be independent of any activity in the other channels. Note that for the two channels in which the model change was confirmed (EEG1A, EEG2B), an obvious change in pattern can be seen.

Thus it can be concluded that no lead-lag relationships exist between the brain channels of the placebo trial. Although the seizures appear in three separate brain channels, there is no evidence to suggest that the appearance of the seizure in one channel directly influences its appearance in any other channel.

This was also accomplished with the four channels of data for the Dilantin trial. The image given in Figure 44 is strikingly different from the image generated with the placebo data. The number and variation of the striations are significantly greater. The striations, indicative of periodic behavior and present from the start, are probably due to the introduction of Dilantin. These were not recognizable in the placebo trial until after the model change.

Channels EEG2A and EEG2B appear to be candidates for a multivariate model. A large section of the two data sets line up fairly well except for a slight lag between them. This may be due to the inaccuracies of starting the recorder at the exact place for each channel. To determine the true

presence of a transfer model, the two channels were re-sampled at the same time. (Because the software samples only in multiples of 100 Hz, three dummy channels were also sampled in order to keep the sampling rate at 60 Hz.)

The resulting WCCF image is shown in Figure 45. The characteristic five lag repetition is clearly obvious as was seen in the placebo data. The correlations, however, are much stronger than those computed for the placebo data. The cross-correlations vary between -.2 and +.5 indicative of a strong relationship between the two channels.

The results are questionable because the correlations previously attributable to the noise of the recorder and sampling software were placed between -.02 and +.02. If this were true then the correlations of the real process should have overshadowed the strict periodic behavior and the true WCCF would have shown through. Since this is evidently not the case, it is difficult to determine exactly how much of the correlation is due to either the true process under study or the artificial correlation of the newly discovered noise process. For now, it is obvious that the WCCF image as shown could not have a physiological origin and therefore can not be used for multivariate analysis.

Analysis of Additional Subjects

Two additional subjects were analyzed in order to validate the methods already developed and to form a comparison for interpretation. The two subjects were selected based on the duration of their trials. Subjects with times that were closest to the durations of the primary subjects' trials were chosen.

The summaries for the four additional trials are given in Tables V and VI. The summary relates trial elapsed time, subject reported symptom level (SSL), major symptoms experienced and corresponding window number.

Analysis of Subject #2. Seven of the ten data channels were collected on this subject. The placebo trial is missing channels EEG1C and EEG2A, the Dilantin trial failed to collect channel EEG2A.

All seven channels exhibited the same behavior across the data, WACF, WPACF and periodogram plots. No model changes were evident and the effects of Dilantin, if any, could not be determined using the methods of this research. A representative channel from the placebo trial, EEG2B, will be discussed.

The raw and differenced data plots are shown in Figure 46. With the exception of several well-defined, long duration motion artifacts, the data appear to be driven by the same process for the duration of the experiment. The plot of the

Table V Summary of Trials for Subject #2

Placebo Trial 14 rpm CW

Time (Sec)	SSL	Window #	Symptoms
0	ASYM	1	NONE
30	2	7.2	NONE
40	6	9.6	Stomach jumps
80	2	19.2	
90	5	21.6	
120	4	28.8	Face feels hot
130	3	31.2	
140	7	33.6	
160	6	38.4	Dry mouth
280	7 or 8	67.2	
310	9	74.4	
340	FS	91.2	Emesis

Dilantin Trial 14 rpm CCW

Time (Sec)	SSL	Window #	Symptoms
0	ASYM	1	NONE
20	2	4.8	Head spinning
50	3	12	Tingling in legs
100	4	24	Queasiness
120	5	28.8	
190	7	45.6	Dry mouth
280	9 or 10	67.2	Gas, nausea
310	9 or 10	74.4	Sweating
570	FS	136.8	Emesis

differenced data highlights three significant artifacts and several other smaller artifacts.

The WACF as given in Figure 47 shows these major artifacts as the horizontal striations that are two to three windows wide. No changes in the model are obvious and there does not appear to be any periodicities present. The WPACF

of Figure 48 confirms this analysis as it remains remarkably consistent throughout the experiment.

The periodogram is given in Figure 49 and confirms the analysis in the time domain. No model change is evident and the low frequency shift characteristic of the motion sickness seizure can not be found. The absence of a significant ridge parallel to the y-axis confirms the absence of significant periodicities.

Analysis of Subject #3. The trial summaries are given in Table VI. The third subject represents the third unique

Table VI Summary of Trials for Subject #3

Placebo Trial 18 rpm CCW

Time (Sec)	SSL	Window #	Symptoms
0	ASYM	1	NONE
50	1	12	Sweating
130	2	31.2	
200	4	48	Nauseous
220	FS	52.8	Emesis

Dilantin Trial 18 rpm CCW

Time (Sec)	SSL	Window #	Symptoms
0	ASYM	1	NONE
180	2	43.2	Dizziness
200	3	48	Sweating
230	4 or 5	55.2	
270	5 or 6	64.8	
300	FS	72	Emesis

set of brain signals analyzed. As was the case in subject #2, this subject also exhibited no abrupt model changes in any of the eight channels that were analyzed. Channel EEG1C failed in both trials. Furthermore, the interpretations of the channels for the two trials were similar enough to warrant the presentation of only one channel from each of the two trials. The similarities where based on each channels' WACF, WPACF and periodogram. A representative channel from both the placebo and Dilantin trials are now presented.

The raw and differenced data for channel EEG1B of the placebo trial are given in Figure 50. Note the large number of equally spaced vertical lines that correspond to head motion artifact. These are equally spaced at ten second intervals and are more dramatic here than in the previous two subjects.

The WACF and WPACF images shown in Figures 51 and 52. A strong vertical striation is noted centered on multiples of lags 5 and 6, which is the now familiar 11 Hz periodicity. As seen previously in the primary subject there is a model change that occurs in the seasonal operators. The periodicities are reasonably well-defined and significant at the beginning of the experiment. The strength of the harmonics dramatically increases over time and becomes more well-defined particularly in the third and fourth harmonic.

The seasonal model appears to go nonstationary in the later windows implying the periodic effects do not die out over large lags. The nonseasonal aspects of the model do not change significantly during the experiment.

The periodogram of these data is given in Figure 53. The unique shape of this periodogram is consistent in all four channels of the placebo trial for subject #3. All the power is contained in the first 45 harmonics. Because the power is fairly evenly distributed, few frequencies test positively for significance. Those that test positively for significance correspond to the harmonics of the 11 Hz periodicity in the seasonal model. There is no apparent change in the periodogram except for the increasing amplitude of the significant peaks.

The final channel to be presented is the EEG1A from the Dilantin trial of subject #3. The plots of the raw and differenced data sets are given in Figure 54. The motion artifact is even more dramatic in the Dilantin trial than in the placebo trial (Figure 50). The peak power levels of these artifacts appear to form a pattern that is more obvious in the plot of the differenced data. The peak values act as though they are in some form of sinusoidal envelope that oscillates in amplitude over time. The significance of this observation is difficult to determine. Maybe the head motions at the beginning and end of the trial result in more

stimulus than those in the middle section of the trial. Perhaps the body is adapting to the stimulus somewhat or it may be attributable to the effects of Dilantin.

The oscillating nature of the motion artifacts can also be seen in the WACF in Figure 55. The horizontal striations that appear every two windows are due to the dominant artifact. Note the length of the striations also follow a similar sinusoidal shape. No evidence of model change can be seen as the WACF remains constant over time. A faint vertical striation at lag 7 indicates a possible weak 8.6 Hz periodicity. The WPACF given in Figure 56 also remains constant for the duration of the experiment and is indicative of a low order AR process.

The periodogram is given in Figure 57 and is representative of the periodograms of the other three channels. No model change can be detected and no frequency shift is found. The periodogram plot is flat except for those windows in which a motion artifact occurs. These windows exhibit the high amplitude long duration periodicities as seen earlier. A significant (in windows where no artifact is present) ridge is present at frequency 74 corresponding to a periodicity at approximately 18 Hz. This correlates with the striation seen in the WACF at lag 7. This places the frequency within the beta wave activity

range of normal brain activity and marks the first time this frequency has been seen in any of the subjects.

The interpretations for each channel for the three subjects are given in Table VII below. Included in the table are the subject number and trial, channel, model condition, time of model change, lag between changes and the presence of periodicities.The table highlights the similarities and differences of within and among the subjects.

Subject #1 exhibits both types of model change. The abrupt change and associated seizure can be tracked for both trials by considering the lag times. The 11 Hz periodicity can be found in 5 of the 8 brain channels. Subject #2 exhibits no model change or periodicities. Subject #3 exhibits periodicities in all but two channels. The seasonal model change is found in channel EEG1B in both trials. It is curious to note that when this type of model change is restricted to channel EEG1B only.

Table VII Summary of Channels

SUBJECT #	CHANNEL	CONDITION	TIME(sec)	LAG	PERIODICITY
1-PLACEBO	EEG1A	MODEL CHANGE	171	0	NO
1-PLACEBO	EEG1B	MODEL CHANGE	*	*	11 Hz
1-PLACEBO	EEG2A	MODEL CHANGE	217	25	11 Hz
1-PLACEBO	EEG2B	MODEL CHANGE	192	21	NO
1-DILANTIN	EEG1A	MODEL CHANGE	292	25	NO
1-DILANTIN	EEG1B	MODEL CHANGE	271	4	11 Hz
1-DILANTIN	EEG2A	MODEL CHANGE	221	0	11 Hz
1-DILANTIN	EEG2B	MODEL CHANGE	267	46	11 Hz
2-PLACEBO	EEG1A	NO CHANGE			NO
2-PLACEBO	EEG1B	NO CHANGE			NO
2-PLACEBO	EEG2B	NO CHANGE			NO
2-DILANTIN	EEG1A	NO CHANGE			NO
2-DILANTIN	EEG1B	NO CHANGE			NO
2-DILANTIN	EEG1C	NO CHANGE			NO
2-DILANTIN	EEG2B	NO CHANGE			NO
3-PLACEBO	EEG1A	NO CHANGE			NO
3-PLACEBO	EEG1B	MODEL CHANGE	*	*	11 Hz
3-PLACEBO	EEG2A	NO CHANGE			NO
3-PLACEBO	EEG2B	NO CHANGE			11 Hz
3-DILANTIN	EEG1A	NO CHANGE			9 Hz
3-DILANTIN	EEG1B	MODEL CHANGE	*	*	11 Hz
3-DILANTIN	EEG2A	NO CHANGE			NO
3-DILANTIN	EEG2B	NO CHANGE			9 Hz

V. Conclusions and Recommendations

Conclusions

Three subjects were analyzed using the methodology developed earlier in this thesis. The primary subjects' data were characterized by two model regions that corresponded to a sick model and a well model. The sick model was typically a white noise process region that transitions into a well model region that was characterized by high order autocorrelations and nonstationary behavior. This transition region was generally well-defined. The model change in the time domain corresponded with a coincident shift in the frequency domain to the low frequency, high amplitude signals previously detected by AFIT researchers.

The second subject acted almost like a control. There were no indications of model changes or periodicities in any of the channels. The subject did experience typical motion sickness symptoms and the experiment ended in the desired result of emesis.

The fi[illegible] subject similarly did not exhibit signs of a model change but did exhibit periodicities in the alpha range as did the primary subject. The periodogram for this subject was unique, however, as all the power in each signal was distributed among the first half of the spectrum.

From this limited data, it cannot be concluded that, in general, a boundary exists between the brain signals of a well subject and a motion sick subject and that the boundary results in a measurable change in the time domain. The evidence seems to point in favor of the hypothesis that each individual may be unique in terms of his brain's response to the motion sickness stimulus. There may be no definitive model or presence of a boundary that can be employed across all subjects.

The effects of Dilantin were noticeable in two of the three subjects. The primary subject exhibited the same indications of a boundary region but that region was delayed much longer into the experiment. Two of the brain channels exhibited the characteristic low frequency power shift from the start of the trial, a result that is attributable to the Dilantin's slowing effects on brain signals. Subject #3 likewise extended his time before emesis. A shift in periodogram behavior may also be attributable to Dilantin.

The usefulness of the time series methodology has been shown. The WACF, WPACF and periodogram all give insight into the data structure by allowing greater samples to be viewed at once. What appears to be insignificant when viewed in one window often becomes significant when viewed in conjunction with a series of windows or when viewed as an image. Low powered periodicities and other data structures can be

highlighted using these techniques. Model changes, model identification, periodicity identification and artifact identification can be performed using the WACF and WPACF. The periodogram can be used to confirm significant behavior noted in the time domain.

Recommendations

The methods developed in this research need to be applied across a wider base of subjects to determine if the brain activity is unique for all subjects. A sample of three is insufficient to make such a claim. An analysis of twenty or thirty subjects could prove worthwhile in developing a set of classes in order to group these subjects.

In one subject the postulated presence of a motion sickness generator looked promising, therefore it is recommended that analysis of the brain channels continue. The number of brain channels monitored needs to be increased in order to more accurately locate and isolate those areas of the brain that are affected by motion sickness.

A way must be found to keep from losing brain channel instrumentation during the experiment. This is especially true regarding channel EEG1C (right temporal). Only one of the six channels analyzed in this thesis had useable data and that channel lasted for only a few minutes before failure. Of the 30 possible channels available, useful data

were collected on 23 channels and only 19 (63%) of tnese were complete.

Possible problems with the sampling software were highlighted during the sampling of multiple channels. The introduction of artificial correlations due to the software does not allow a reliable multivariate analysis to be performed. It is suggested that either a new program be looked into or another method of multiple sampling of channels be developed.

A multivariate approach is suggested due to indications from some of the WCCFs. In the case where definite model changes occur, a transfer model could be employed to determine the relationships that exist between the other brain channels. Furthermore, when the number of channels collected is increased, there will be a need for data reduction. Principal components and factor analysis should be prime candidates as analysis tools in order to decrease the dimensionality of the data.

A final recommendation concerns the development of a means of classifying the models generated by the time series methods. It is suggested that a high order AR model be fit to the data in each window as an approximation to the exact model. These parameters can then be used to perform a discriminant analysis to determine if multiple states exist during the transition from the start of head motions to

emesis. This method looks promising as it was experimented with briefly but not reported.

Appendix

Additional Plots and Images

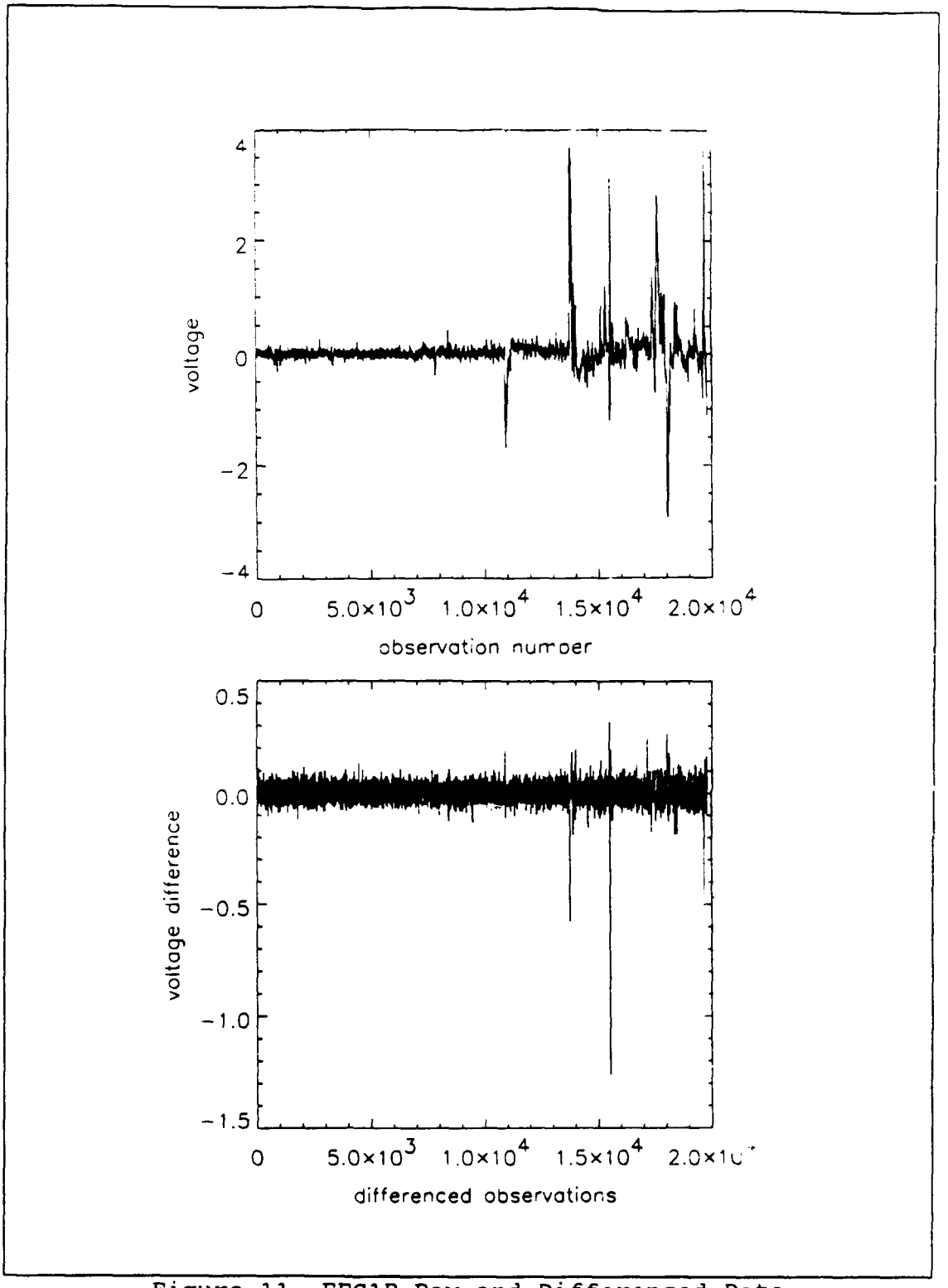

Figure 11. EEG1B Raw and Differenced Data

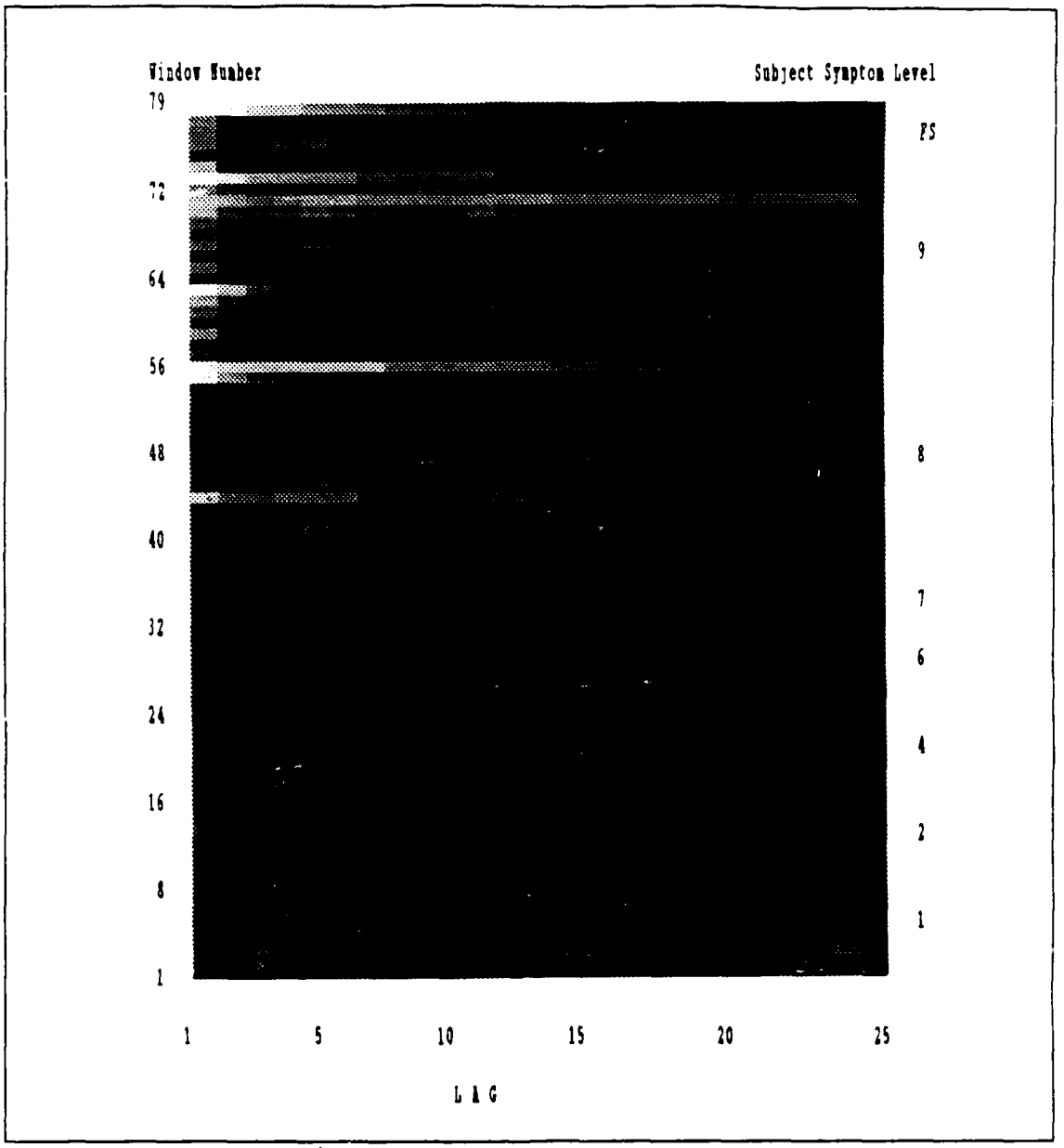

Figure 12. EEG1B WACF Image

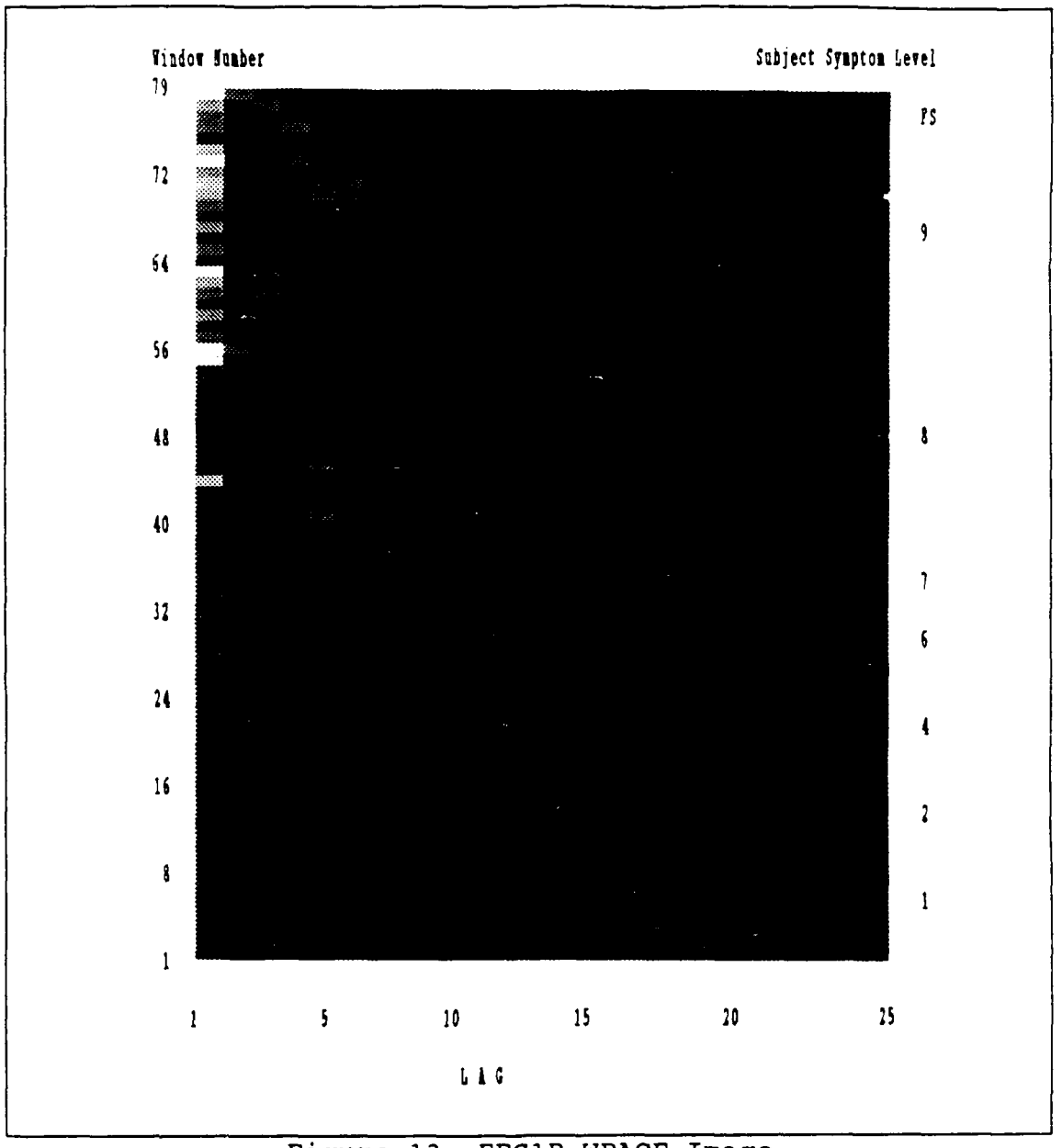

Figure 13. EEG1B WPACF Image

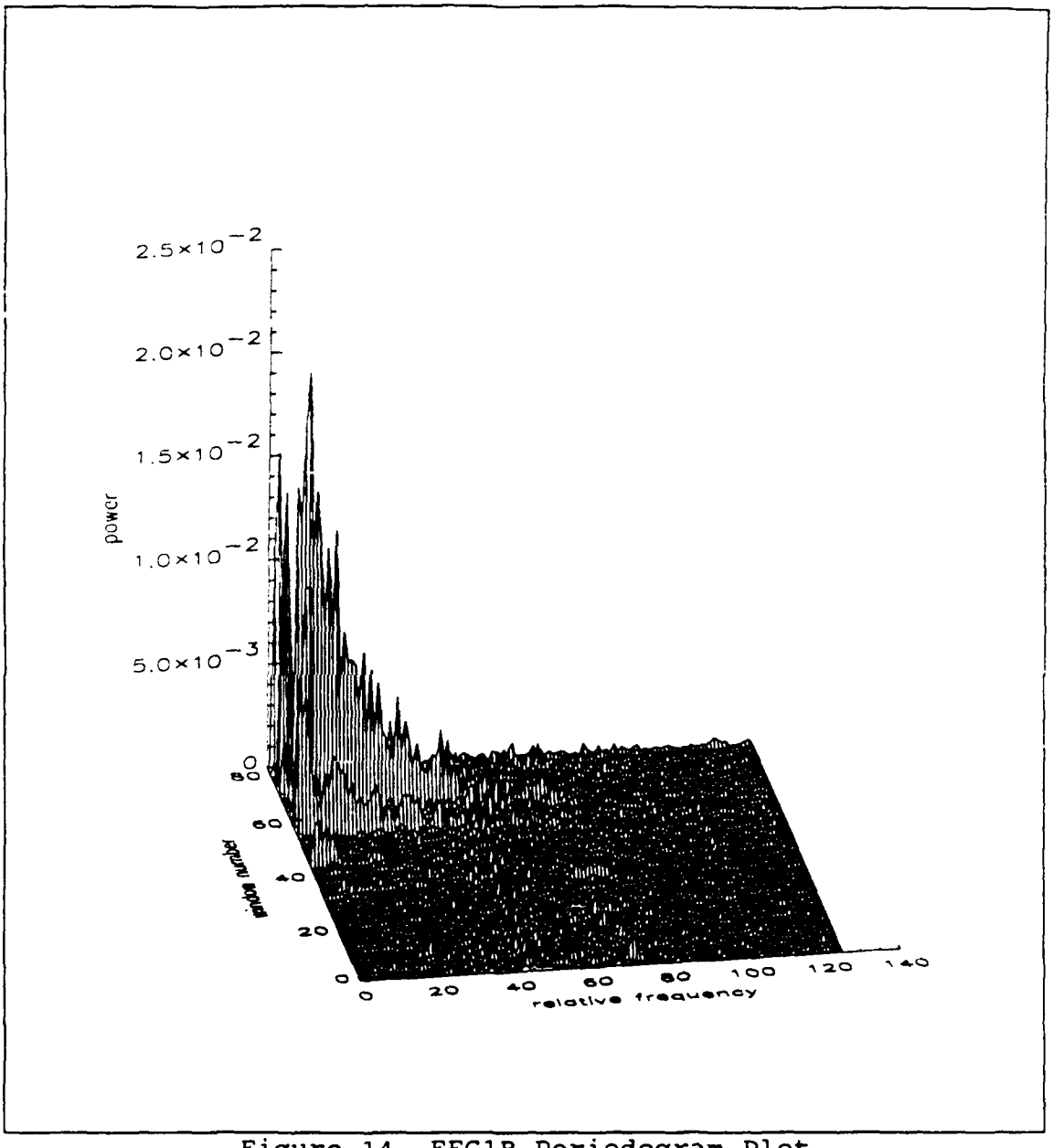

Figure 14. EEG1B Periodogram Plot

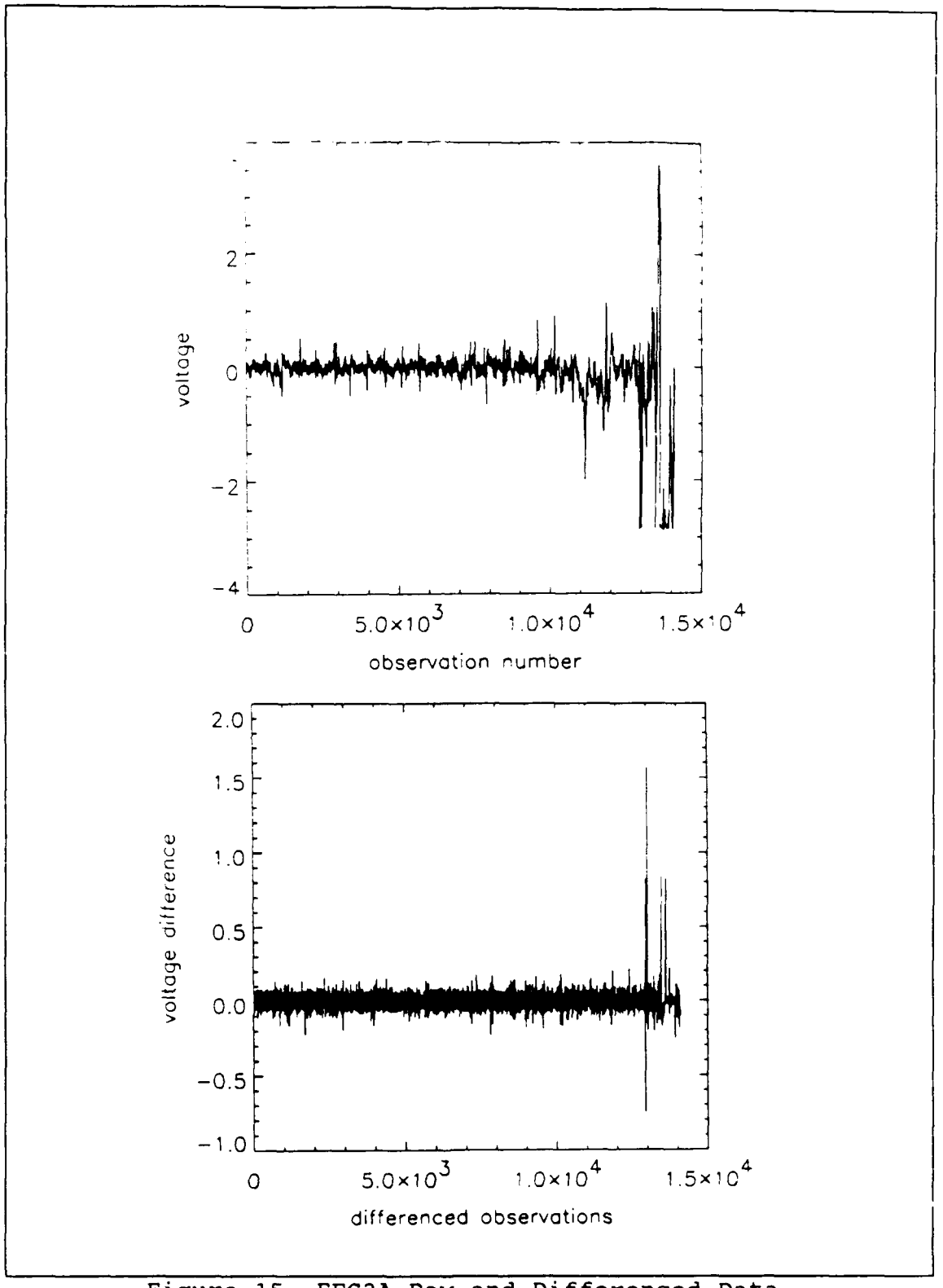

Figure 15. EEG2A Raw and Differenced Data

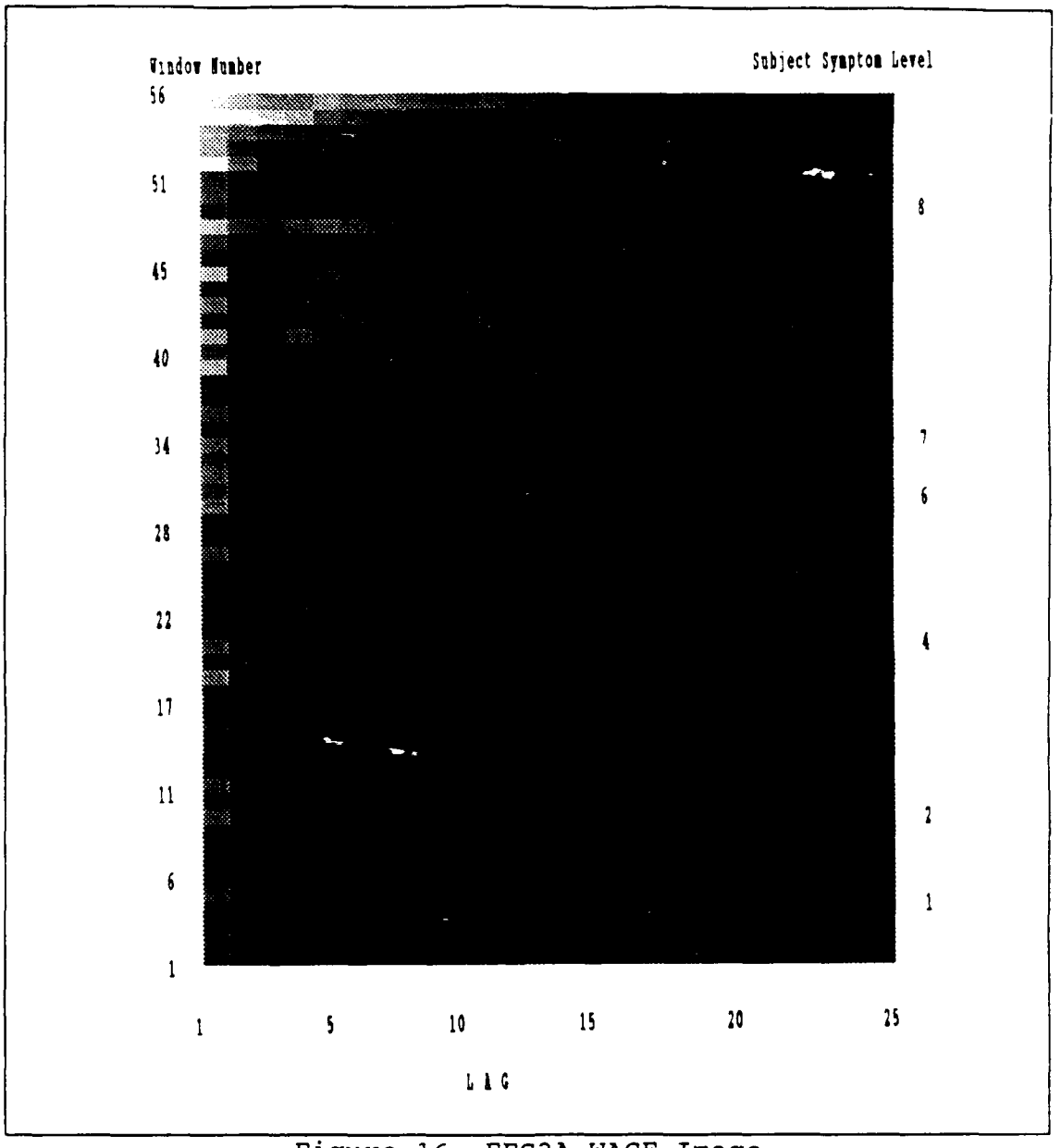

Figure 16. EEG2A WACF Image

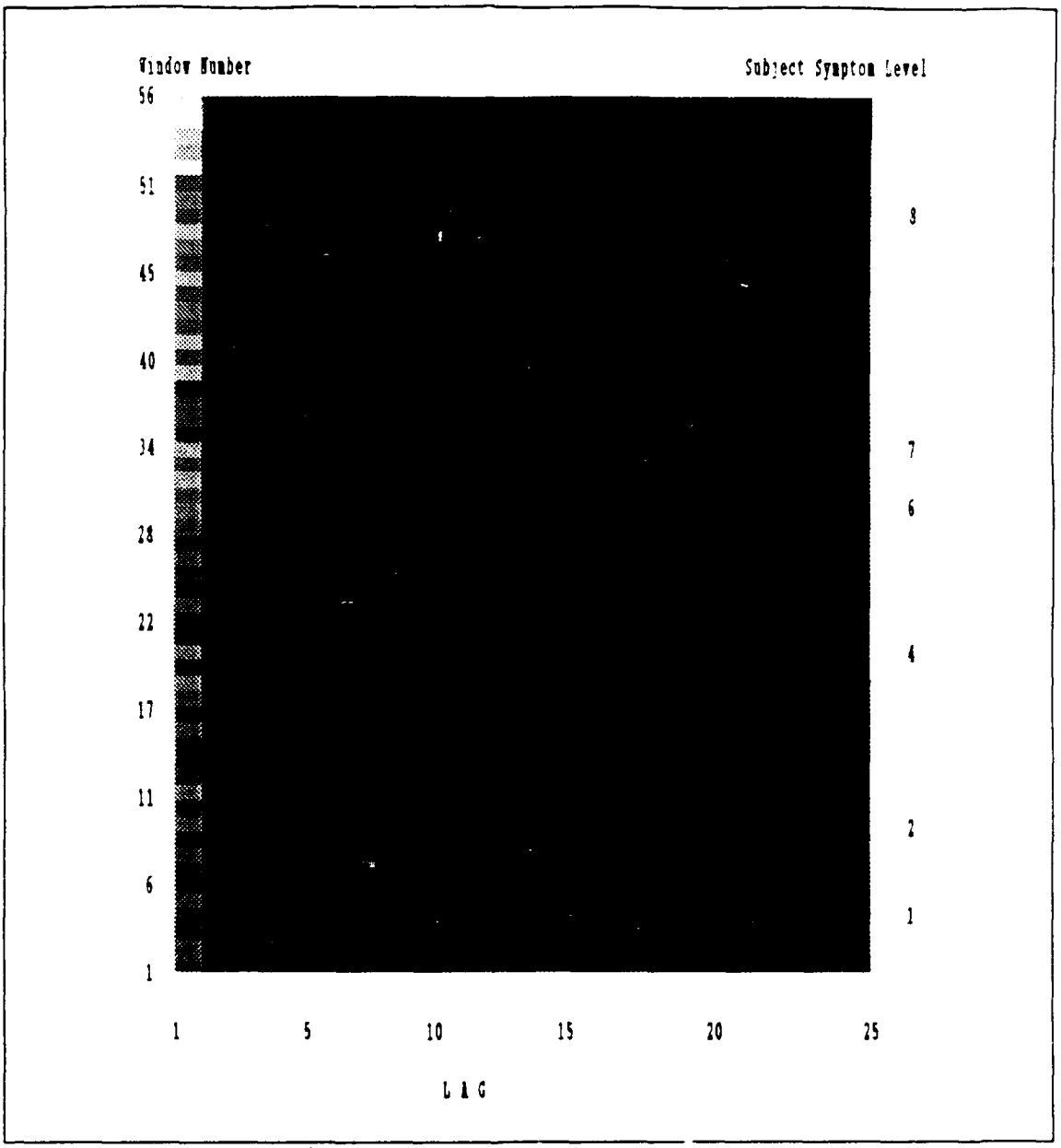

Figure 17. EEG2A WPACF Image

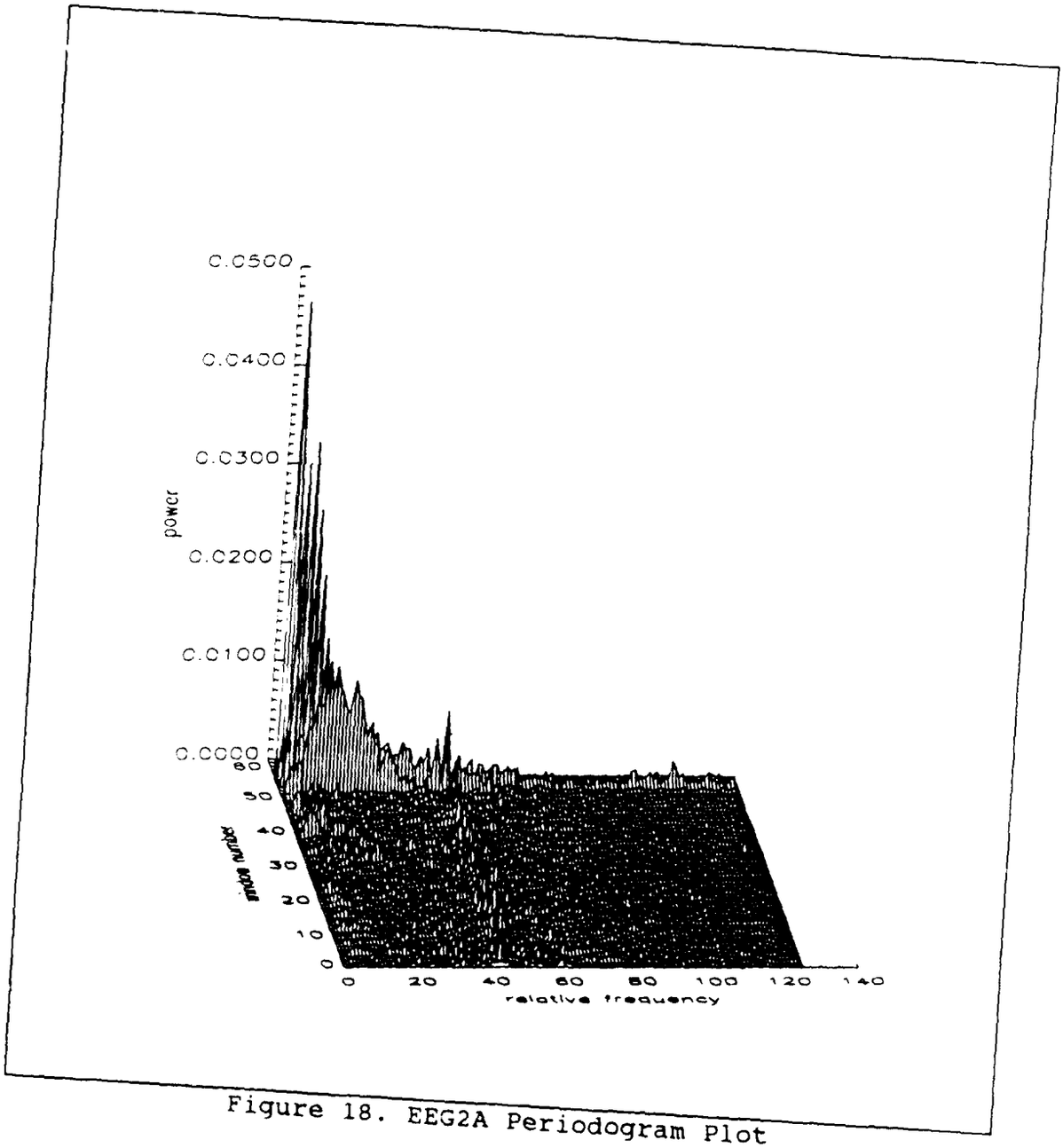

Figure 18. EEG2A Periodogram Plot

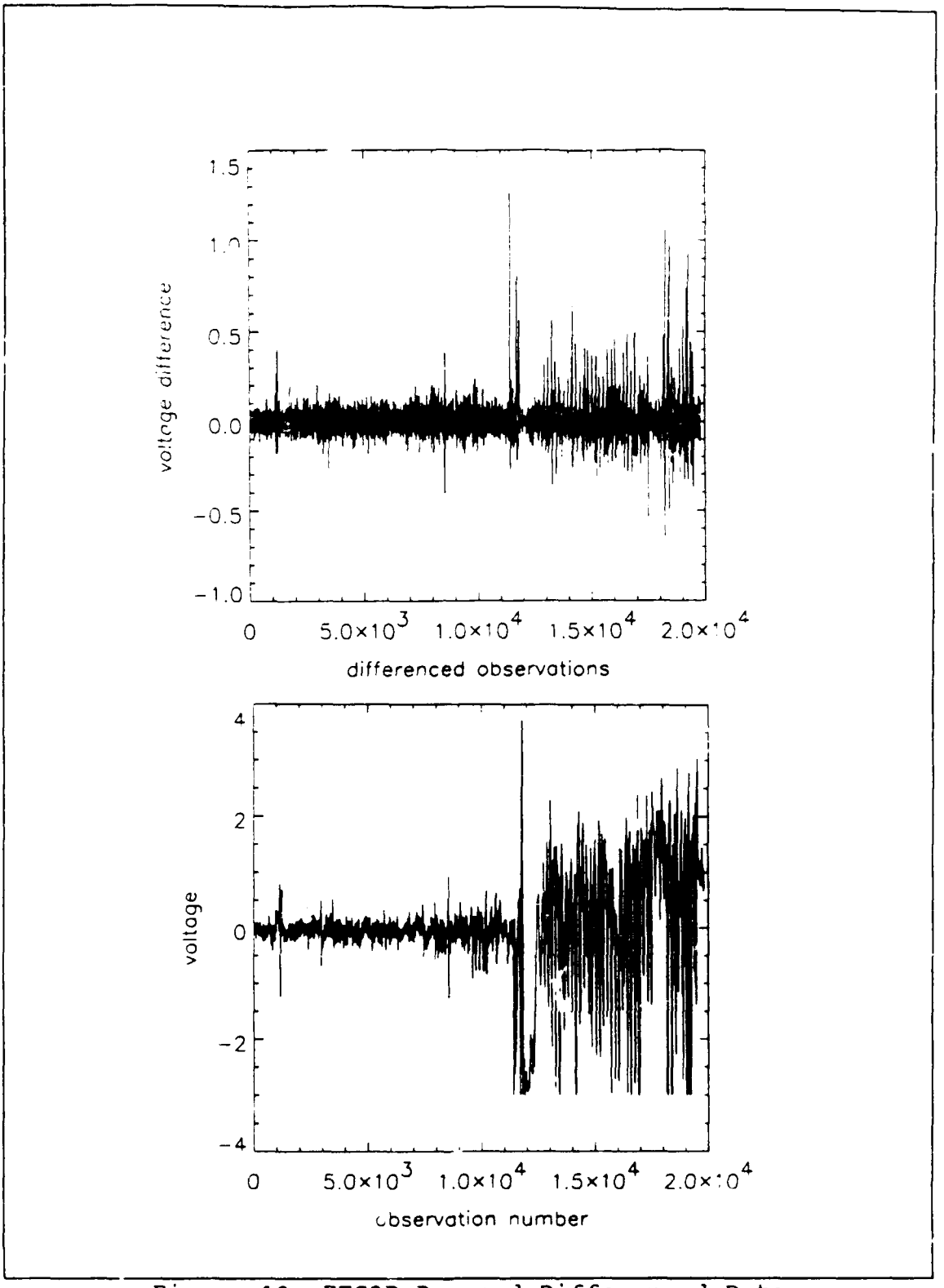

Figure 19. EEG2B Raw and Differenced Data

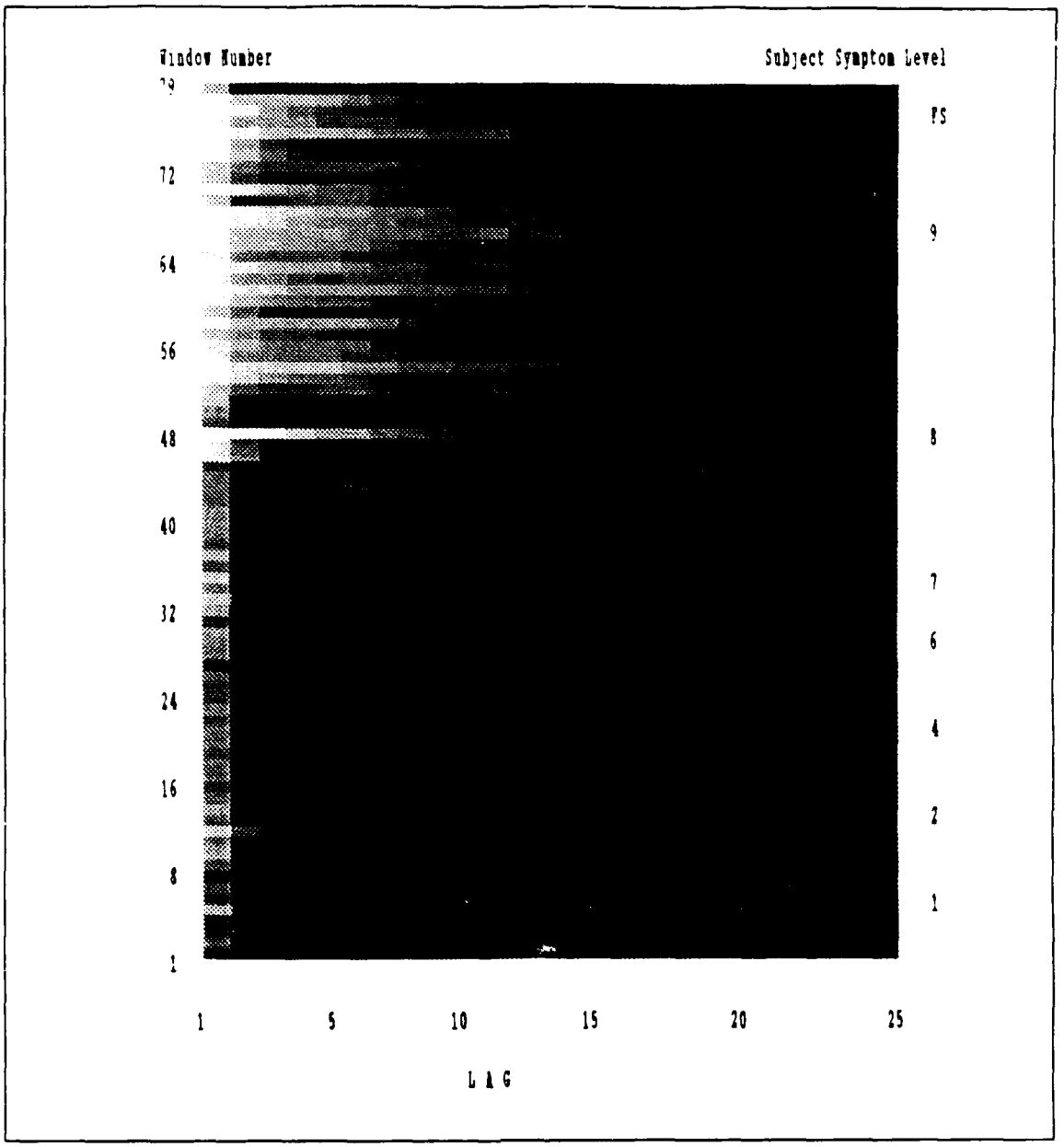

Figure 20. EEG2B WACF Image

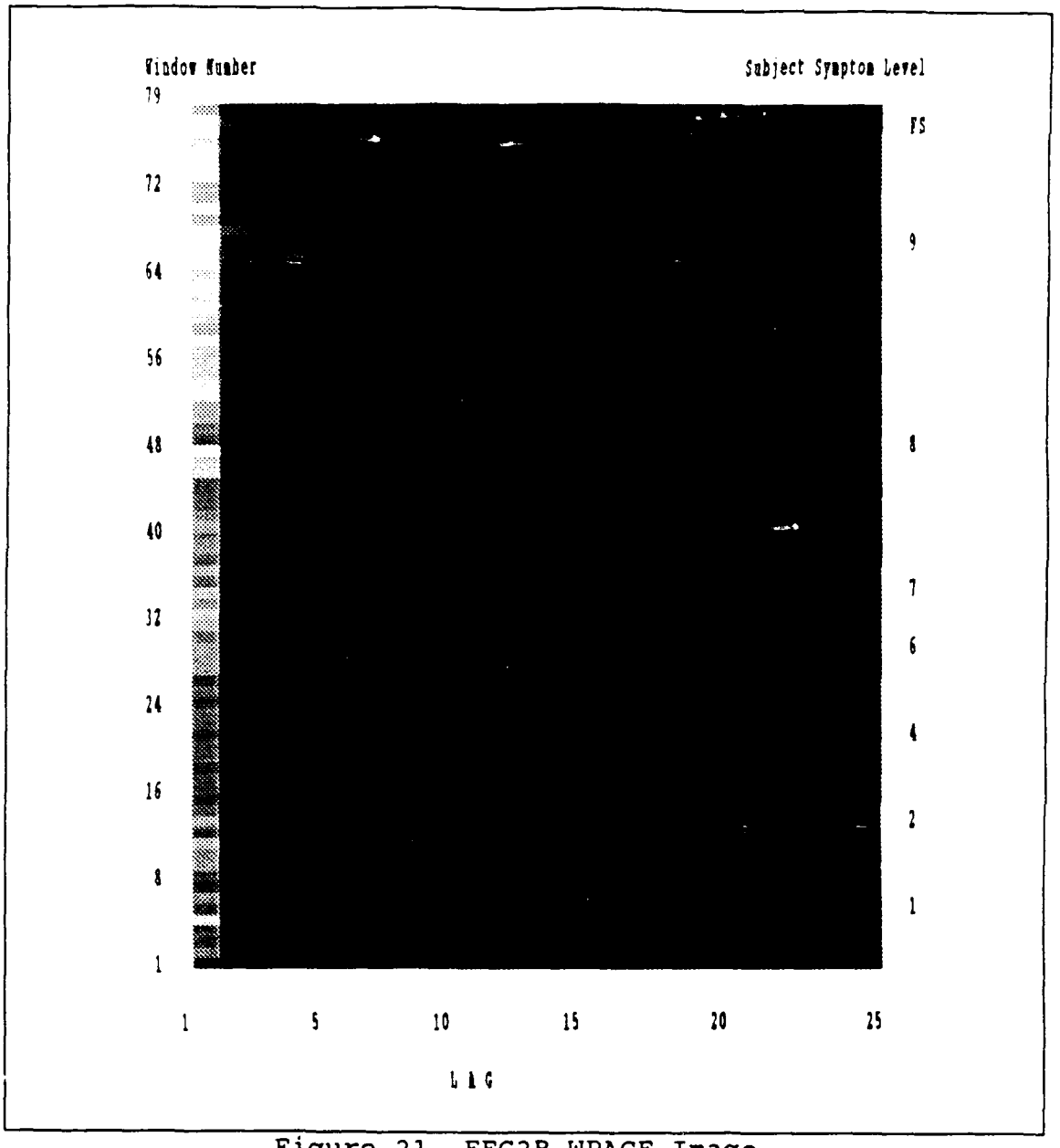

Figure 21. EEG2B WPACF Image

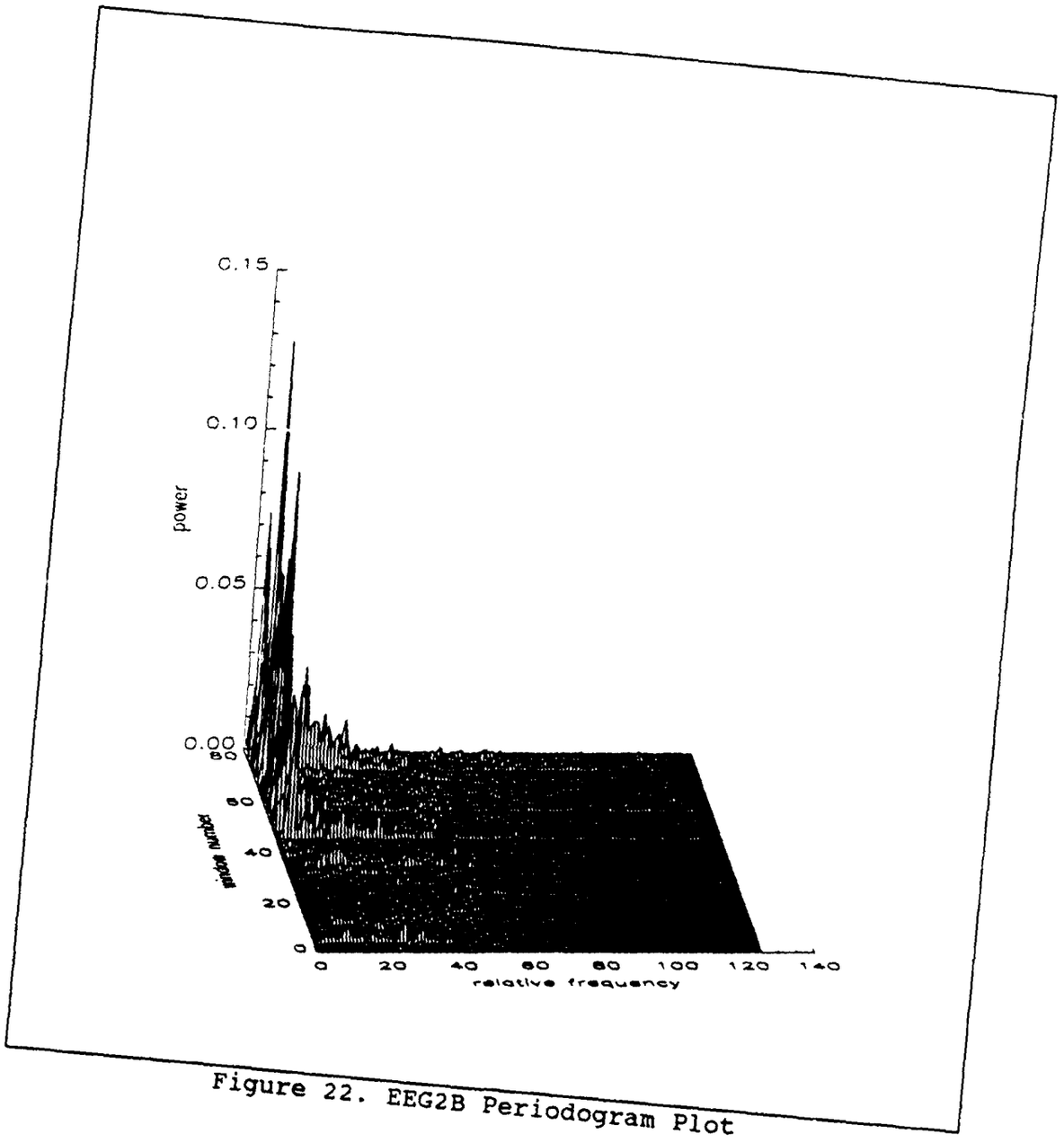

Figure 22. EEG2B Periodogram Plot

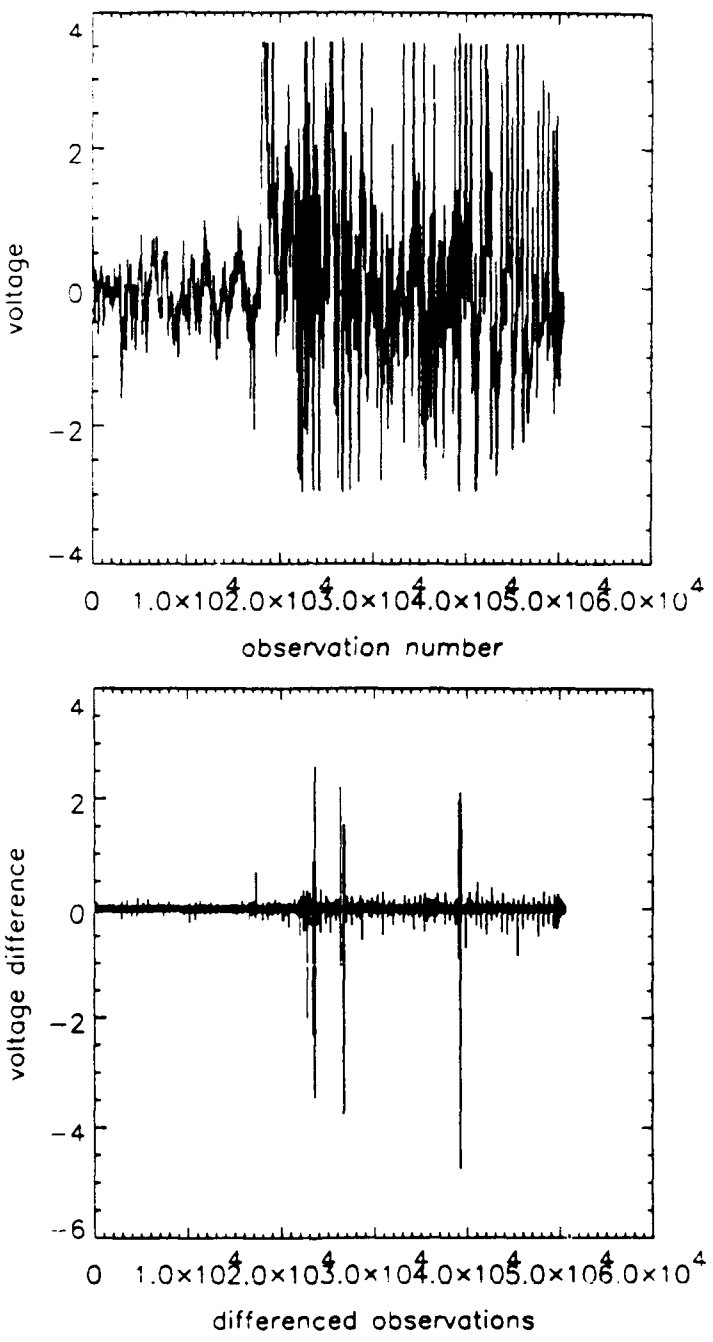

Figure 23. EEG1A Raw and Differenced Data

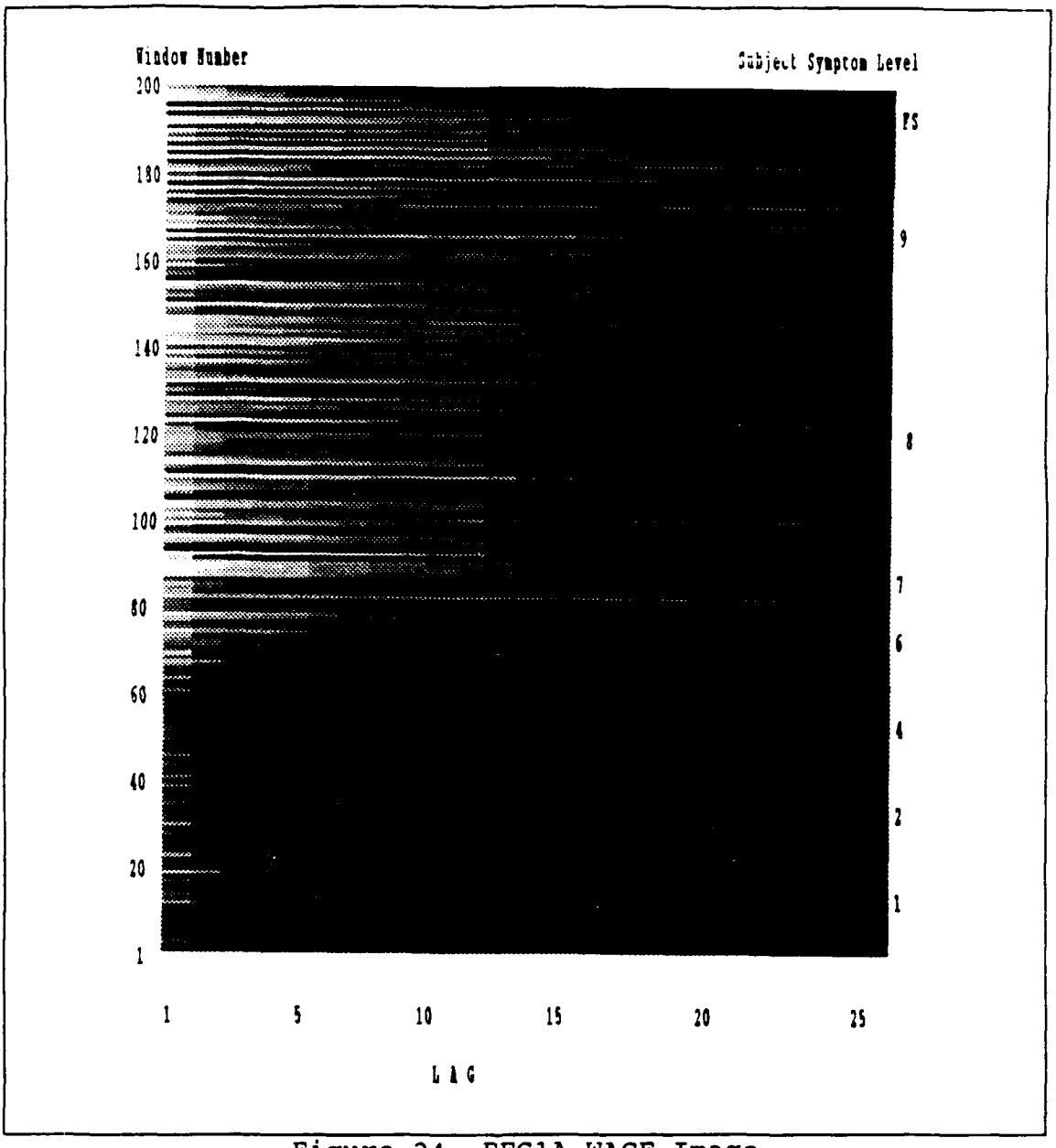

Figure 24. EEG1A WACF Image

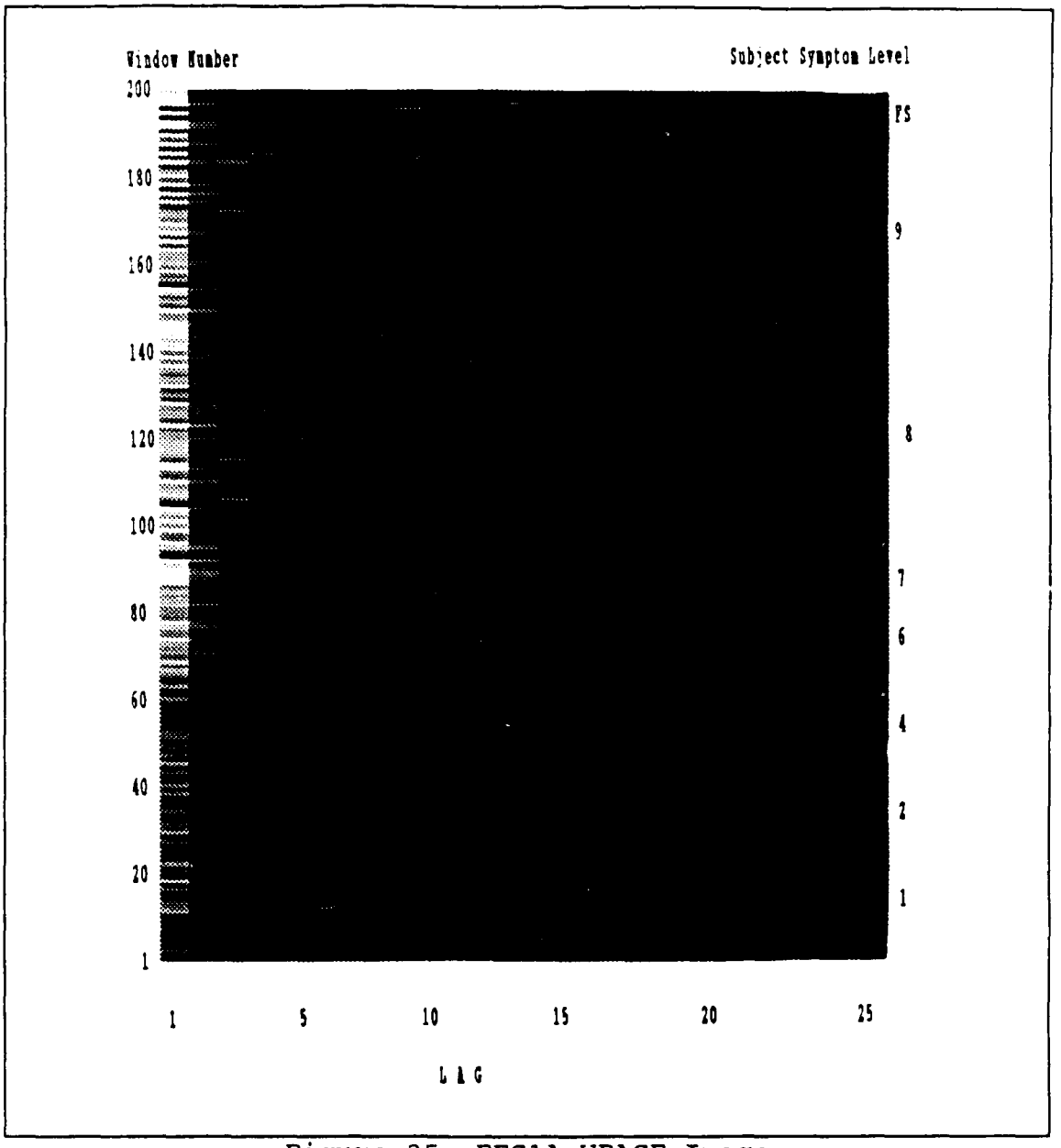

Figure 25. EEG1A WPACF Image

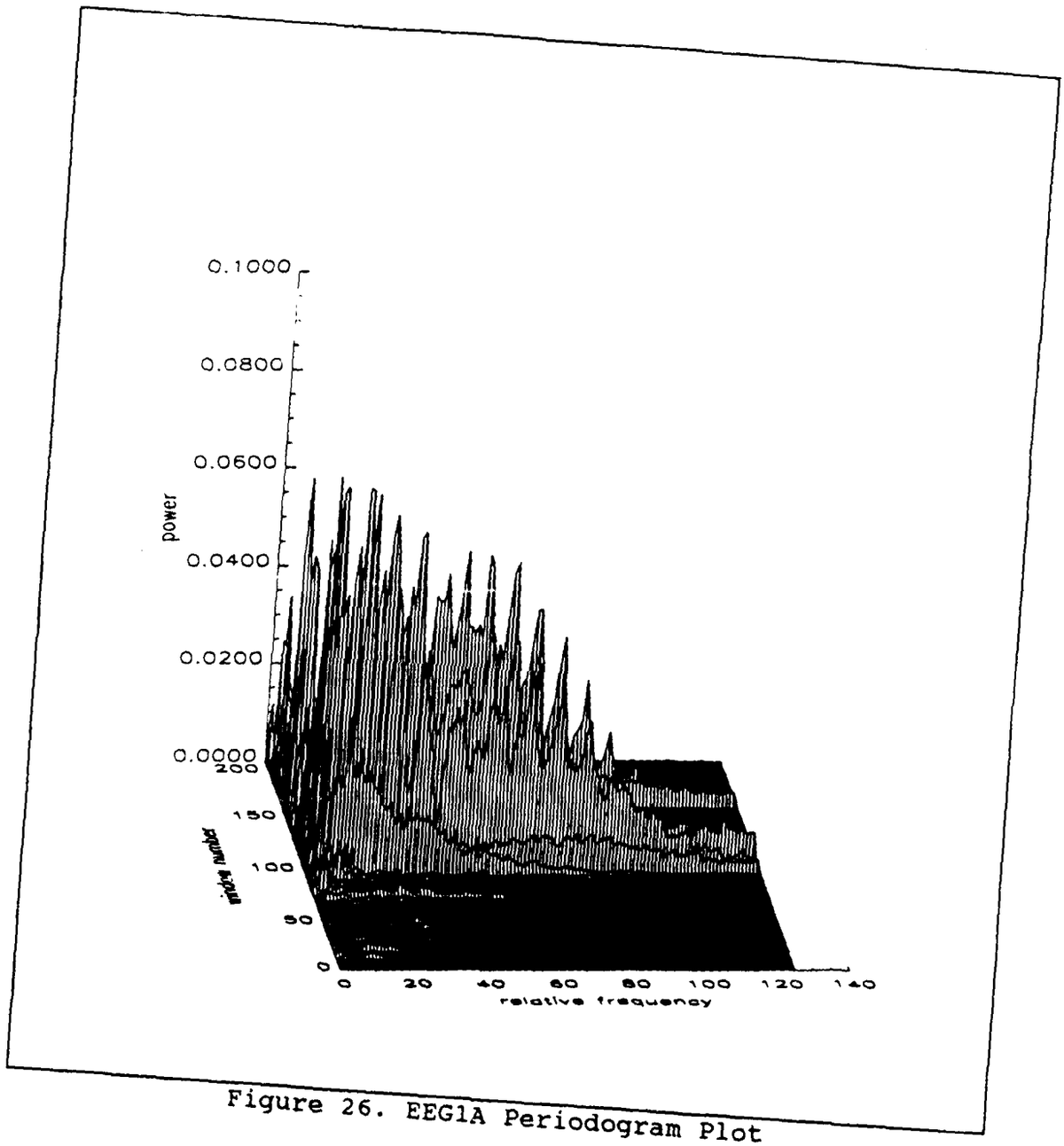

Figure 26. EEG1A Periodogram Plot

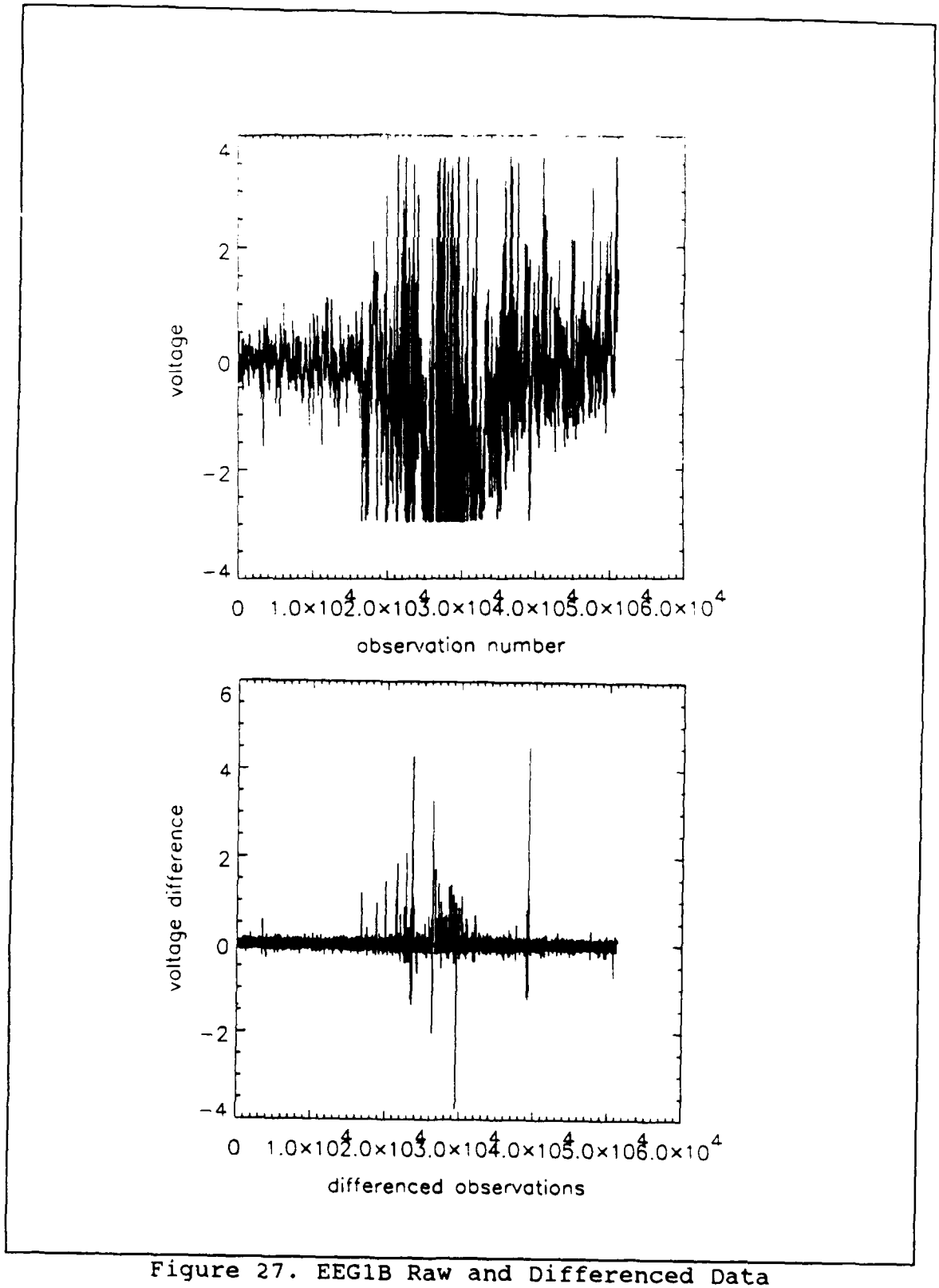

Figure 27. EEG1B Raw and Differenced Data

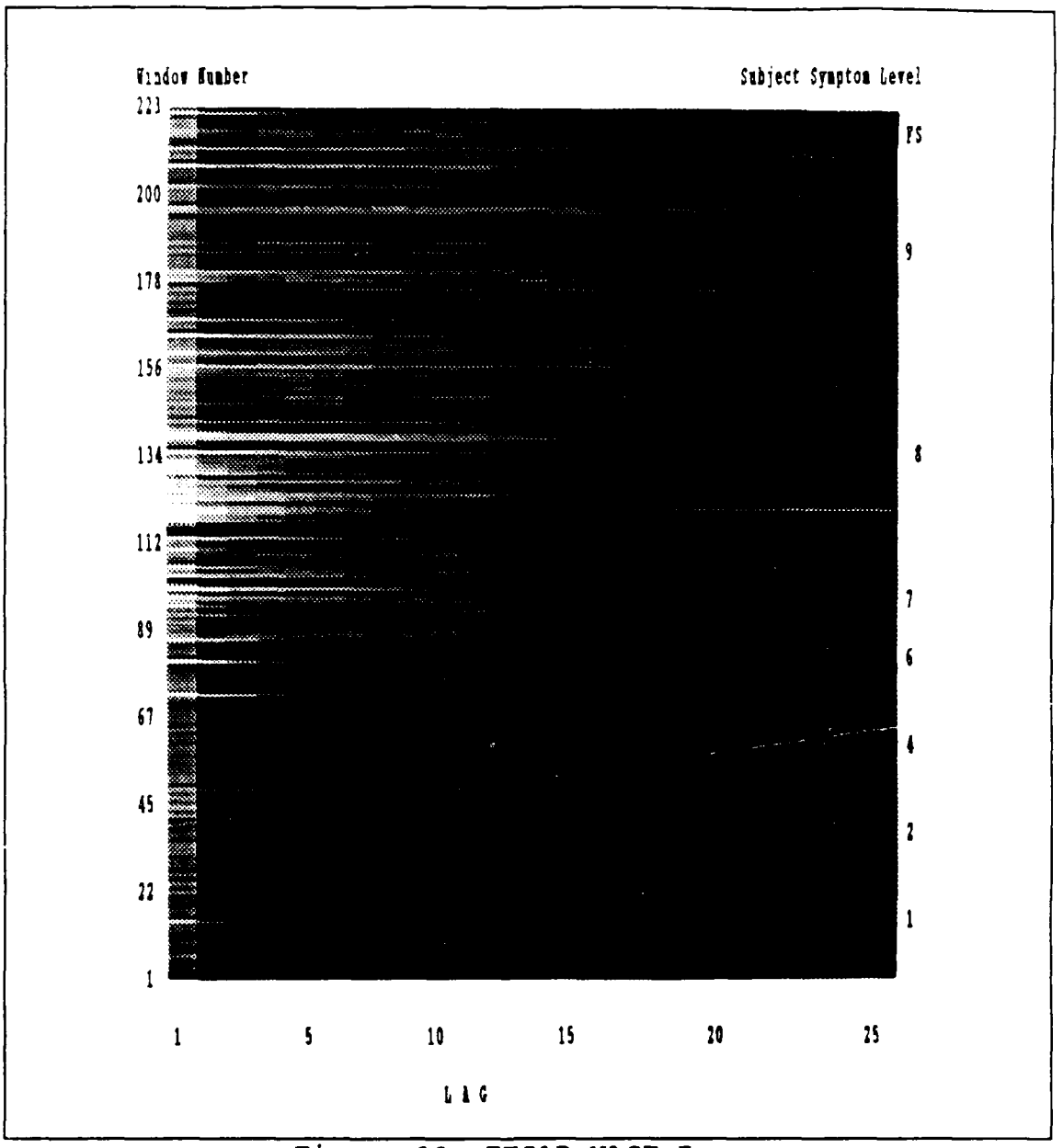

Figure 28. EEG1B WACF Image

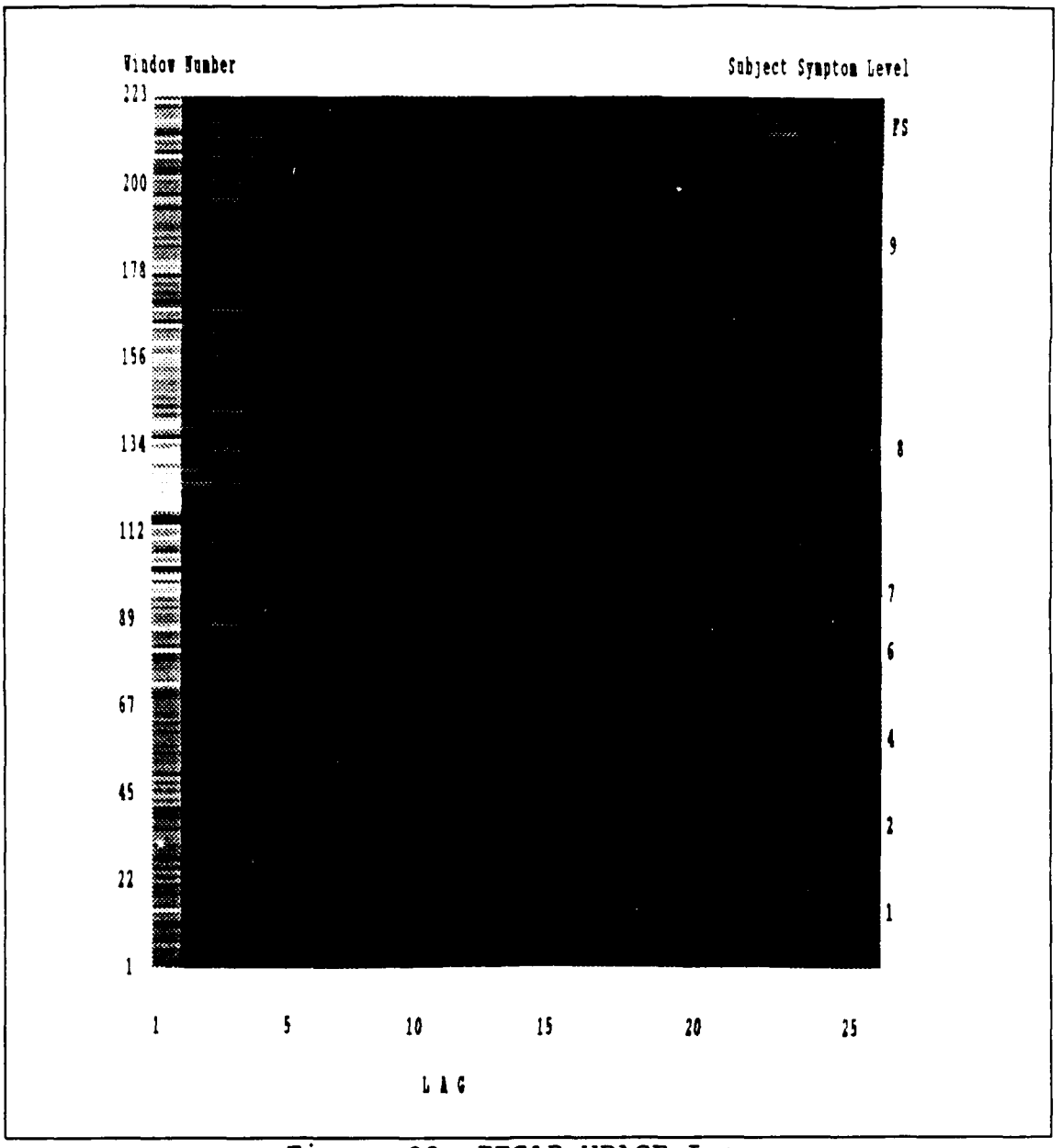

Figure 29. EEG1B WPACF Image

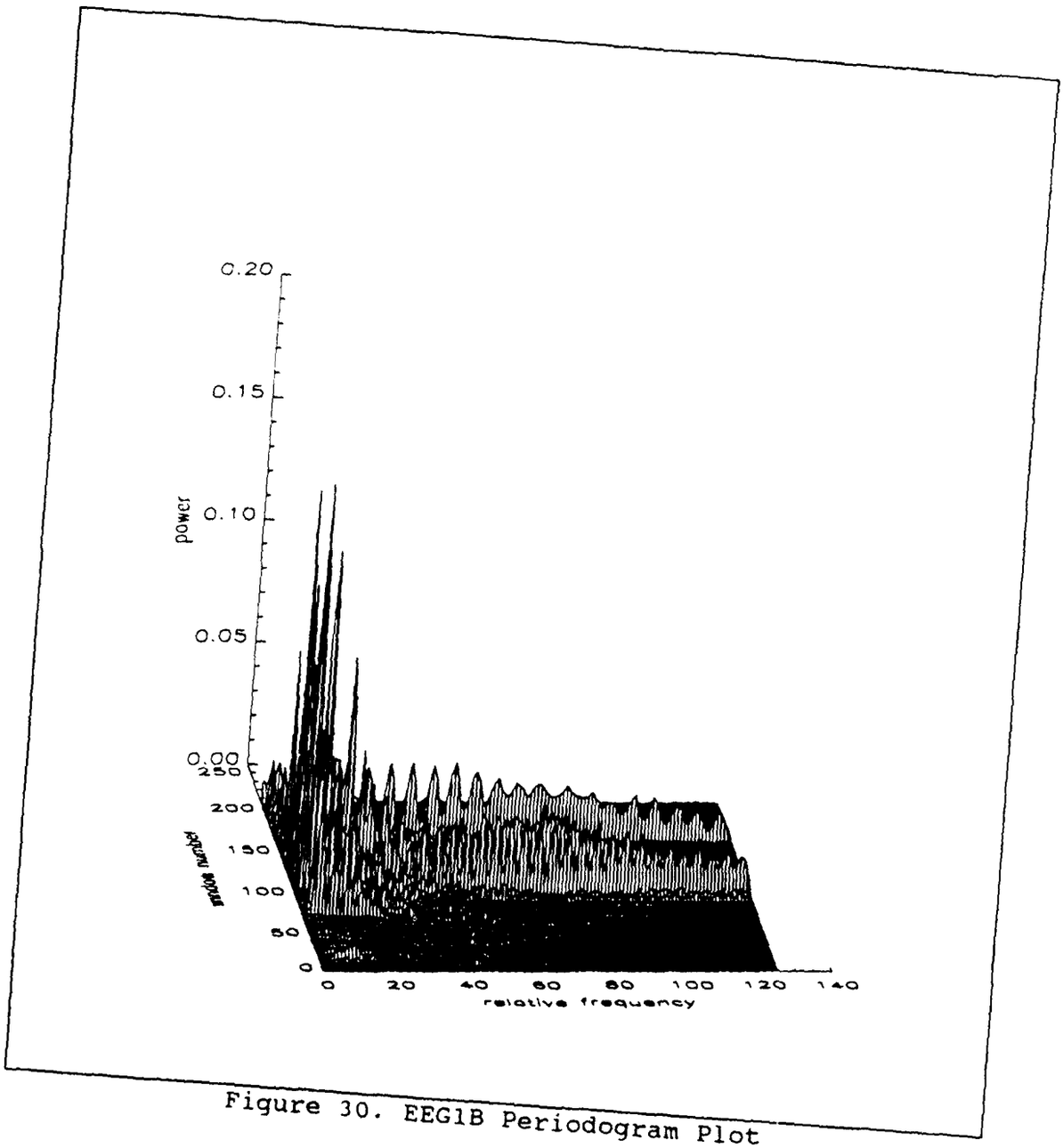

Figure 30. EEG1B Periodogram Plot

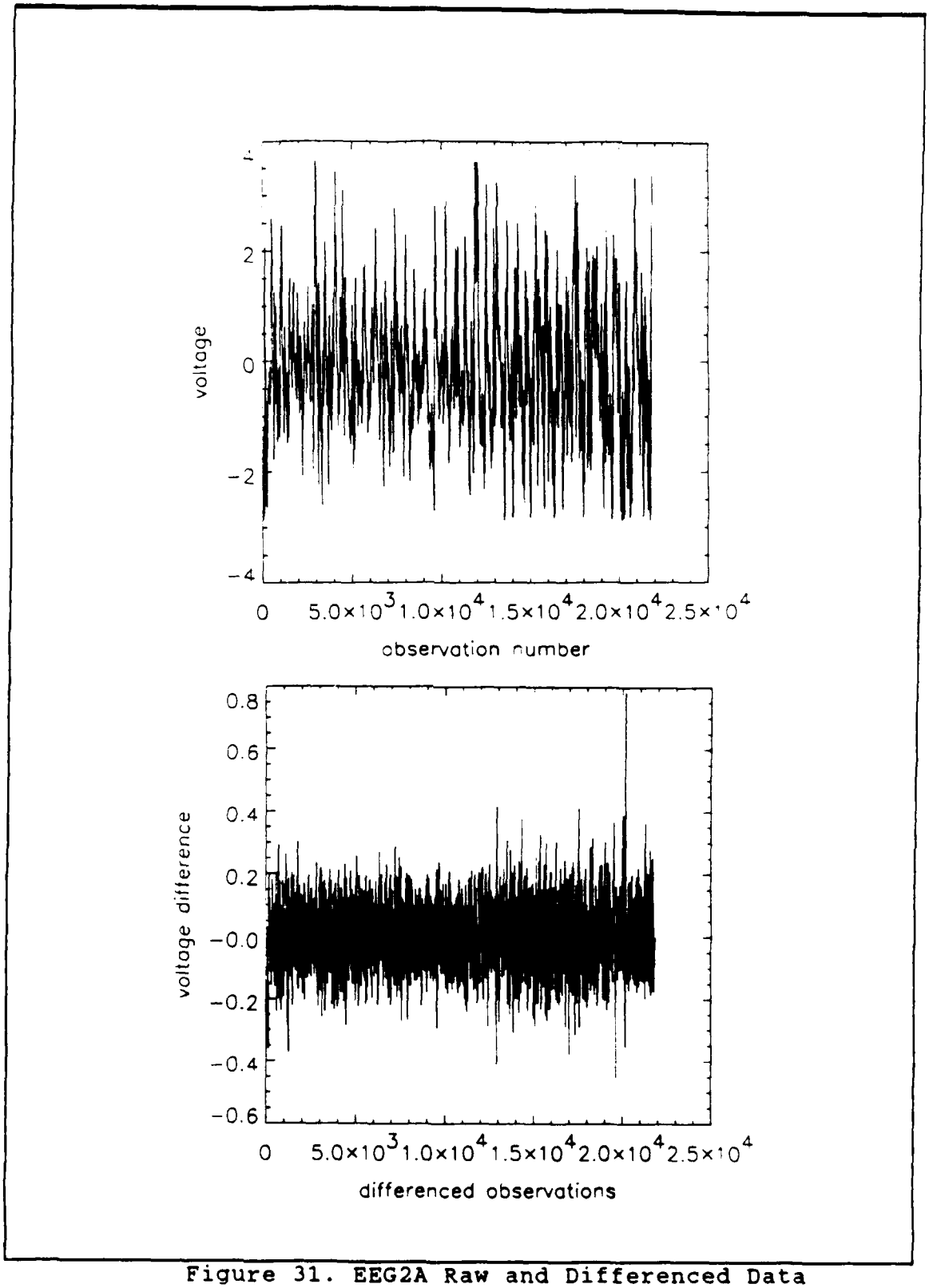

Figure 31. EEG2A Raw and Differenced Data

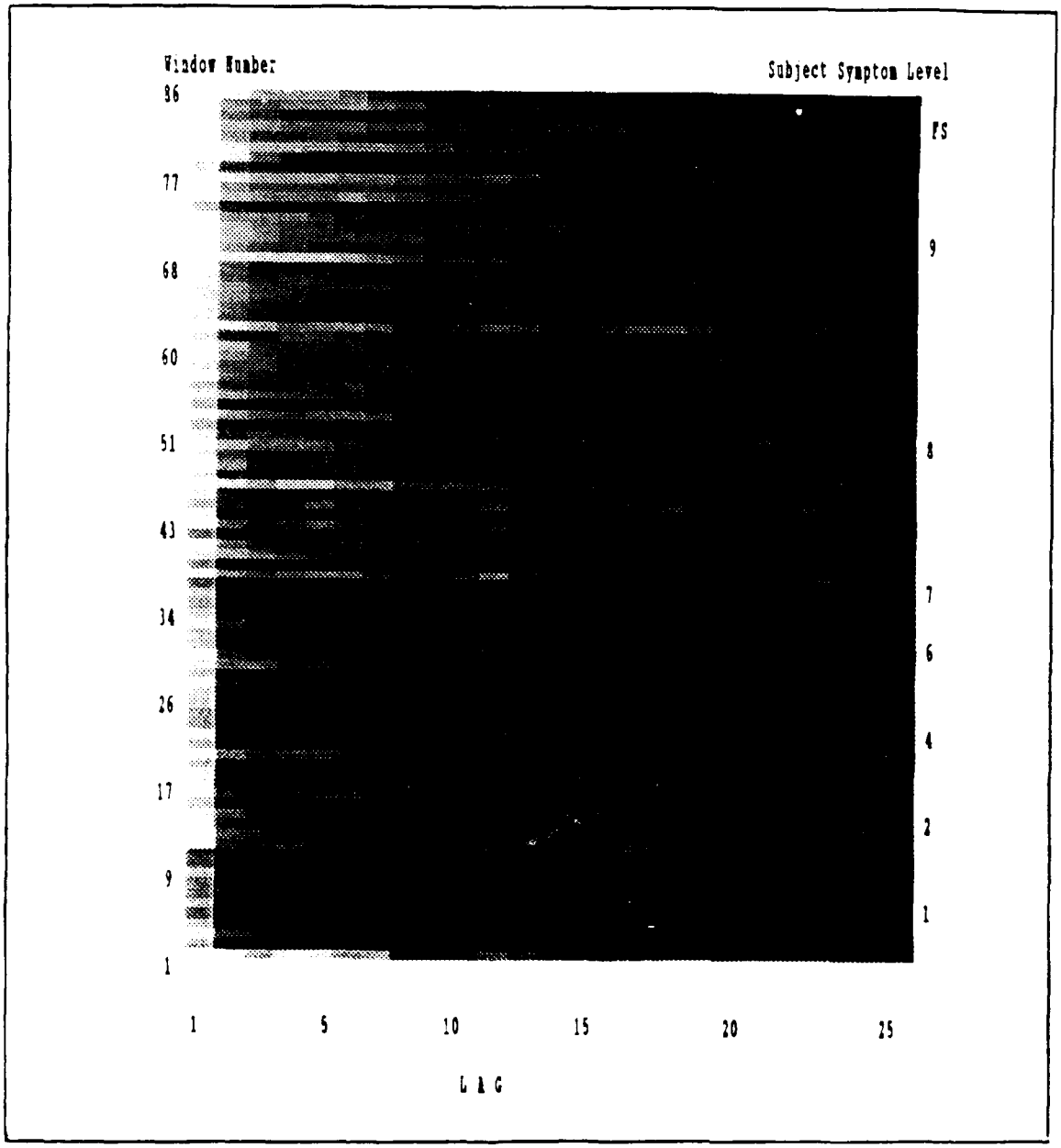

Figure 32. EEG2A WACF Image

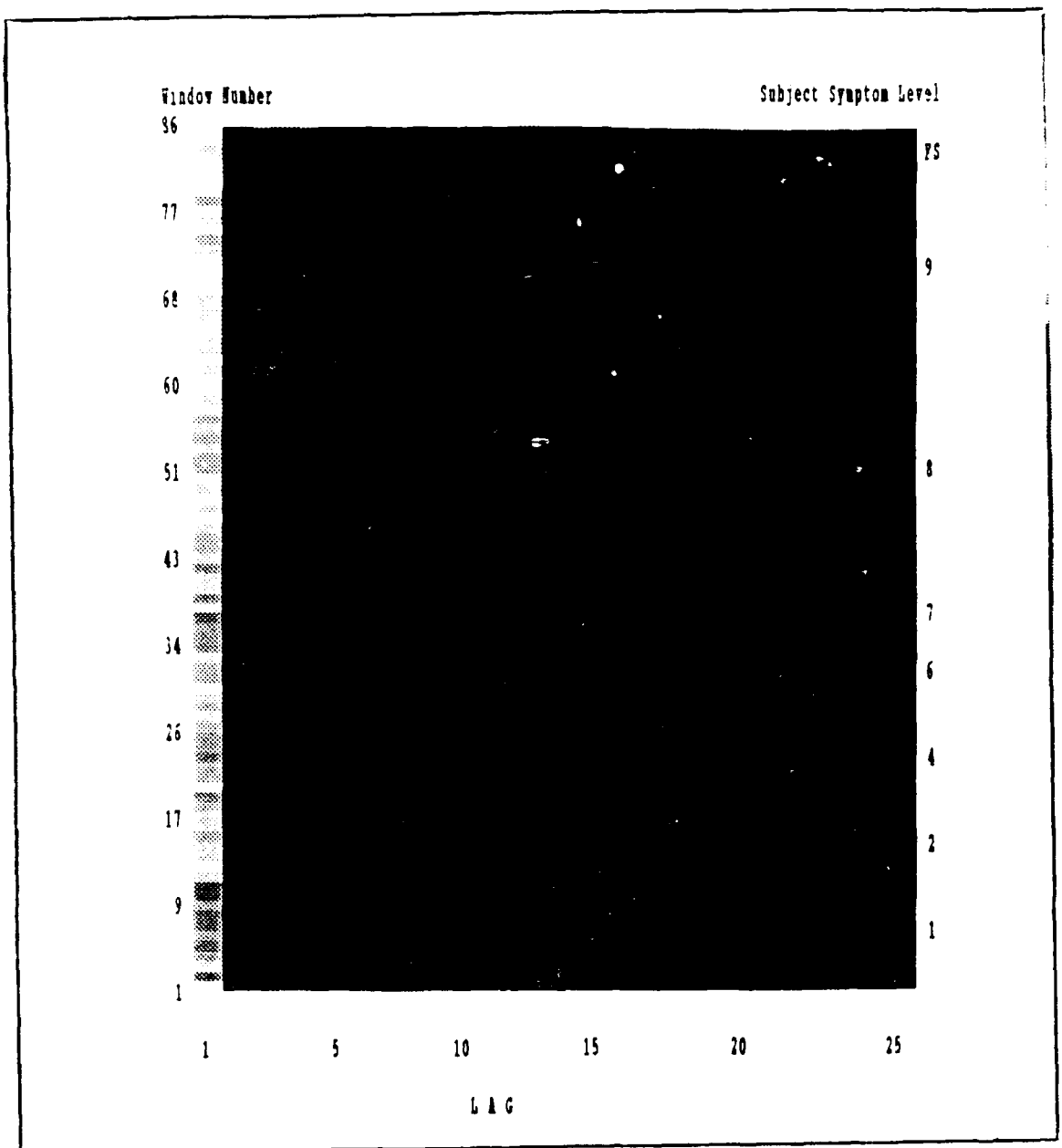

Figure 33. EEG2A WPACF Image

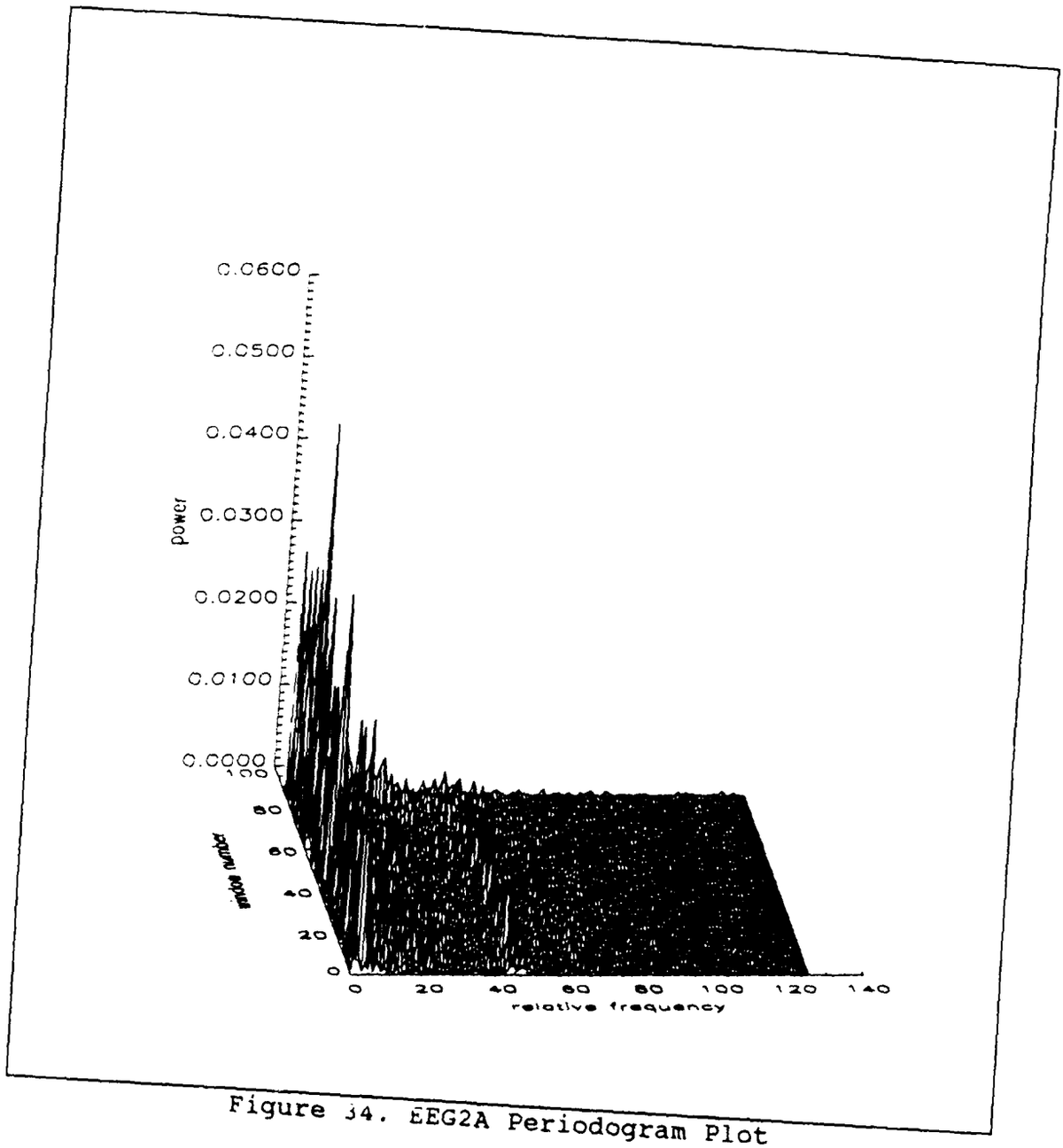

Figure 34. EEG2A Periodogram Plot

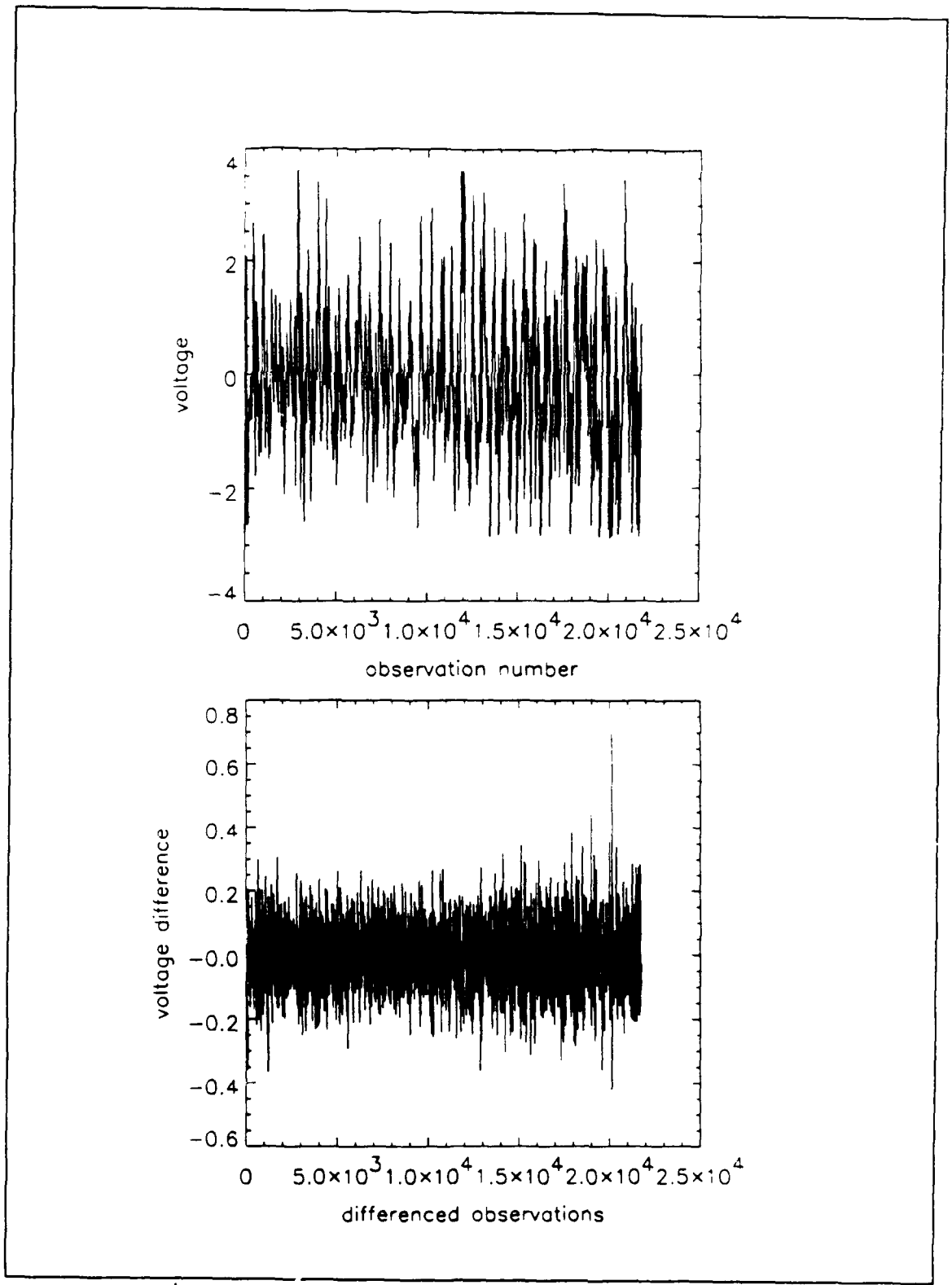

Figure 35. EEG2B Raw and Differenced Data

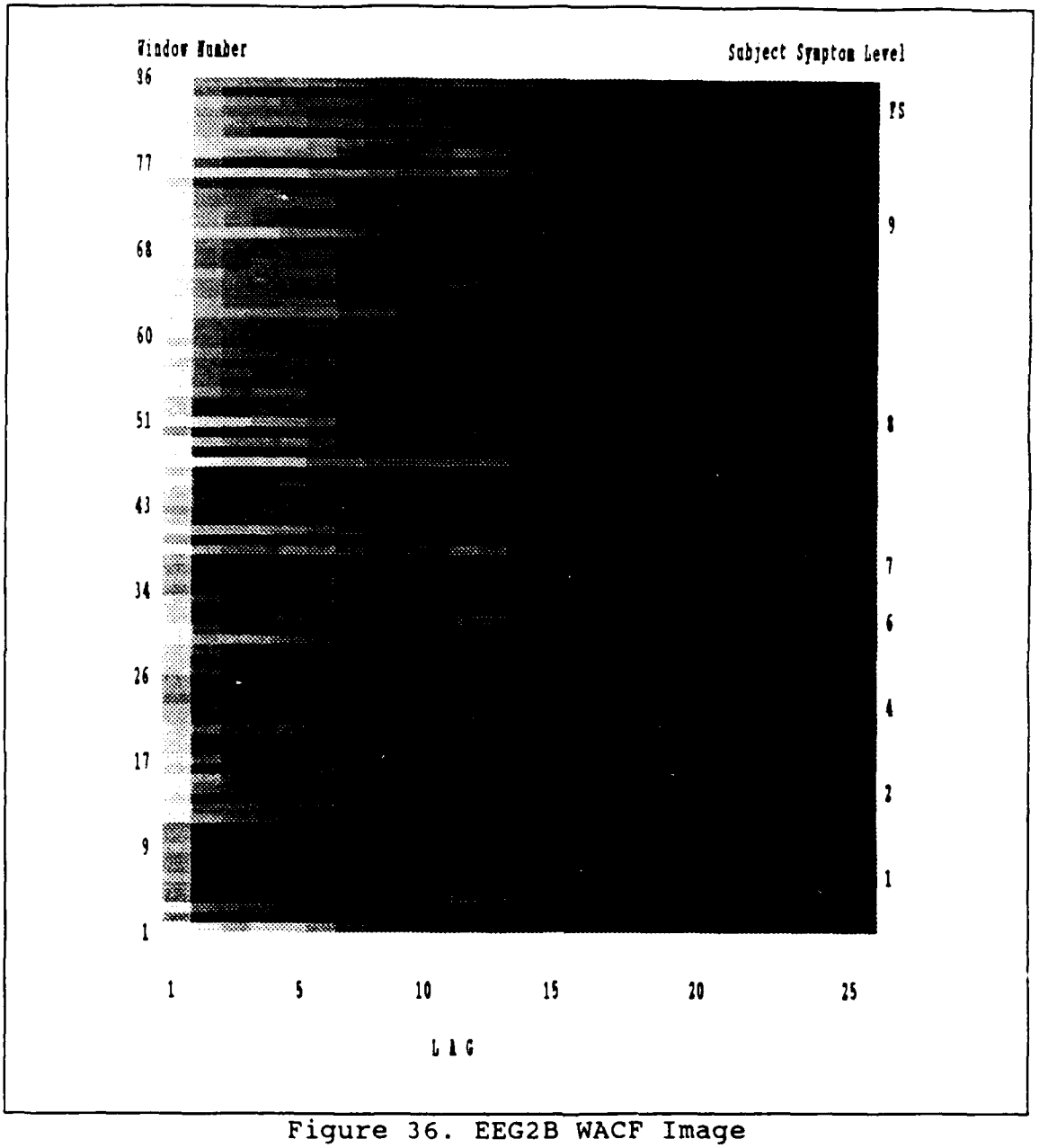

Figure 36. EEG2B WACF Image

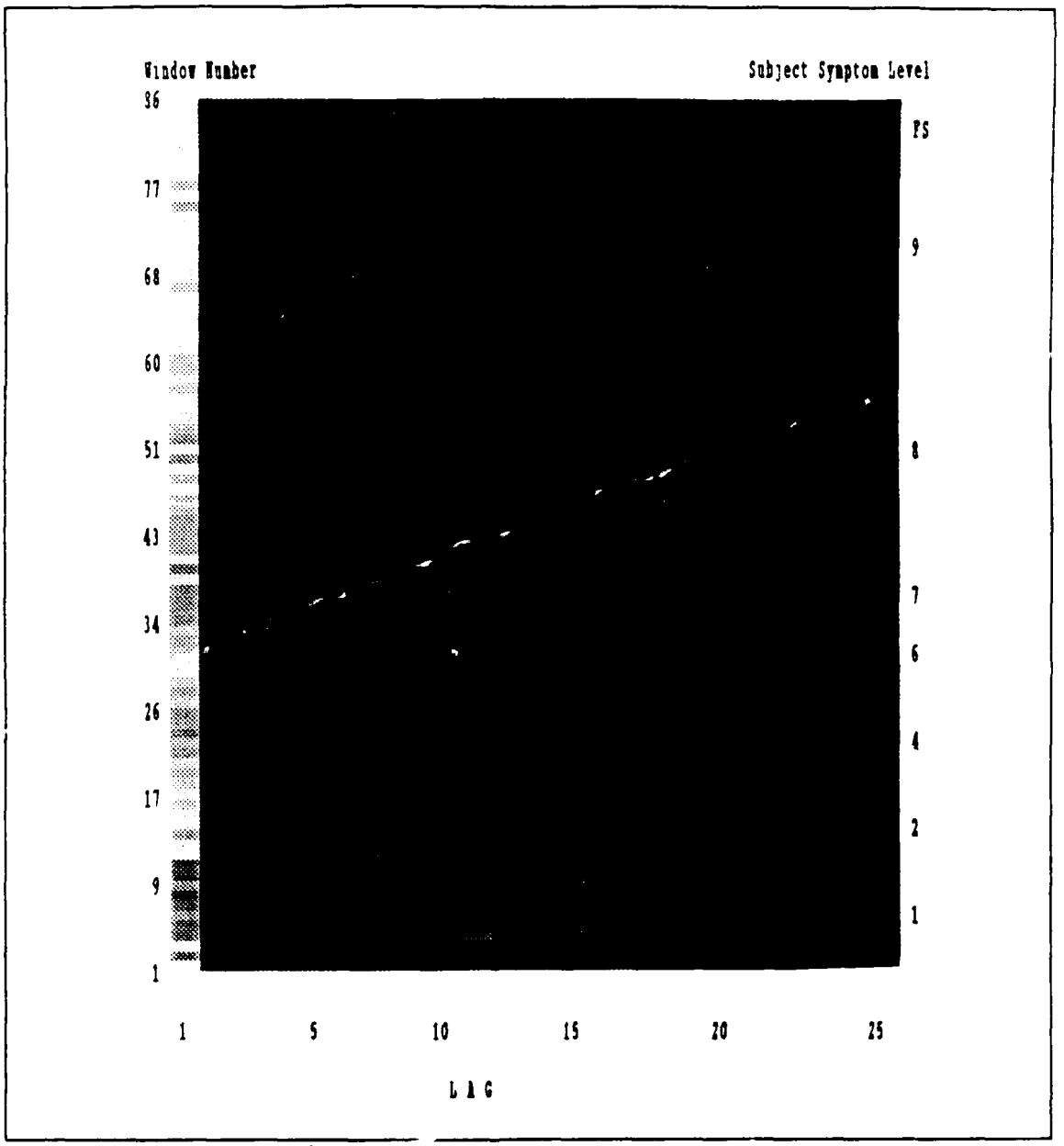

Figure 37. EEG2B WPACF Image

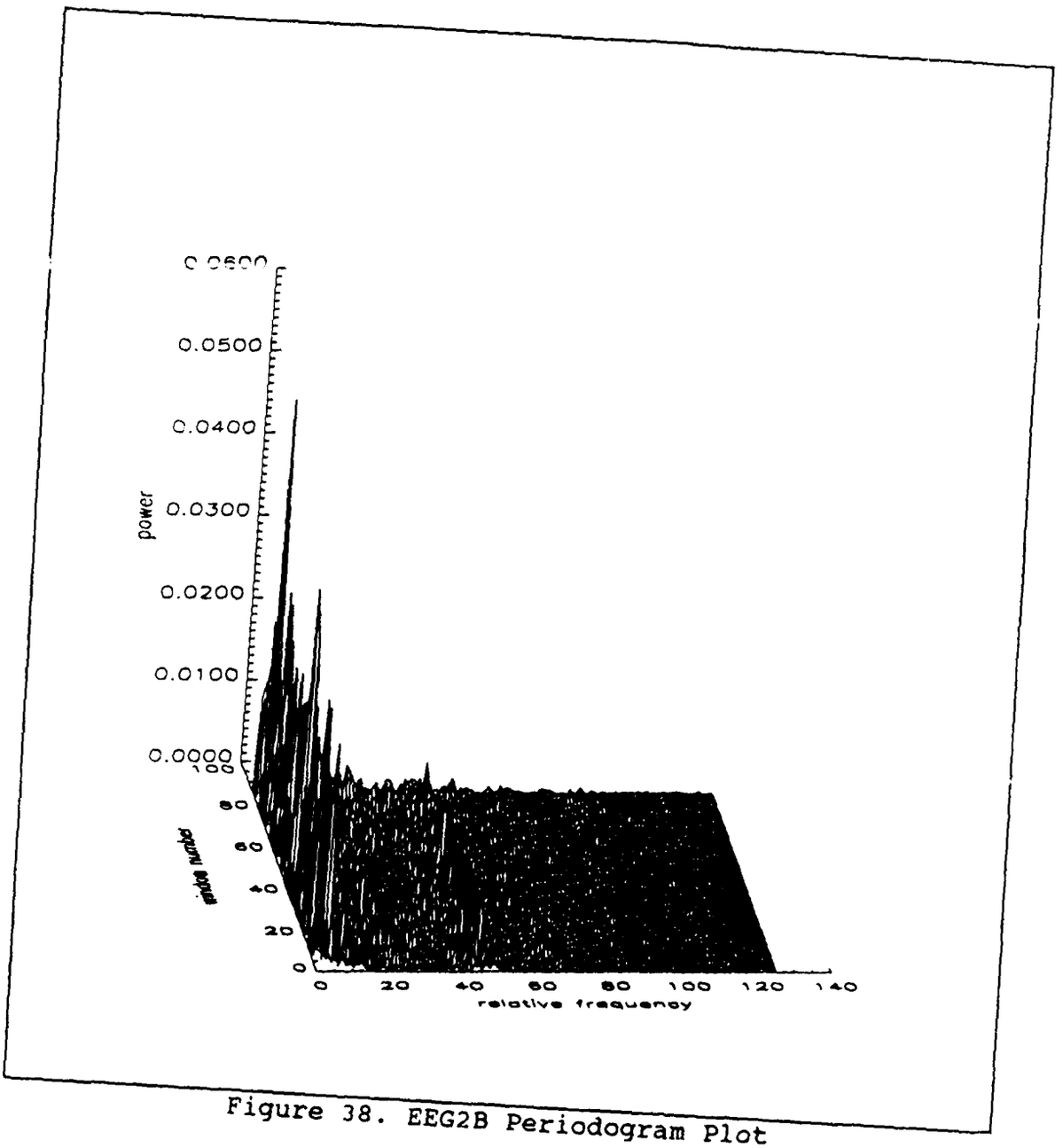

Figure 38. EEG2B Periodogram Plot

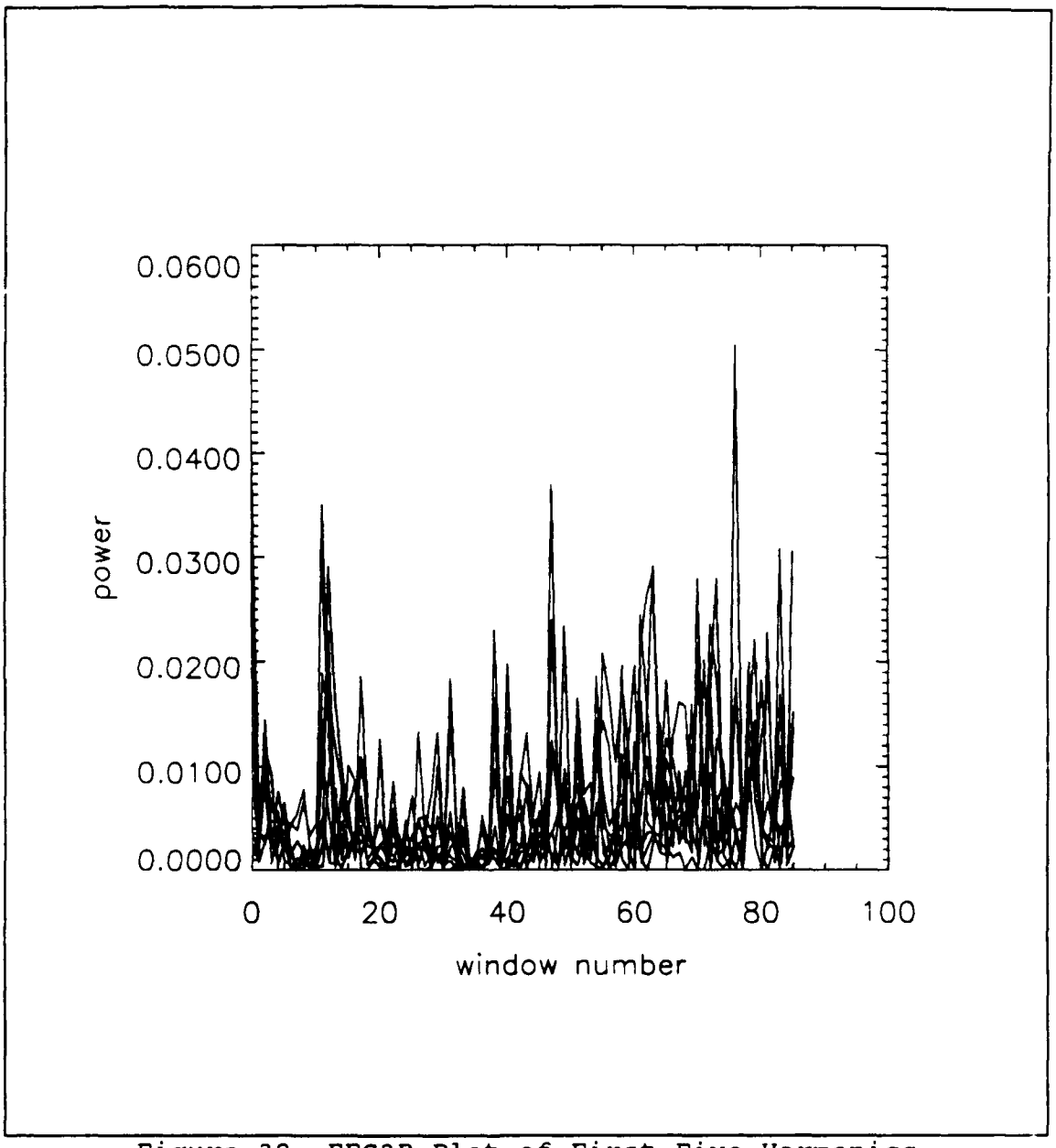

Figure 39. EEG2B Plot of First Five Harmonics

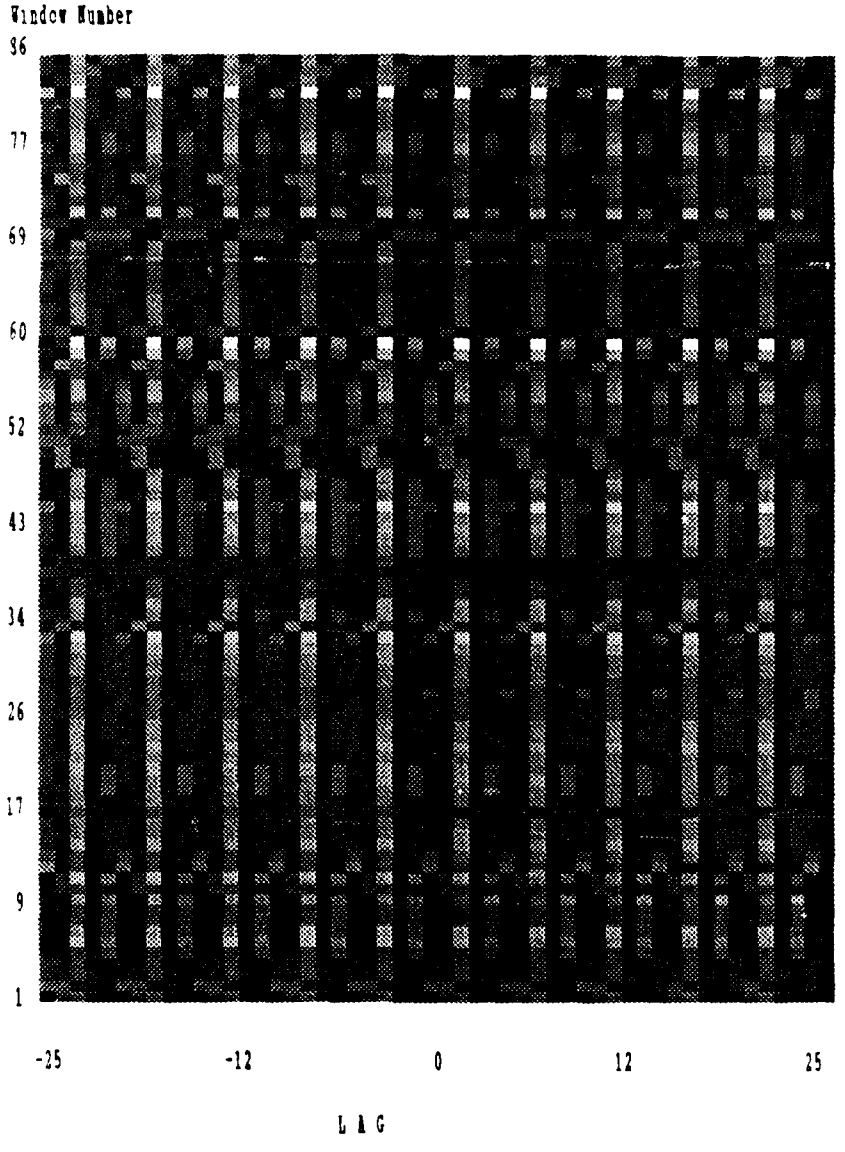

Figure 40. EEG1A-EEG1B WCCF Image

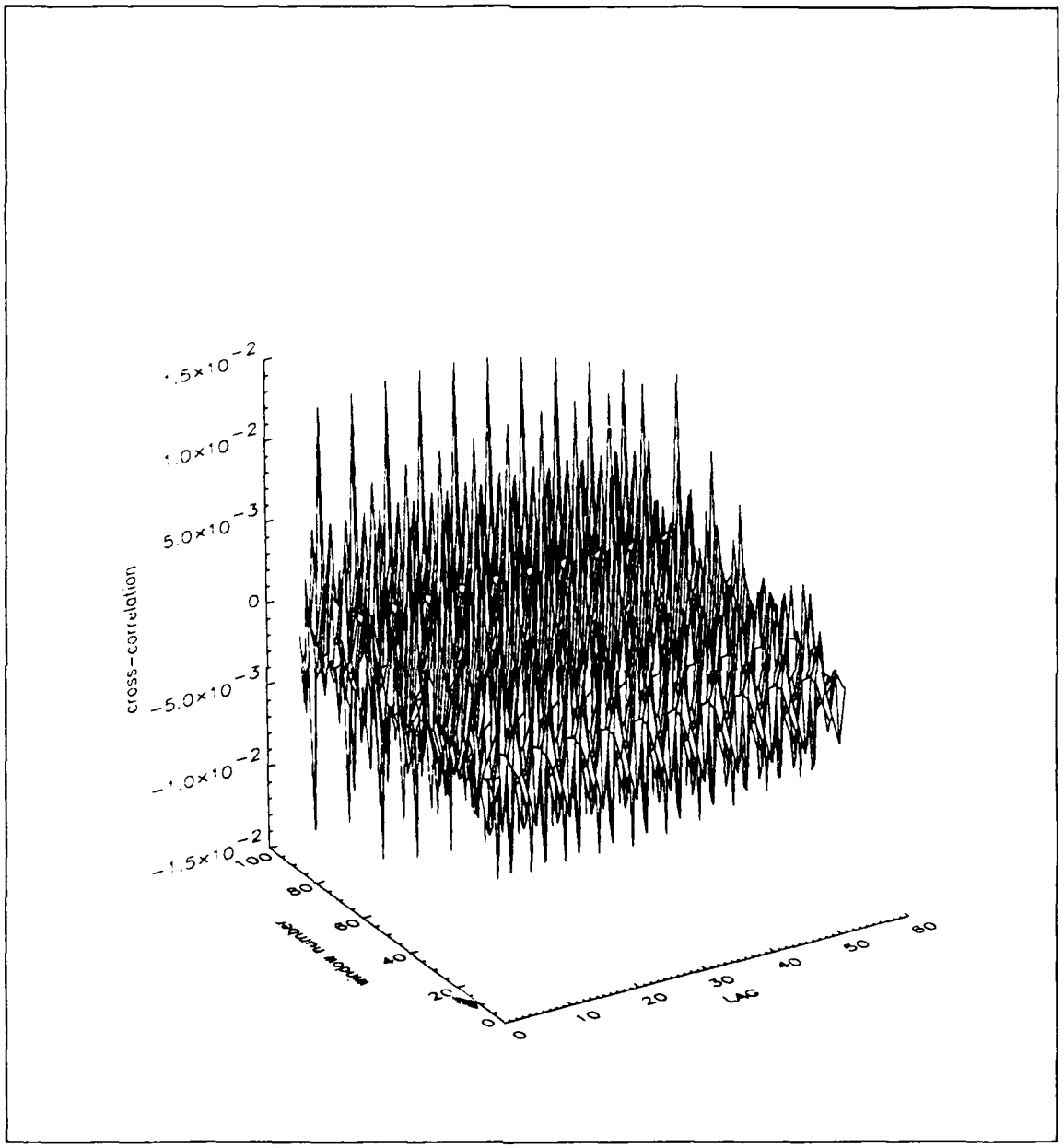

Figure 41. EEG1A-EEG1B WCCF Plot

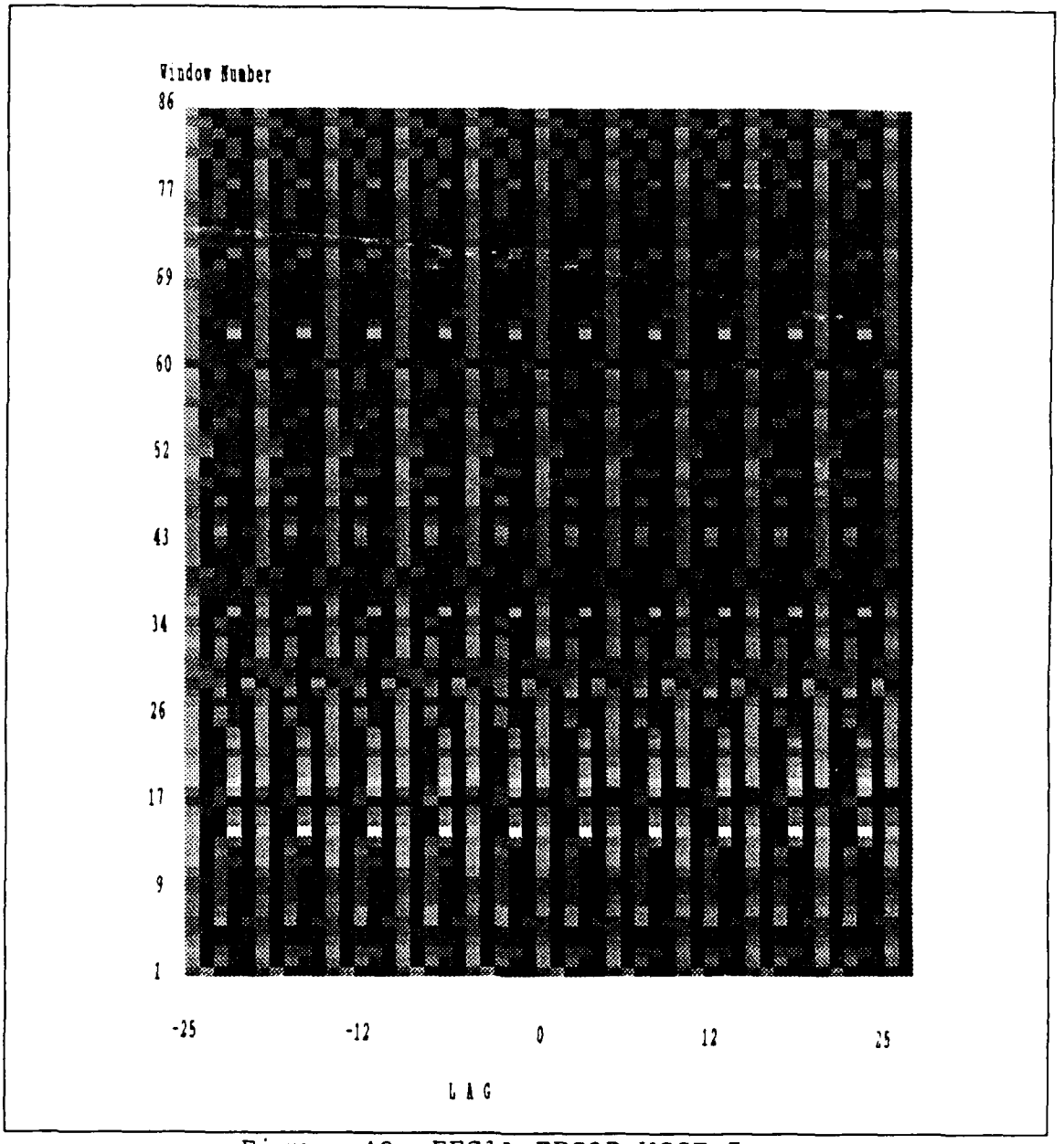

Figure 42. EEG1A-EEG2B WCCF Image

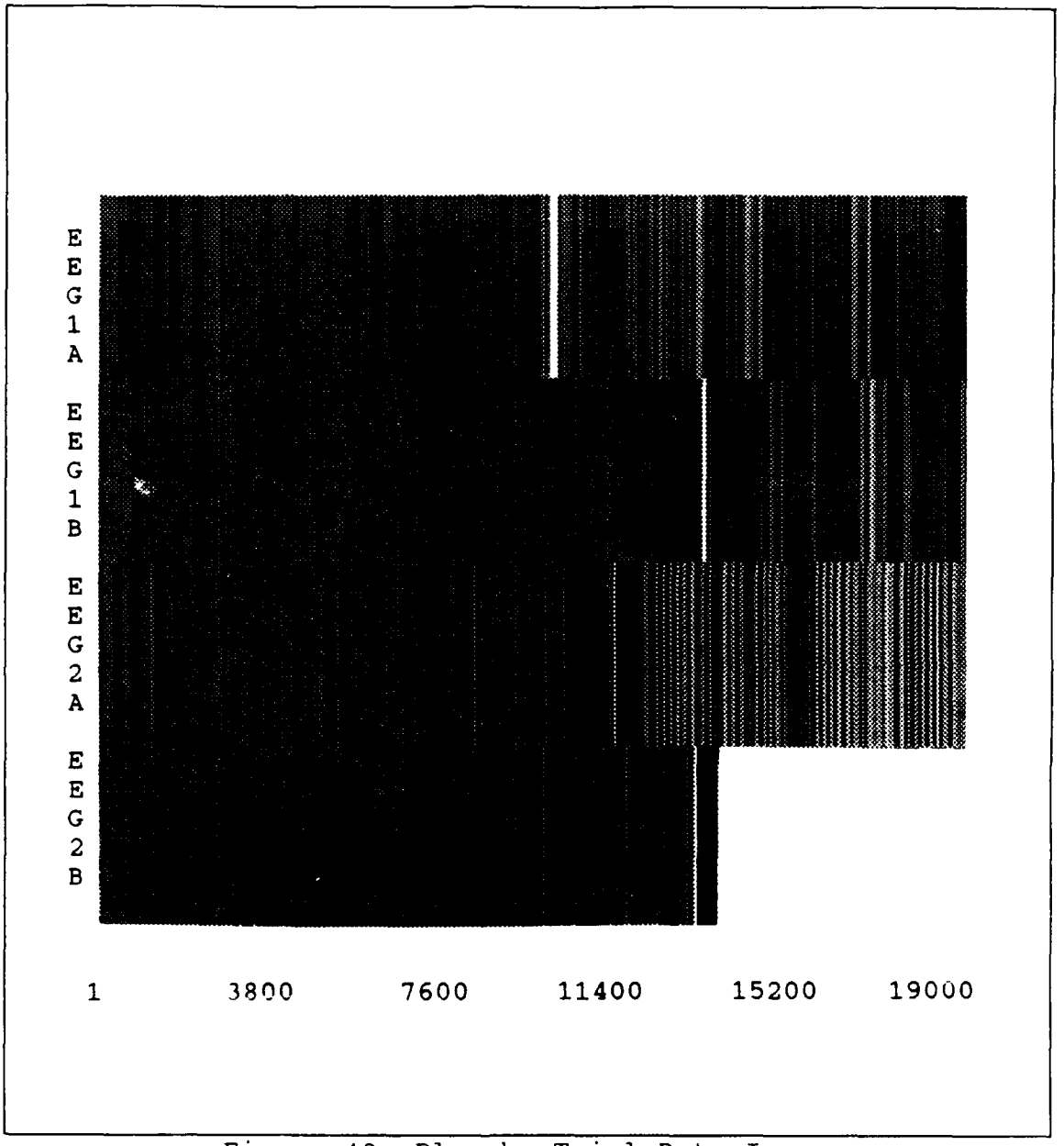

Figure 43. Placebo Trial Data Image

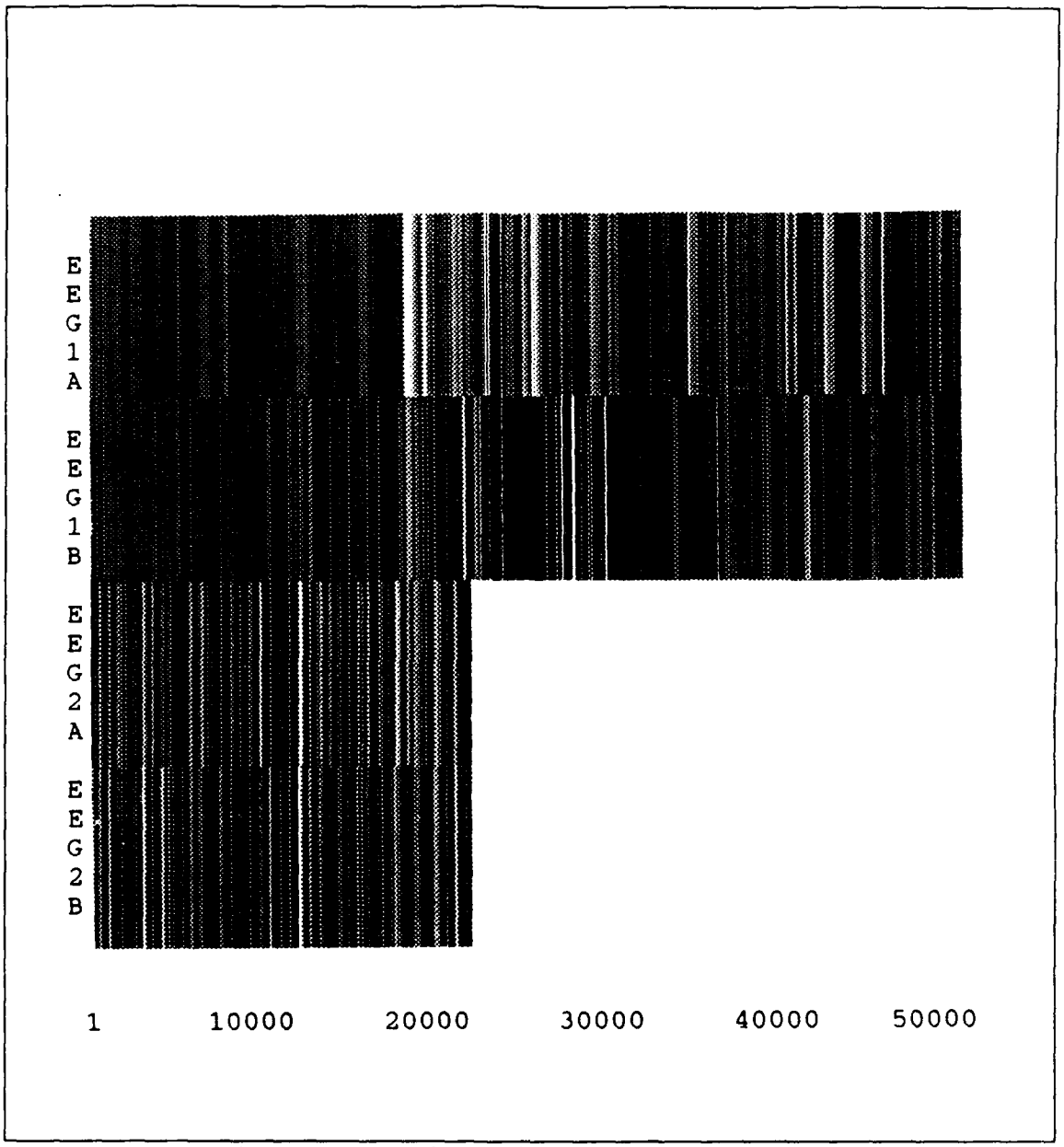

Figure 44. Dilantin Trial Data Image

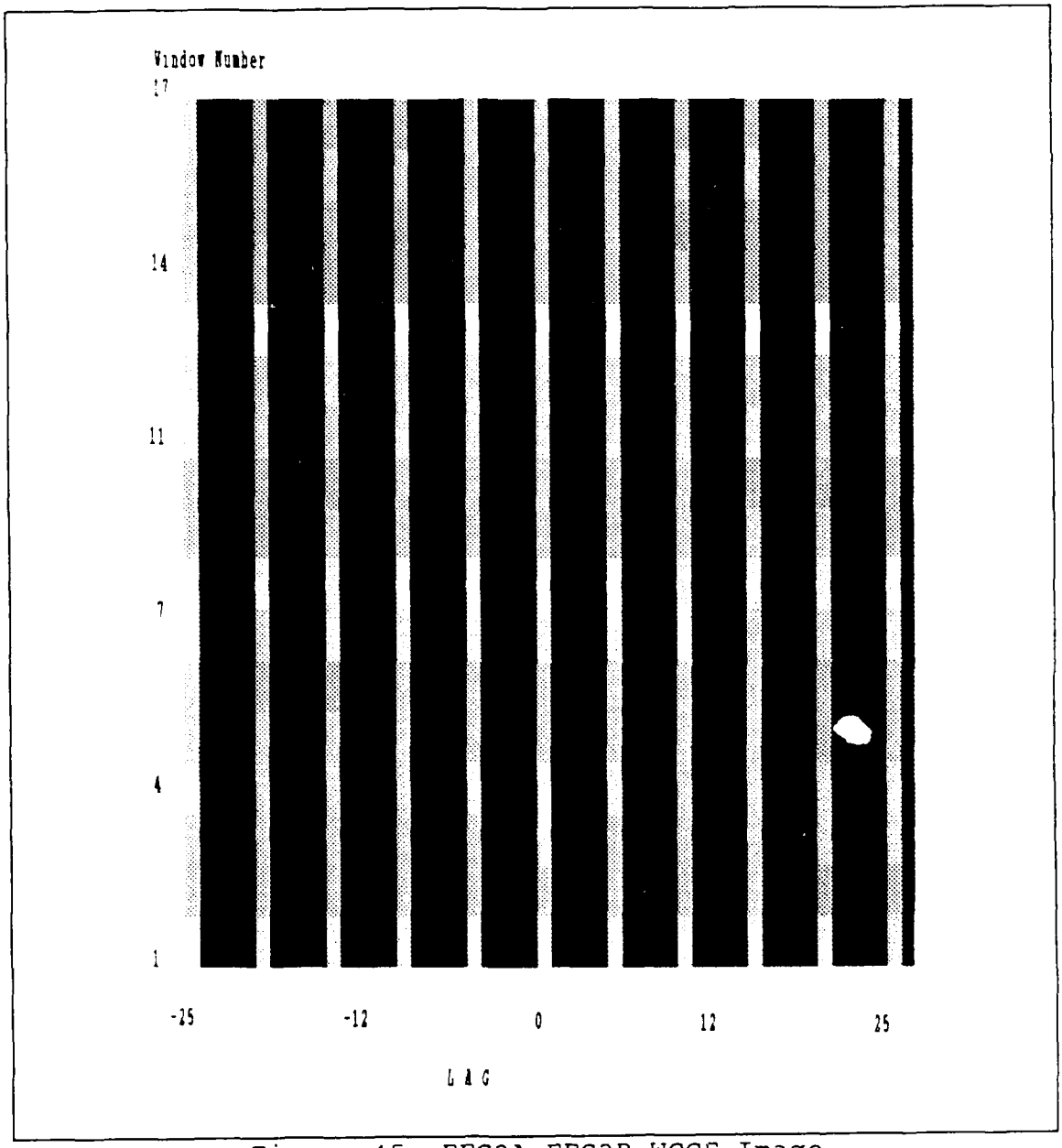

Figure 45. EEG2A-EEG2B WCCF Image

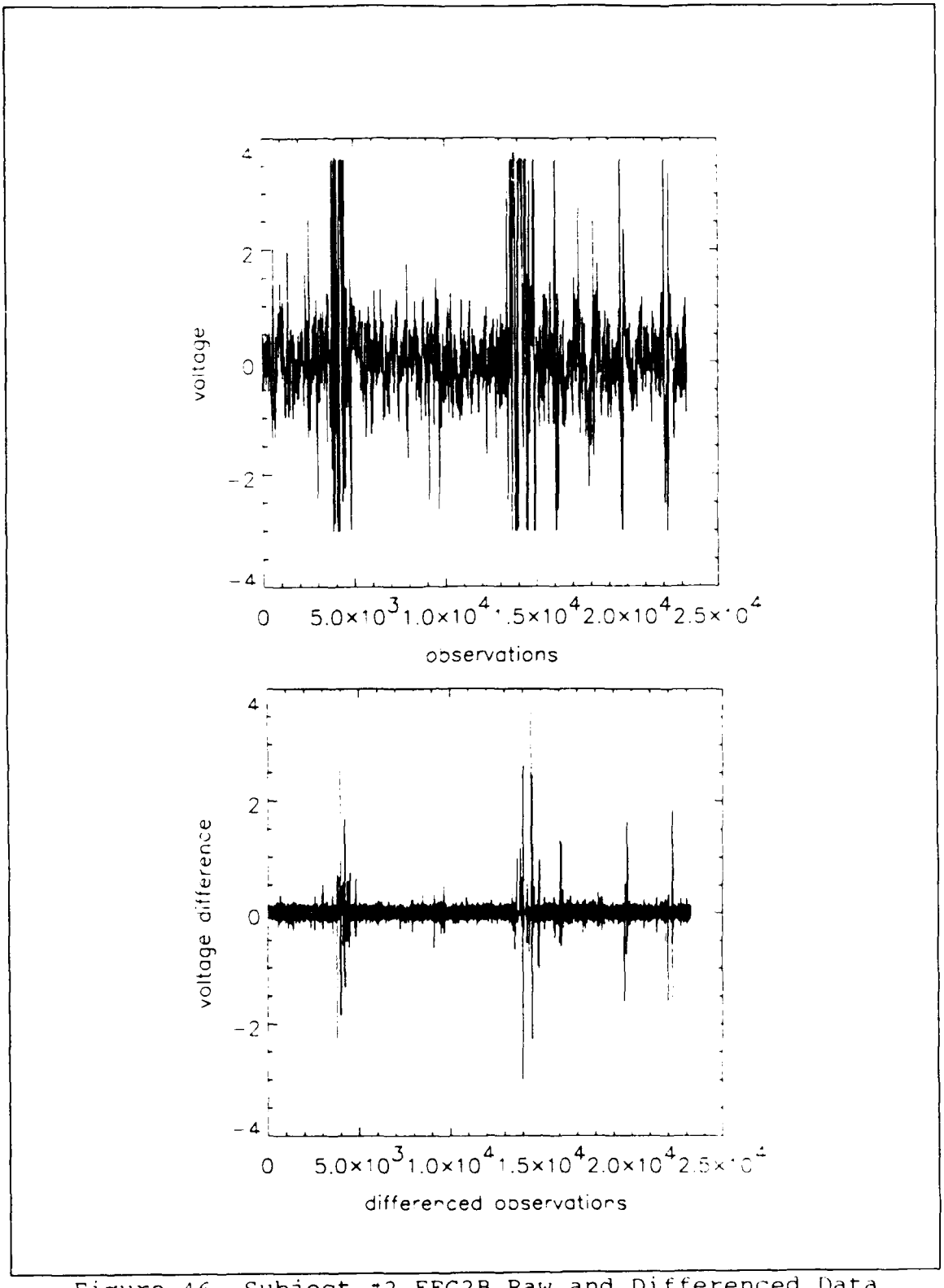

Figure 46. Subject #2 EEG2B Raw and Differenced Data

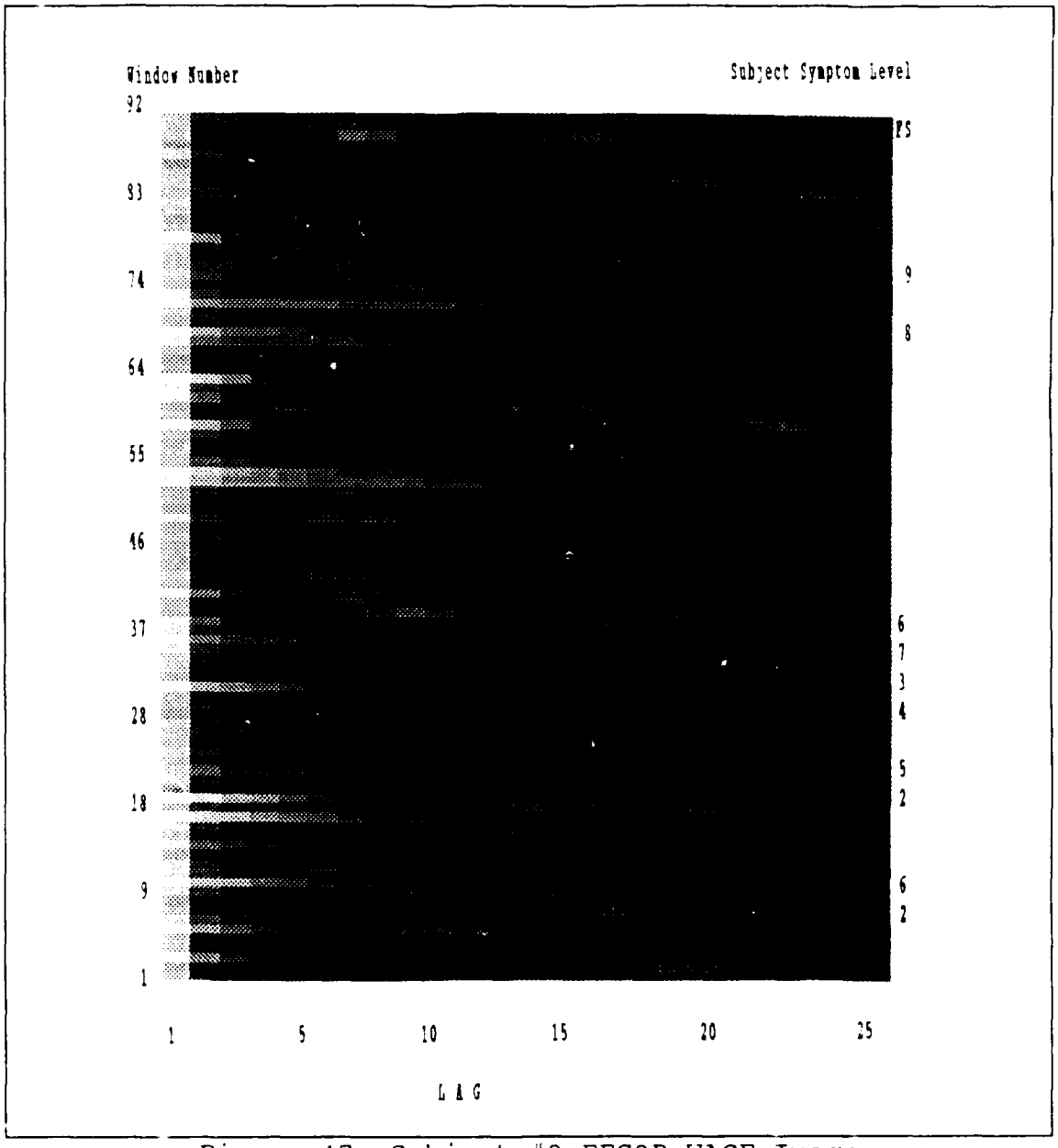

Figure 47. Subject #2 EEG2B WACF Image

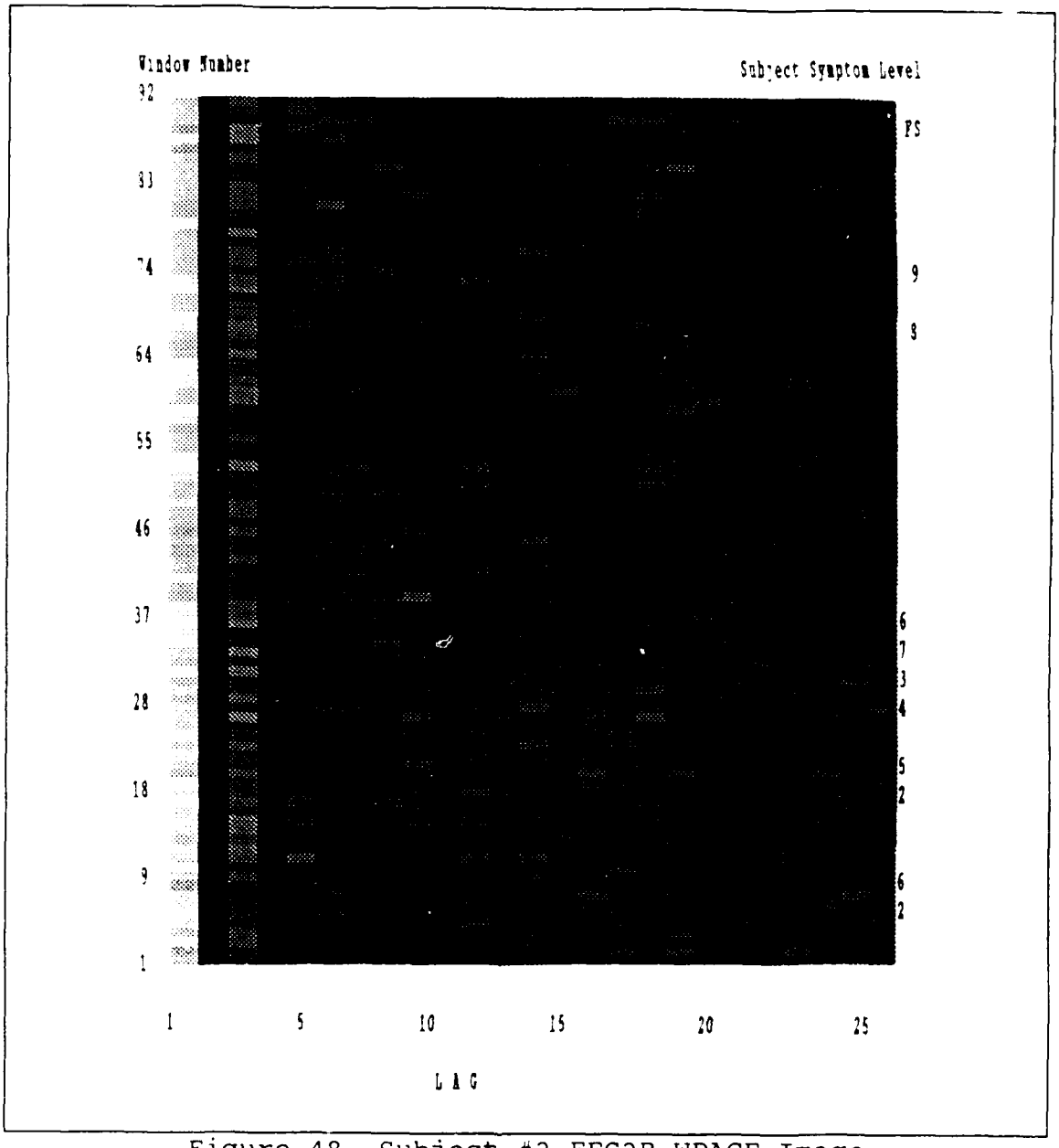

Figure 48. Subject #2 EEG2B WPACF Image

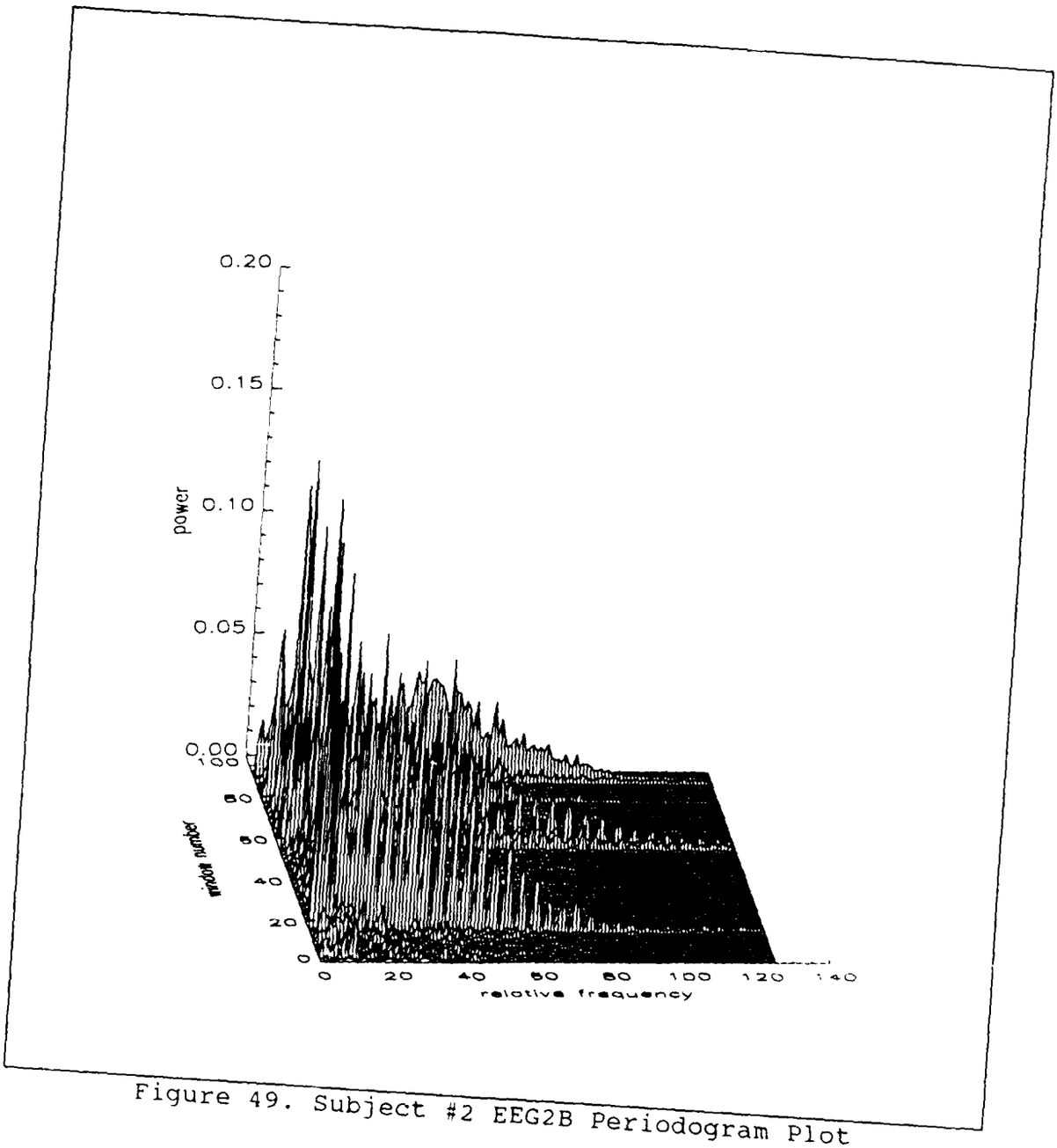

Figure 49. Subject #2 EEG2B Periodogram Plot

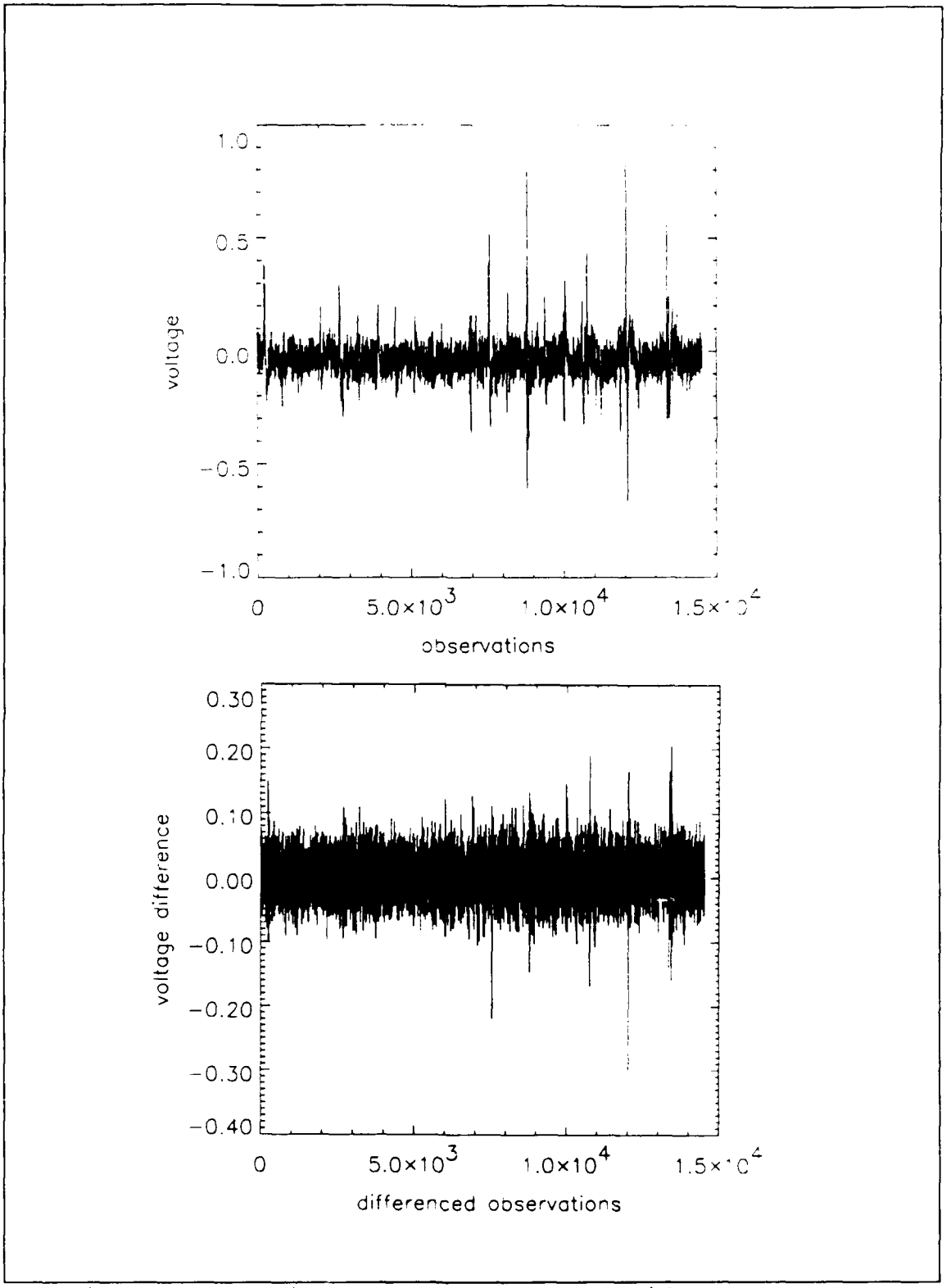

Figure 50. Subject #3 EEG1B Raw and Differenced Data

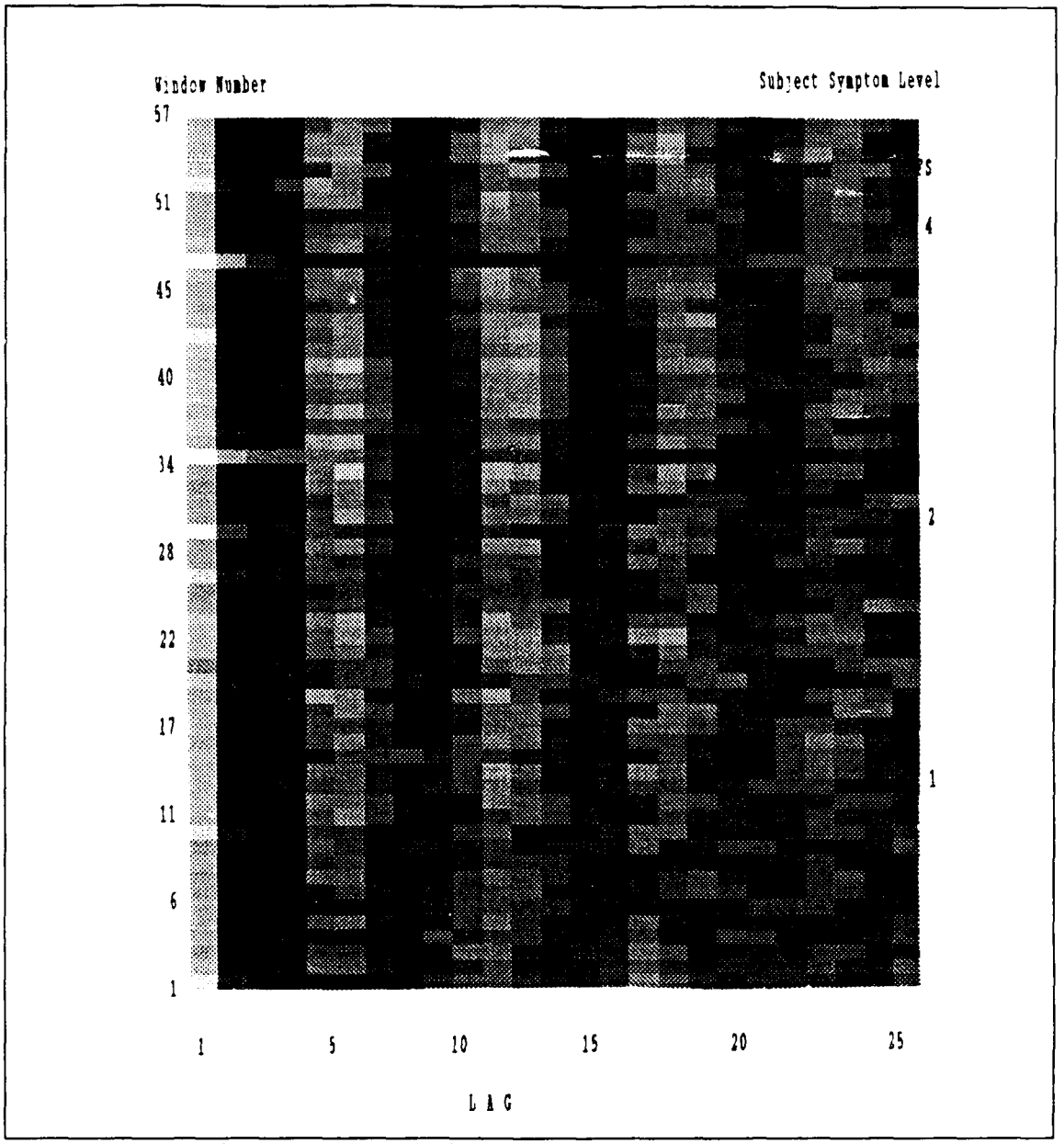

Figure 51. Subject #3 EEG1B WACF Image

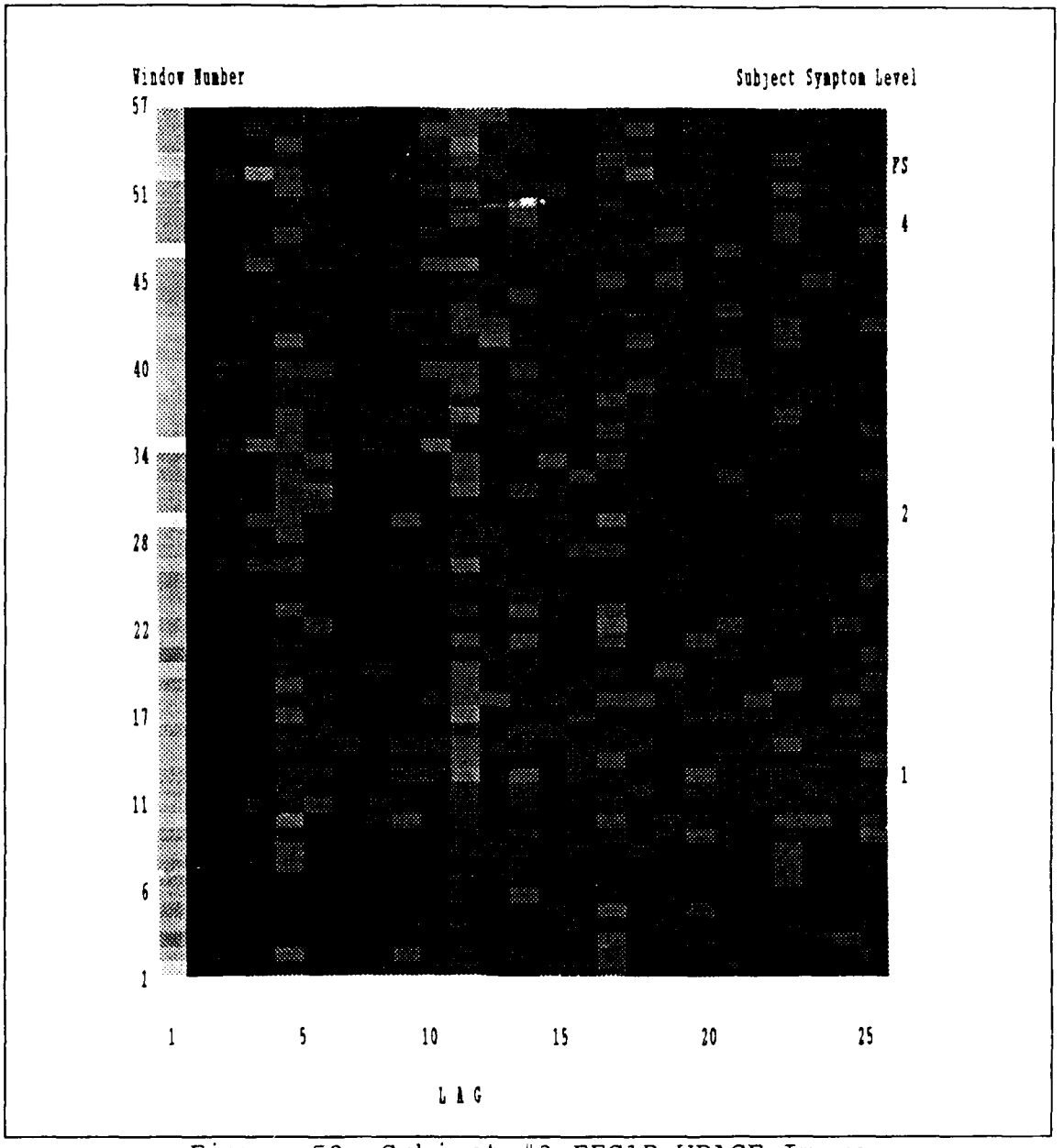

Figure 52. Subject #3 EEG1B WPACF Image

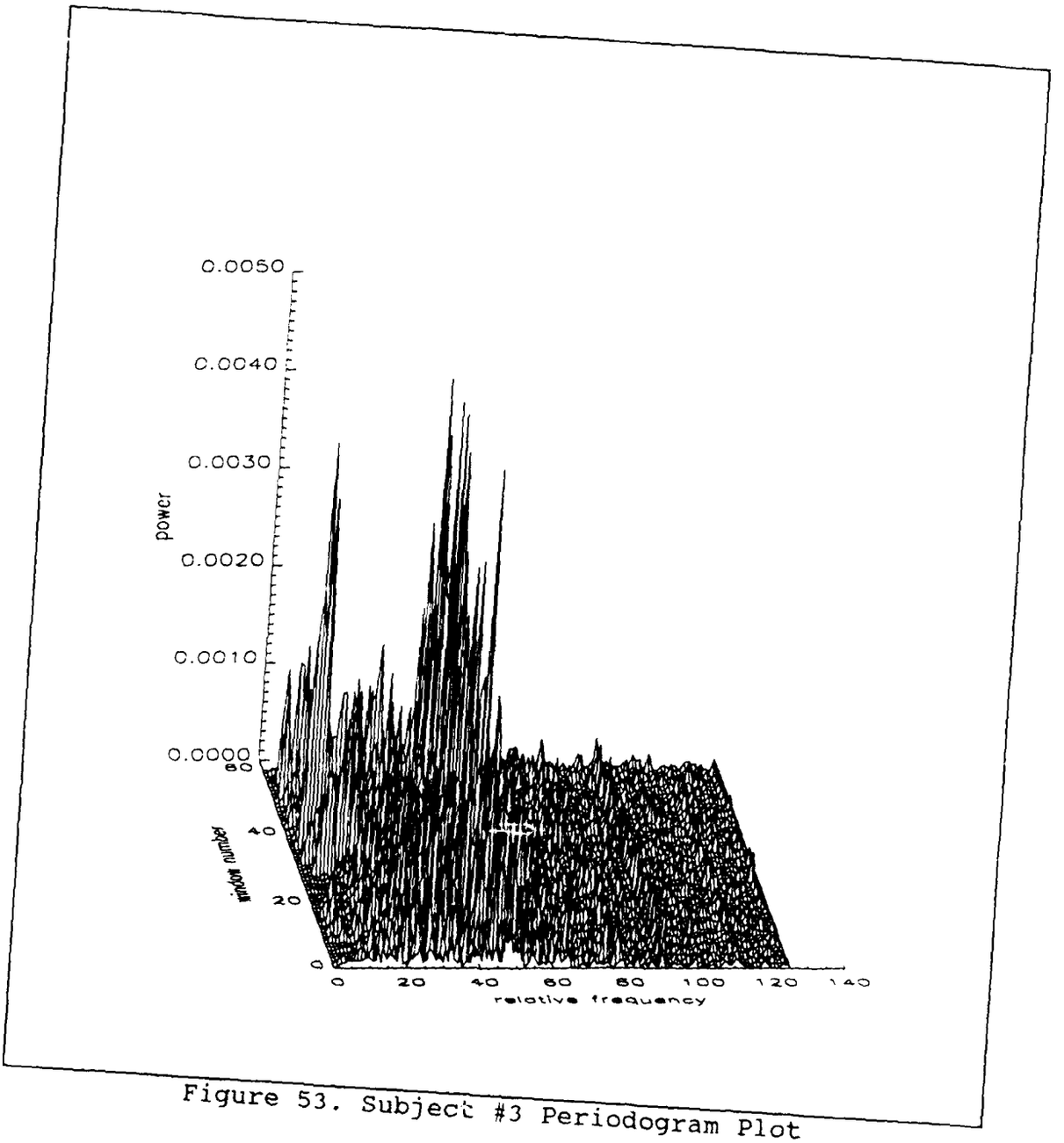

Figure 53. Subject #3 Periodogram Plot

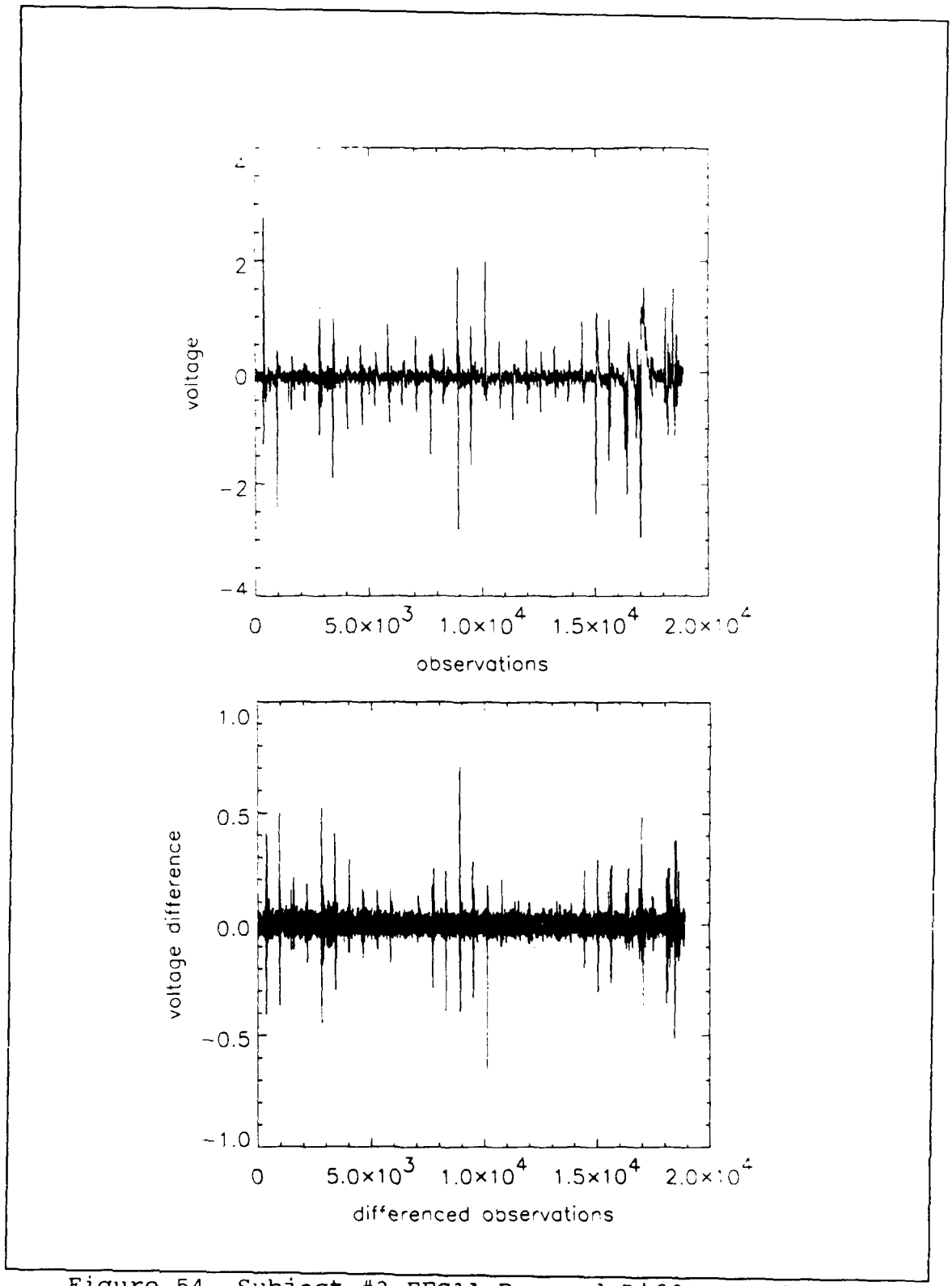

Figure 54. Subject #3 EEG1A Raw and Differenced Data

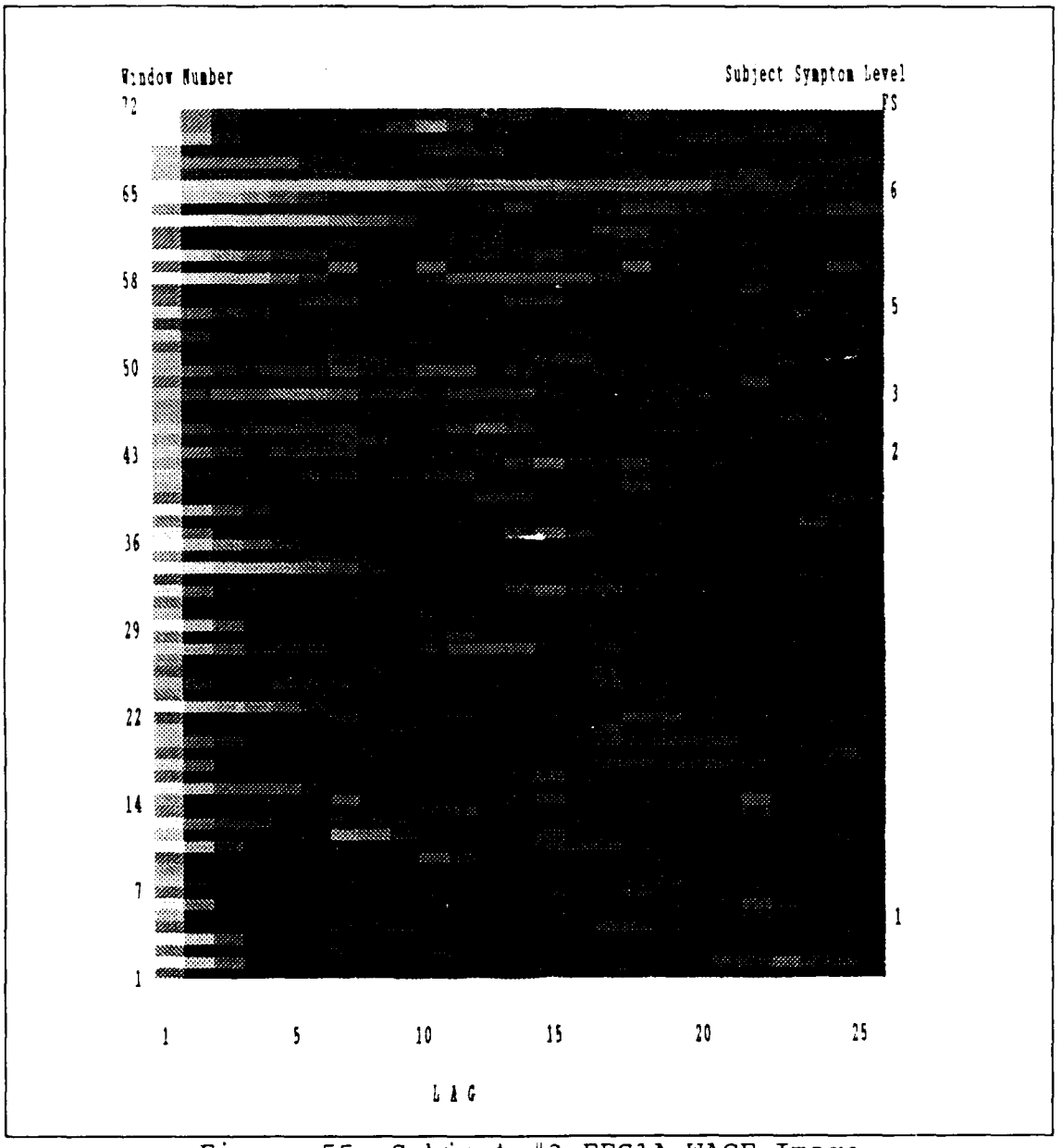

Figure 55. Subject #3 EEG1A WACF Image

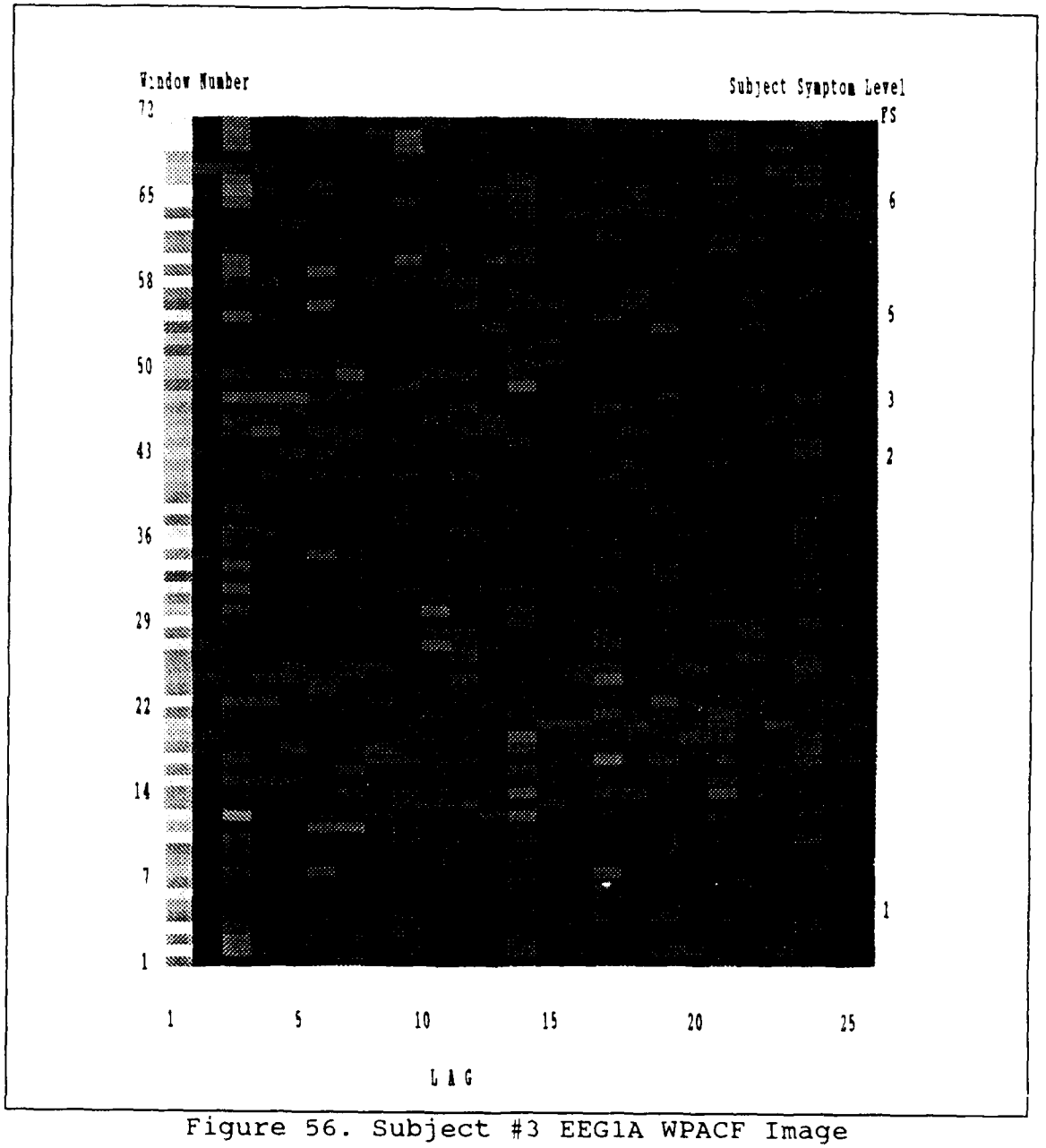

Figure 56. Subject #3 EEG1A WPACF Image

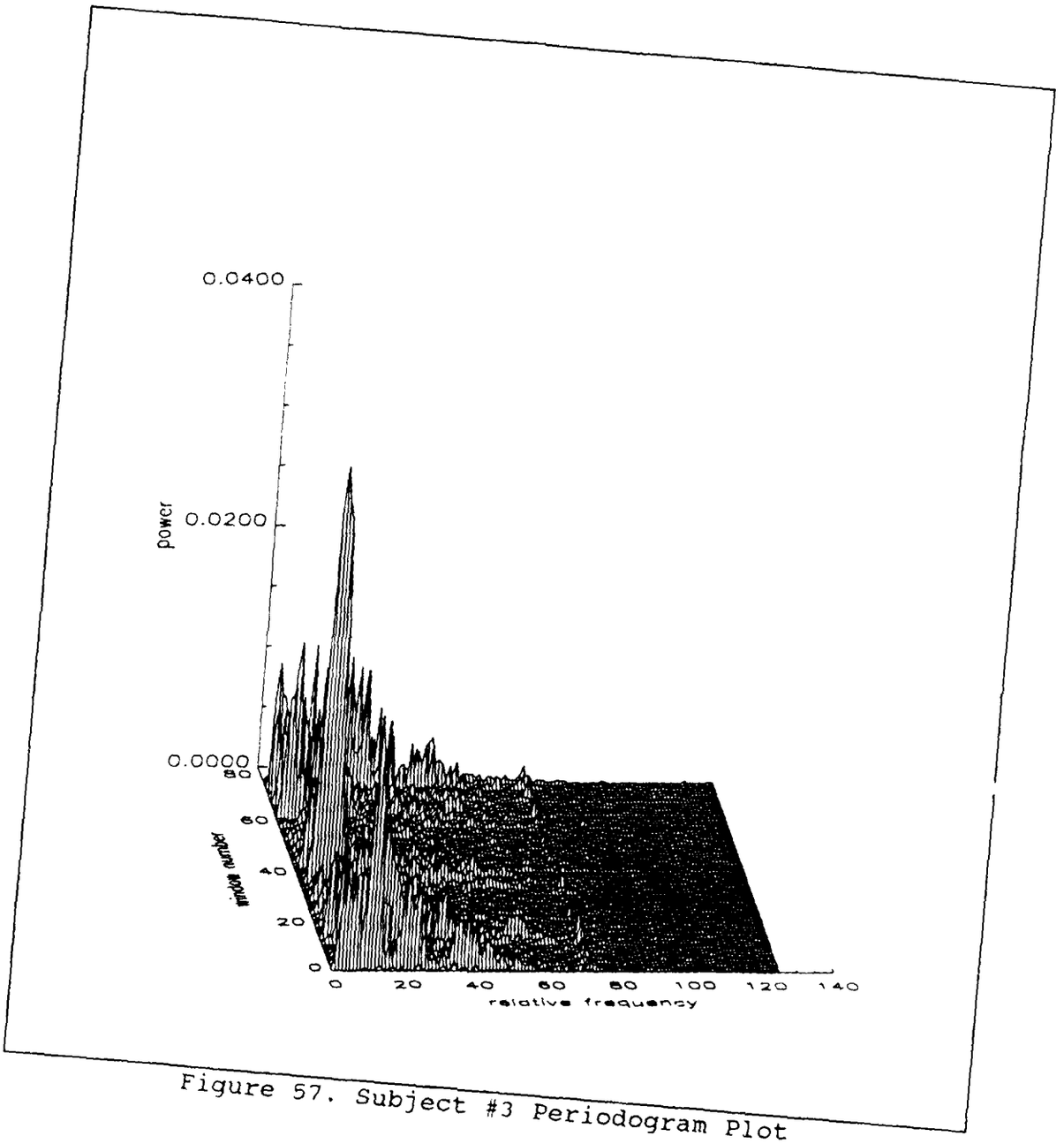

Figure 57. Subject #3 Periodogram Plot

Bibliography

1. Bowerman, Bruce L. and Richard T. O'Connell. Time Series Forecasting: Unified Concepts and Computer Implementation. Boston: Duxbury Press, 1987

2. Box, George E. P. and Gwilym M. Jenkins. Time Series Analysis Forecasting and Control. Oakland: Holden-Day, 1976

3. Chelen, Dr. William. Research Contractor, AFIT/ENG. Personal conversations. AFIT/EN, Wright-Patterson AFB OH, March-April, 1989.

4. Chelen, Dr. William et al. "Electroencephalographic Changes During Motion Sickness," Unpublished article. AFIT/EN, Wright-Patterson AFB OH, 1987.

5. Cohen, Arnon. Biomedical Signal Processing. Boca Raton: CRC Press, 1986

6. Cowings, Patricia S. et al. "General Autonomic Components of Motion Sickness," Psychophysiology, 23: 542-551 (May 1986)

7. Fix, Edward L. Motion Sickness: Quantitative, Algorithmic Malaise Indication in Real Time. MS Thesis AFIT/GE/ENG/87D-18. School of Engineering, Air Force Institute of Technology (AU), Wright-Patterson AFB OH, December 1987. (AD number not available).

8. Glaser, Edmund M. and Daniel S. Ruchkin. Principles of Neurobiological Signal Analysis. New York: Academic Press, 1976.

9. Isaksson, Anders et al. "Computer Analysis of EEG Signals with Parametric Models," Proceedings of the IEEE, 69: 451-460 (April 1981)

10. Kabrisky, Matthew. Professor, AFIT/ENG. Personal conversations, AFIT/EN, Wright-Patterson AFB OH, Oct-Nov 1989

11. McPherson, Michael R. Collection and Statistical Analysis of Biophysical Data to Predict Motion Sickness Incidence. MS Thesis AFIT/GCS/ENG/86D-2J. School of Engineering, Air Force Institute of Technology (AU), Wright-Patterson AFB OH, December 1986. (AD-A178874)

12. Morales, Rogelio Jr. A New Perspective in the Etiology, Treatment, Prevention and Prediction of Space Motion Sickness. MS Thesis AFIT/GSO/ENG/88D-2. School of Engineering, Air Force Institute of Technology (AU), Wright-Patterson AFB OH, December 1988.

13. Priestley, M. B. Spectral Analysis and Time Series. London: Academic Press, 1981

14. Scott, Capt Mark F. A Study of Motion Sickness: Mathematical Modeling and Data Analysis. MS Thesis AFIT/GEO/ENG/88D-4. School of Engineering, Air Force Institute of Technology (AU), Wright-Patterson AFB OH, December 1988. (AD number not available).

Vita

Captain David C. Thompson [redacted] He graduated from Fairborn Baker High School in Fairborn Ohio in June 1979. He received his A.B. degree in Mathematics from Washington University in Saint Louis in May 1983. He was commissioned a second lieutenant in the United States Air Force in May 1983. His first assignment on active duty was with the North American Aerospace Defense Command (NORAD) at the Cheyenne Mountain Complex, Colorado. After working in the Norad Space Surveillance Center (NSSC) he was assigned to the Training and Exercise division in May 1985.

He was assigned to the Air Force Institute of Technology at Wright-Patterson AFB, Ohio in May 1988.

[redacted]

Unclassified
SECURITY CLASSIFICATION OF THIS PAGE

REPORT DOCUMENTATION PAGE

Form Approved
OMB No. 0704-0188

1a. REPORT SECURITY CLASSIFICATION Unclassified	1b. RESTRICTIVE MARKINGS
2a. SECURITY CLASSIFICATION AUTHORITY	3. DISTRIBUTION / AVAILABILITY OF REPORT Approved for public release; distribution unlimited.
2b. DECLASSIFICATION / DOWNGRADING SCHEDULE	
4. PERFORMING ORGANIZATION REPORT NUMBER(S) AFIT/GSO/ENS/89d-15	5. MONITORING ORGANIZATION REPORT NUMBER(S)
6a. NAME OF PERFORMING ORGANIZATION School of Engineering 6b. OFFICE SYMBOL (If applicable) AFIT/ENS	7a. NAME OF MONITORING ORGANIZATION
6c. ADDRESS (City, State, and ZIP Code) Air Force Institute of Technology Wright Patterson AFB, OH 45433	7b. ADDRESS (City, State, and ZIP Code)
8a. NAME OF FUNDING / SPONSORING ORGANIZATION 8b. OFFICE SYMBOL (If applicable)	9. PROCUREMENT INSTRUMENT IDENTIFICATION NUMBER
8c. ADDRESS (City, State, and ZIP Code)	10. SOURCE OF FUNDING NUMBERS PROGRAM ELEMENT NO. / PROJECT NO. / TASK NO / WORK UNIT ACCESSION NO.

11. TITLE (Include Security Classification)
An Exploratory Analysis of Motion Sickness Data: A Time Series Approach

12. PERSONAL AUTHOR(S)
Thompson, David Clinton, A.B., Capt USAF

13a. TYPE OF REPORT	13b. TIME COVERED	14. DATE OF REPORT (Year, Month, Day)	15. PAGE COUNT
MS Thesis	FROM _____ TO _____	1989 December	148

16. SUPPLEMENTARY NOTATION

17. COSATI CODES			18. SUBJECT TERMS (Continue on reverse if necessary and identify by block number)
FIELD	GROUP	SUB-GROUP	Time Series Analysis, Autocorrelation Function Periodogram, Motion Sickness, Dilantin
12	01		
06	10		

19. ABSTRACT (Continue on reverse if necessary and identify by block number)

Thesis Chairman: James Robinson, PhD. (Lt Col)
Proffessor of Operational Sciences
Department of Operational Sciences

(Abstract on Back)

20. DISTRIBUTION / AVAILABILITY OF ABSTRACT ☒ UNCLASSIFIED/UNLIMITED ☐ SAME AS RPT ☐ DTIC USERS	21. ABSTRACT SECURITY CLASSIFICATION Unclassified
22a. NAME OF RESPONSIBLE INDIVIDUAL James Robinson, PhD, Lt Col	22b. TELEPHONE (Include Area Code) (513) 255-3362 22c. OFFICE SYMBOL AFIT/ENS

DD Form 1473, JUN 86 *Previous editions are obsolete.* SECURITY CLASSIFICATION OF THIS PAGE

Block 19. Abstract

A methodology was developed in order to characterize the prodigious amount of electroencephalographic (EEG) data collected during motion sickness experiments at the Air Force Institute of Technology. The analog data are sampled and digitized into a time series. Stationarity transformations and a windowing operation are performed on the data to produce local areas of stationarity.

Windowed versions of the autocorrelation function, partial autocorrelation function and periodogram are discussed and employed. The windows are analyzed over time in order to view the underlying structure of the model that is hidden in the data. These functions are converted into image files to aid interpretation. The images are directly interpreted for model determination, model changes, artifact assessment and stationarity determination.

A primary subject and two confirming subjectsare analyzed. Both a placebo trial and Dilantin trial were analyzed for each subject to determine the nature of motion sickness and the efficacy of the drug treatment. The results are inconclusive as all three subjects brain data proved to be unique with respect to the placebo trials. A definite model change or pattern cannot be determined based on the subjects used. The effects of Dilantin on the brain signals, however, were marked in two of the three subjects.

The methodology is shown to be an effective means of representing the underlying structure of large amounts of data. Both significant and weak periodicities can be highlighted for analysis and interpretation.